CONTRIBUTIONS OF GENETICALLY DEFINED CELL POPULATIONS IN THE EXTENDED AMYGDALA TO EMOTIONAL BEHAVIOR

Christopher Mazzone

A dissertation submitted to the faculty at the University of North Carolina at Chapel Hill in partial fulfillment of the requirements for the degree of Doctor of Philosophy in the Neuroscience Curriculum.

Chapel Hill
2017

Approved by:

Fulton T. Crews

Todd E. Thiele

Garret D. Stuber

Spencer L. Smith

Thomas L. Kash

ABSTRACT

Christopher Mazzone: Contributions of Genetically Defined Cell Populations in the Extended Amygdala to Emotional Behavior
(Under the direction of Thomas Kash)

Emotional disorders, including anxiety, remain pervasive and debilitating conditions throughout the world despite decades of progress in the development of pharmacological treatments. Limitations in treatment efficacy exist, in part, due to our lack of understanding of the precise neural pathways and mechanisms underlying emotional disorders. Here I focus on the extended amygdala, an area of the brain that has long been implicated in the regulation of emotional behaviors. In this dissertation work, I use combinatorial approaches to determine the cellular identity and receptors that contribute to anxiety so that we may better develop more selective drug treatments for emotional disorders.

In Chapter 2, I use Designer Receptors Exclusively Activated by Designer Drugs (DREADDs) to manipulate G protein-coupled signaling pathways in a population of inhibitory cells of the bed nucleus of the stria terminalis (BNST), a component of the extended amygdala. This approach allowed us to identify that activation of Gq-coupled signaling pathways within inhibitory cells of the BNST is sufficient to induce an anxiety-like state in mice. I then identified endogenous Gq-coupled receptors expressed by inhibitory cells of the BNST, ultimately creating a list of potential candidate receptors for alleviating anxiety.

In Chapter 3, I further dissect BNST anxiety circuitry by focusing on the impact of serotonin on BNST corticotropin-releasing factor (CRF) expressing neurons. I show that the serotonergic input from the dorsal raphe (DR) nucleus to the BNST can induce both serotonin release and anxiety-like behavior. Using electrophysiological tools we found that serotonin produces opposing effects on membrane properties within BNST CRF neurons. Interestingly, selective serotonin reuptake inhibitors (SSRIs) are known to exacerbate learned fear responses and we found that inhibition of BNST CRF neurons is able to occlude the SSRI-induced enhancements of fear. These results highlight inhibition of BNST CRF neurons

as a potential therapeutic strategy for SSRI-induced increases in anxiety seen in patients during the early stages of SSRI-based therapies.

Together, these studies untangle part of the complex emotional circuits that may contribute to pathological emotional states and provide new therapeutic targets for the alleviation of both acute and SSRI-induced anxiety.

ACKNOWLEDGEMENTS

First, I'd like to thank the University of North Carolina at Chapel Hill and the Curriculum in Neurobiology for providing an outstanding environment for my graduate studies. The program directors, Dr. Bill Snider, Dr. Aldo Rustioni, and Dr. Garret Stuber, all oversaw and contributed to my progress as a student, and I'm grateful for the support they provided.

I'd like to especially thank my graduate mentor, Dr. Tom Kash, for all of his guidance throughout this work. I can unequivocally say I will miss working in his lab and am deeply grateful for his mentorship during the past five years. As a mentor, he could not have been more supportive or understanding of life both within and beyond the lab. His perspective on mentorship is something I will carry with me well beyond graduate school. I'd also like to thank all of the current and former members of the Kash Lab for their help and wealth of support. Chapter 3 of this dissertation would not have been possible without the remarkable contributions of Dr. Catherine Marcinkiewcz, and I'm honored that our work together led to my co-first authorship on that manuscript. Beyond the Kash Lab, I'd like to especially thank Dr. Zoe McElligott who has been an invaluable mentor and friend, and who collected the fast scan cyclic voltammetry work in Chapter 3. I'd like to thank other members of the UNC Neuroscience community, including Dr. Todd Thiele, Dr. Bryan Roth, Dr. Fulton Crews, Dr. Spencer Smith, Dr. Ben Philpot, Dr. Scott Magness, Dr. Robert Currin, and Dr. Vladimir Ghuskasyan who all contributed greatly to my training across a breadth of techniques. Additionally, all of the work in this dissertation would be impossible without the incredibly attentive and compassionate animal care staff at UNC, particularly Ashley Meadows and Matt Ehinger. I'll be forever grateful for their attention to detail and for their patience with all of my numerous requests and questions. To put it bluntly, I cannot imagine working with a better community of scientists and researchers than the team I've been fortunate to be a part of at UNC.

Beyond the UNC community, I'd like to thank the many collaborators from other institutions that contributed to the work in this dissertation. In particular, I'd like to thank Dr. Yasmin Hurd and Dr. Michael Michaelides for assisting with the DREADD Assisted Metabolic Mapping study in Chapter 2, and Dr. Jom

Hammack, Dr. William Falls, and Dr. Andrew Fox for providing the data assessing 5-HT2CR effects on anxiety in the BNST in Chapter 2. I would like to thank Dr. Francisco Javier Rubio Gallego for providing the protocol used for single-cell dissociations. In work presented in Chapter 3, I'd like to thank Dr. Lindsay Halladay and Dr. Andrew Holmes for collecting the *in vivo* electrophysiology data, Dr. Giuseppe D'Agostino, Dr. Claudia Cristiano, and Lora Heisler for conducting the 5HT2C-Cre DREADD study, and Dr. Charu Ramakrishnan and Dr. Karl Deisseroth for providing the INTRSECT constructs. Lastly, I'd be remiss to not thank all of the incredible scientists I met at various conferences over the past five years: thank you all for inspiring my own work and providing semi-annual reminders of how fortunate I am to work in a field with great people far beyond the Research Triangle.

Prior to graduate school, I worked as a technician in a neuropeptide laboratory run by Dr. Richard Mains and Dr. Betty Eipper at the University of Connecticut Health Center. There are no words that can convey my gratitude for my time in their lab, and for their continued friendship. I'd also like to thank Dr. James Chrobak for allowing me to volunteer in his lab while I was an undergraduate student at the University of Connecticut. His research and teaching ignited my initial interest in neuroscience. Lastly, I'd like to thank my high school AP Biology teacher Jerry Lentz. I have no doubt that the root of my scientific interests can be traced back to his enthusiastic lectures and challenging assignments. The ways our earliest mentors and teachers shape our lives cannot be overstated and I am so grateful to have been raised by great teachers.

Lastly, I'd like to thank my family for their unwavering love and support throughout all stages of my life. To my mother, my father, and my sister: thank you for everything.

TABLE OF CONTENTS

LIST OF TABLES

LIST OF FIGURES

LIST OF ABBREVIATIONS

5-HT	5-hydroxytryptamine; serotonin
BLA	Basolateral amygdala
BNST	Bed nucleus of the stria terminalis
CeA	Central nucleus of the amygdala
ChR2	Channelrhodopsin-2
CRF	Corticotropin-releasing factor
CS	Conditioned stimulus
DR	Dorsal raphe nucleus
DREADD	Designer Receptor Exclusively Activated by a Designer Drug
DREAMM	DREADD-Assisted Metabolic Mapping
EPM	Elevated plus maze
EZM	Elevated zero maze
FACS	Fluorescence-activated cell sorting
GABA	γ-Aminobutyric acid
ICV	Intracerebroventricular
LH	Lateral hypothalamus
mCPP	*meta*-cholorophenylpiperazine
NAc	Nucleus Accumbens
NSF	Novelty-induced suppression of feeding
PFC	Prefrontal cortex
PVN	Paraventricular nucleus of the hypothalamus
SSRI	Selective serotonin reuptake inhibitor
US	Unconditioned stimulus
VTA	Ventral tegmental area

CHAPTER 1 INTRODUCTION

1.1 Anxiety in Humans

Anxiety disorders remain widely prevalent despite decades of research and pharmaceutical drug development. Each year, nearly 18% of the United States population can be diagnosed with an anxiety disorder, and lifetime prevalence affects nearly a third of the population (Kessler, 2005; Kessler et al., 2007).These widespread chronic conditions are characterized by excessive fear and hypervigilance that can exert both high personal and economic costs (Whiteford et al., 2013; DiLuca & Olesen, 2014). Existing medical options for the treatment of anxiety-related conditions primarily focus on targeting the γ-aminobutyric acid (GABA) and serotonin (5-HT) neurotransmitter systems through the actions of benzodiazepines and selective serotonin reuptake inhibitors (SSRIs), respectively. Other drug classes may be prescribed, such as 5-HT norepinephrine reuptake inhibitors, monoamine oxidase inhibitors (MAOIs), and tricyclic antidepressants, though benzodiazepines and SSRIs remain the first-line options (Griebel & Holmes, 2013). Unfortunately, side effect profiles or a reduction of drug efficacy mar the potential for long-term treatment of persistent anxiety disorders. For example, chronic treatment with benzodiazepines suffers from abuse potential, while SSRIs may take weeks of treatment before the alleviation of symptoms (O'brien, 2005; Hoffman & Mathew, 2008). This highlights the need to better understand the underlying neural circuitry for anxiety disorders so that we may better target and modulate the activity of defined cell types involved in the generation of anxiety states.

In humans, functional magnetic resonance imaging (fMRI) studies have provided insights into the brain regions associated with anxiety-related conditions. Studies assessing the blood-oxygen-level dependent (BOLD) signal in patients with generalized anxiety disorder (GAD), social anxiety, or panic disorder (PD), have identified dysregulation in cortical areas, including the prefrontal cortex (PFC) and

anterior cingulate cortex (ACC) (Blair et al., 2008; Greenberg et al., 2013; Mochcovitch et al., 2014). Many studies have observed altered activity in subcortical structures as well, including the amygdala (Hoehn-Saric et al., 2004; Nitschke et al., 2009; Costafreda et al., 2008; Sergerie et al., 2008), however it should be noted that some studies have shown no differences, or a reduction, in amygdalar activity to emotional stimuli (Whalen et al., 2008; Etkin et al., 2010; Blair et al., 2008; Yassa et al., 2012). Interestingly, it has been proposed that in adult patients with GAD, there is reduced amygdala activity that correlates with enhanced activity in the bed nucleus of the stria terminalis (BNST), a component of the extended amygdala (Yassa et al., 2012). In keeping with this, previous studies have shown that BNST activity is elevated in humans during anxiety-evoking stimuli (Straube et al., 2007; Somerville et al., 2010; Avery et al., 2016). In one study, human patients with arachnophobia had elevated activity in the BNST that correlated with self-reports of anxiety following being told they would be presented with an image of a spider, while non-arachnophobic patients did not show elevated BNST activity during the same protocol (Straube et al., 2007). Similarly, in a study with human subjects without a diagnosed anxiety disorder, perceiving a spider to be near their feet elevated activity in the BNST in a proximity-dependent manner that correlated with self-reports of anxiety (Mobbs et al., 2010). Such studies have highlighted the BNST as a neural locus that is engaged during aversive emotional states. It is important to note that the small size of the BNST in humans makes it difficult to identify reactivity of discrete subregions, though recent advances in segmentation approaches may yield more discrete results (Theiss et al., 2016).

Non-human primates also show similar increases in BNST activity during anxiety-evoking states. Changes in freezing behavior, a behavioral manifestation of anxiety and fear, correlated with BNST activity in rhesus macaques using positron emission tomography (PET) imaging (Kalin et al., 2005). These studies in humans and non-human primates highlight the BNST as a promising node in the regulation of anxiety. Although the BNST has been linked with anxiety in humans and non-human primates, the majority of the literature has used rodent models to characterize the involvement of brain nuclei and discrete cell populations in anxiety-related behavior, which we discuss below.

1.2 Rodent Models of Anxiety- and Fear-Related Behavior

While fMRI and PET imaging technologies allow for remarkable assessments of activity-driven changes in neural and metabolic function in humans, they unfortunately do not provide insights into the

specific contributions of discrete anatomical connections between brain nuclei or genetically defined cell populations to producing emotional states. We thus turn to animal models of emotional behavior to overcome these limitations and untangle the complex circuitry that governs emotion processing. Additional complexities arise given the subjectivity of emotional experiences and the controversial nature of associating animal behavior with human emotion (Anderson & Adolphs, 2014; LeDoux, 2012). Nonetheless, we can use emotional behavior in models organisms where the behavioral readout gives clues to the internal emotional state (Anderson & Adolphs, 2014).

Importantly, a key aspect of an anxiety state is whether the emotional response can be defined as either trait or state anxiety. Trait anxiety refers to a non-evoked stable degree of anxiety, such as baseline anxiety levels, while state anxiety refers to anxiety experienced in a particular moment, especially following a stimulus (Lister, 1990). Due to the difficulty in assessing trait anxiety in animals, studies in rodents often capitalize on the state anxiety induced by exposure to novel environments. Generally, these tests involve a motivational conflict: the desire to explore the entirety of a novel environment versus remaining in safer aspects of the potentially threatening arena. One of the most common anxiety assays in rodents is the elevated plus maze (EPM). It consists of two intersecting platforms that create a plus-shaped environment with four arms. Two of the arms are walled, thus generating two “safe” arms (walled) and two potentially threatening arms (open). When placed into the maze, a typical mouse will spend more time in the closed arms relative to the exposed open arms (Pellow et al., 1985). This general approach-avoidance principle drives other exploratory-based anxiety assays as well. The light-dark box, for instance, features a two-compartment box with a well-lit “exposed” compartment, and one that is enclosed by dark walls. Similarly, an open field assay consists of a single large enclosed space, and the duration spent in the central area, as opposed to being near the walls, serves as an inverse measure of the degree of anxiety.

Another assessment of anxiety-like behavior is the startle response to an unexpected stimulus. This is most commonly an acoustic stimulus in rodents. This acoustic startle response can be enhanced by a number of anxiogenic conditions, such as fear-potentiated, light-enhanced, and corticotropin releasing-factor (CRF)-enhanced startle (Davis et al., 2010). Fear-potentiated startle refers to the evoked startle amplitude in the presence of a conditioned stimulus (CS) that was previously paired with an

aversive unconditioned stimulus (US), which is most often a foot shock in rodents (Brown et al., 1951). It is important to note that in this assay, fear potentiates the existing startle response and is dependent on a learned conditioned fear. As described above, rodents are averse to bright lights. Taking advantage of this, the acoustic startle assay was modified to assess the effect of bright light exposure on the startle response, or light-enhanced startle (Walker & Michael Davis, 1997). Because light-enhanced startle capitalizes on an innate anxiogenic stimulus, it is independent of learning and thus allows probing of the effects of drugs selectively on an anxiety-dependent and not a learned fear-dependent behavior. In contrast to rodents, both humans and non-human primates show an enhanced startle response in dark environments. The magnitude of this dark-enhanced startle can be in exacerbated in human patients with post-traumatic stress disorder (PTSD) and rhesus monkeys separated from their mothers (Grillon et al., 1997; Grillon et al., 1998; Parr et al., 2002). Thus, the amplitude of the acoustic startle response serves as an index anxiety. Lastly, in addition to both fear- and light-enhanced acoustic startle, the startle response can be potentiated by intracerebroventricular (ICV) infusion of corticotropin-releasing factor (CRF), a peptide involved in the stress response (Swerdlow et al., 1986). This is not an exhaustive list of assays designed to probe anxiety-related behavior. Others have adapted to include more motivated behaviors, such as novelty-induced suppression of feeding in which palatable food consumption is suppressed by a potentially threatening novel environment (Merali et al., 2003; Bodnoff et al., 1988).

A critical aspect of behavioral assay design is whether it satisfies face, construct, and predicative validity. Face validity refers to the degree of similarity between the assayed phenotype and what is observed in the human state being modeled. For example, in the exploratory assays described above, a reduction in the time spent in the aversive zones is representative of avoidance of cues or contexts that trigger anxiety in people. To meet construct validity in animal models, the underlying biological mechanisms for the observed phenotype must be similar to those in humans. Construct validity is thus critical if an animal model is being used to identify potential circuits or therapeutic targets of interest for a given condition. Appropriate construct validity in rodent models of anxiety is what allows us to identify discrete neural circuits potentially involved in the generation of anxiety in humans. Lastly, the predicative validity of rodent models of anxiety-like behavior refers to the ability of the assay to screen therapeutic effects of pharmacological agents in humans. Thus, if an assay shows a compound is anxiolytic in

rodents, then the same compound should reduce anxiety in humans (Cryan & Holmes, 2005; Belzung & Griebel, 2001; Calhoon & Tye, 2015). However, drug side effect profiles may create potential caveats for the predictive efficacy of an assay. Benzodiazepines, for example, reduce anxiety in people, but also have sedative properties. As the anxiety assays described above are dependent on exploration of a novel environment, pharmacologically-induced sedation would produce a reduction in locomotor activity that is independent of anxiety. It is therefore crucial to interpret results of behavioral assays carefully, particularly with respect to changes in locomotion.

1.3 Involvement of the Extended Amygdala in Anxiety and Fear

Decades of work using electrolytic lesioning, pharmacological manipulations, transgenic rodent lines, optogenetics, and chemogenetics have aided in untangling the neural circuits that drive anxiety and fear behavior (for review, see Calhoon & Tye, 2015; Adhikari, 2014; Janak & Tye, 2015). The results of these studies identified numerous brainwide networks that contribute to multiple components of anxiety and fear. Much work has implicated the prefrontal cortex, the basolateral amygdala (BLA), the hippocampus, and the extended amygdala, which consists of the CeA and the BNST (Alheid & Heimer, 1988). In a pioneering study in rhesus macaques, aspiration of the amygdala reduced fear-related behavior and cue-related learning behavior (Weiskrantz, 1956). Similar results were later obtained through excitotoxic lesions of the amygdala that spared damage to fibers of passage, implicating the amygdala indeed played a role in the effect (Meunier et al., 1999). Human subjects with damage to the amygdala also show reductions in conditioned fear learning without impaired learning of declarative memories, thus highlighting the importance of amygdala in human fear (Bechara et al., 1995). Beyond humans and non-human primates, a wealth of studies in rodents further established that disruption of the BLA impairs fear and anxiety-related behavior (LeDoux, 2000; Shin & Liberzon, 2010; Janak & Tye, 2015). As the BLA has direct projections to the extended amygdala, including the CeA and BNST, and the extended amygdala has direct projections to areas of the hypothalamus and brainstem known to be involved in anxiety, these regions and circuits became of high interest for the potential regulation of anxiety-related behavior.

The extended amygdala was initially defined following early characterizations of the CeA and BNST that remarked on the similarities of these structures with respect to anatomical connectivity and

neurochemical makeup (Alheid & Heimer, 1988). To determine the unique contributions of the BNST and CeA to anxiety and fear behavior, seminal studies used electrolytic or pharmacological lesions to inactivate components of the extended amygdala nuclei during fear-related tasks (Davis et al., 1997; Walker et al., 2003; LeDoux et al., 1988; Gewirtz et al., 1998). In particular, lesions of the CeA abolished fear-potentiated startle, while BNST lesions had no effect (LeDoux et al., 1988; Lee & Davis, 1997; Hitchcock & Davis, 1991). Conversely, pharmacological inhibition of the BNST, but not CeA, blocked light-potentiated startle (Walker & M Davis, 1997). Pharmacological inhibition of the BLA, an upstream target of both the CeA and BNST, was sufficient to impair both fear-potentiated and light-potentiated acoustic startle (Walker & M Davis, 1997). These initial findings led to the theory that the BNST is not involved in shock-predicting cues (Walker et al., 2003). Together, these formative studies led to a model in which the CeA regulates fear (immediate predictable threats), while the BNST is involved in anxiety (ambiguous threats) (Walker et al., 2003).

The drivers of anxiety and fear behavior are distinct between fear- and light-potentiated startle. In fear-potentiated startle a discrete cue predicts a temporally near aversive stimulus, while light-potentiated startle uses an innately anxiogenic stimulus to exacerbate startle responding. In other words, in one situation there is a cue predicting a known immediate threat, while in the other the threat is ambiguous and possibly nonexistent. In agreement with this, light-potentiated and fear-potentiated startle produce different effects on the duration of the startle increase following offset of the potentiating stimulus (De Jongh et al., 2003). Startle amplitude returns to baseline within seconds following offset of the conditioned stimulus in fear-potentiated startle, while startle amplitude remains elevated on the order of minutes in light-enhanced started (De Jongh et al., 2003). To better dissect the role of temporal proximity between a CS and US in engaging anxiety or fear behavior through BNST function, a critical study from Waddell et al. used a classic fear conditioning paradigm in which an auditory CS preceded a US of a foot shock (Waddell et al., 2006). BNST lesions did not disrupt the acquisition of conditioned fear learning when a short duration CS (1 minute) preceded a footshock, but impaired the acquisition of fear learning when a long-duration CS (10 minutes) preceded shock. This study further demonstrated that BNST lesions disrupt the reinstatement of fear responding and was sufficient to reduce anxiety-like behavior in the elevated plus maze (Waddell et al., 2006). It is important to consider that these findings do not entirely

dissociate the BNST and CeA functionally. Indeed, the CeA has direct projections to the BNST and lesions to the CeA can reduce CRF labeling in the BNST (Sakanaka et al., 1986). While the findings discussed above demonstrate that they are differentially engaged by select anxiety- or fear-provoking stimuli, the CeA and BNST are functionally interconnected and may serve feedback loops that contribute to broader circuit changes in activity. This interconnectivity is important to consider when assessing the modulatory roles various neurotransmitter and neuropeptide inputs have on BNST function (Kash et al., 2015).

1.4 Anatomical Characterization of the BNST

Early observations that the BNST shared structural similarities with the CeA led to the idea of these structures forming an "extended amygdala" (Alheid & Heimer, 1988). In addition to structural parallels, the CeA and BNST were similar with respect to cellular morphology, anatomical connectivity, and cellular composition as determined by immunohistochemistry (Alheid & Heimer, 1988). As described above, decades of research has since dissected the unique contributions of the CeA and BNST to various fear-related and motivated behaviors to better distinguish the differences between these similar structures. However, discerning precisely how the BNST contributes to emotional behavior is made difficult by the structure's diverse, and often reciprocal, projections throughout the brain (Figures 1.1 and 1.2). The BNST receives glutamatergic projections from the medial prefrontal cortex, paraventricular thalamus, ventral hippocampus, and the BLA (Dong & Swanson, 2003; Hong Wei Dong et al., 2001; Kim et al., 2013). In addition to glutamatergic inputs, the BNST receives dopaminergic afferents from the ventral tegmental area (VTA) and the A10dc located in the periaqueductal gray (PAG) (Park et al., 2013; Hasue & Shammah-Lagnado, 2002; Meloni et al., 2006), serotonergic inputs from the dorsal raphe (DR) (Phelix et al., 1992), and noradrenergic inputs from the locus coeruleus (LC) and the nucleus of the solitary tract (NTS) (Forray et al., 2000; Park et al., 2009). The BNST also receives dense GABAergic and CRFergic inputs from the CeA (Sakanaka et al., 1986; Erb et al., 2001; Morin et al., 1999; Cummings et al., 1983; Silberman et al., 2013). The BNST sends direct projections to numerous nuclei throughout the brain, including areas of the hypothalamus, amygdala, VTA, PAG, DR, and parabrachial nucleus (PBN) that allow the BNST to modulate a diverse array of behaviors (Hong Wei Dong et al., 2001; Hong W. Dong et al., 2001; Choi et al., 2007; Kim et al., 2013).

Beyond having a complex connectivity architecture, the BNST itself can be subdivided into more than a dozen subnuclei in rodents. Early topographical tracing studies in rats aided to rigorously characterize the discrete connectivity differences between BNST subregions with respect to local and distal projections (Dong & Swanson, 2003; Dong et al., 2006; Dong & Swanson, 2006b; Dong & Swanson, 2004a; Hong Wei Dong et al., 2001; Dong & Swanson, 2006a; Dong & Swanson, 2004b; H W Dong et al., 2001). Although the exact number of subcompartments of the BNST remains controversial, it can be generally divided by its medial-lateral and anterior-posterior axes (Bota et al., 2012). Under this schematic, the anterior division can be divided into the following nuclei: anterolateral, anteromedial, oval, juxtacapsular, rhomboid, dorsomedial, fusiform, ventral, and magnocellular (Bota et al., 2012; Lebow & Chen, 2016). Conversely, the posterior compartments of the BNST consist of the principal, interfasicular, transverse (Lebow & Chen, 2016; Dong & Swanson, 2004a).

1.5 Neuromodulation of BNST Function by Corticotropin-Releasing Factor and Serotonin

Corticotropin-releasing factor (CRF)

CRF is the most studied neuropeptide within the BNST, and CRF overexpression is sufficient to induce anxiety-like behavior (Coste et al., 2001). Likewise, stress-inducing stimuli elevates expression of c-fos, an intermediate early gene, in CRF-expressing cells in of the paraventricular nucleus of the hypothalamus (PVN) and other brain nuclei (Ceccatelli et al., 1989). Originally viewed for its initiation of the HPA stress axis via release of CRF from neurons of the PVN, CRF expression has been observed in non-hypothalamic structures including the CeA and BNST (Heinrichs & Koob, 2004; Bale & Vale, 2004; Vale et al., 1981; Merchenthaler et al., 1982; Phelix & Paull, 1990; Cummings et al., 1983; Herman et al., 2003). Further, CRF positive fibers within the BNST were found to be in close proximity to serotonergic fibers, highlighting the potential interplay between neurotransmitter and neuropeptide systems (Phelix et al., 1992). In agreement with this, a study demonstrated that exposure to a novel environment enhances intermediate early gene (IEG) c-fos expression in BNST CRF neurons, but this effect is absent in mice lacking the 5-HT2C receptor (Heisler et al., 2007). Adding to the complexity, BNST CRF neurons also express the neurotransmitter GABA (Dabrowska et al., 2013). ICV and systemic treatment with CRF has been shown to elevate stress-related behaviors, and stress exposure elevates CRF mRNA within the BNST (Dunn & Berridge, 1990; Funk et al., 2006). Of note, the density of CRF-expressing cells is largely

similar between mice and rats, though differences in CRF neuron density do exist (Wang et al., 2011). These data implicate the BNST, and the extended amygdala generally, as critical loci for CRF-mediated stress-induced behavior.

Building upon this, intracerebroventricular (ICV) CRF enhances the startle response, which can be blocked by pharmacological lesions of the BNST using NMDA (Lee & Davis, 1997). Further, ICV α-helical CRF, a CRF antagonist, is sufficient to blunt light-enhanced startle without altering fear-potentiated startle (De Jongh et al., 2003). Infusion of α-helical CRF directly into the BNST also blunts light-enhanced startle, indicating the BNST is a critical locus for anxiety-induced startle responding (Lee & Davis, 1997). As prior reports observed that cerebroventricular infusion of CRF could potentiate the acoustic startle response (Swerdlow et al., 1986), this finding further positioned the BNST as a critical component of the CRF-induced increase in anxiety. Importantly, CRF-enhanced startle persists despite lesioning of the paraventricular nucleus of the hypothalamus (PVN) (Liang et al., 1992). Together, these studies demonstrate that CRF-potentiated acoustic startle requires BNST CRF receptor activation and is independent of CRF-induced engagement of the hypothalamic-pituitary-adrenal (HPA) stress axis. Building upon this, a study assessing the involvement of the CeA and BNST in the expression of a learned cued fear identified that electrolytic lesions of the CeA disrupted expression of cued and contextual fear, while lesions of the BNST only disrupted the expression of contextual fear (Sullivan et al., 2004). Corticosterone levels in this study paralleled the expression of learned fear, such that BNST lesions blunted context-induced increases in corticosterone (Sullivan et al., 2004).

Interestingly, CRF infusions to the BNST can induce reinstatement of cocaine seeking, while antagonism of CRF receptors in the BNST disrupts stress-induced drug seeking (Erb & Stewart, 1999; Wang et al., 2006). Interestingly, overexpression of CRF in the BNST using a lentiviral approach led to no changes in baseline anxiety behavior (Sink et al., 2013). Further, overexpression of CRF in the BNST prior to a startle conditioning task impairs acquisition of fear responding, while overexpression post training exacerbates fear behavior (Sink et al., 2013). These data highlight the complexities of CRF effects on anxiety and fear within the BNST.

Part of the variance in behavioral response to CRF manipulations in the BNST may be attributed to the activation of CRF receptor subtypes. CRF binds to two types of G protein-coupled receptors: CRF-

1 and CRF-2 (CRF1R and CRF2R, respectively) (Hauger et al., 2006; Chalmers et al., 1995; Lovenberg et al., 1995). Although both of these receptors are preferentially coupled to a Gs alpha subunit, activation of CRF1 and CRF2 receptors can produce differing responses within the BNST (Tran et al., 2014). Of note, however, CRF receptors are capable of binding other types of G proteins as well, including the Gq subunit (Grammatopoulos et al., 2001). CRF receptors may also be bound by the CRF-related urocortin (UCN) peptides UCN 1, UCN 2 (also called stresscopin-related peptide), and UCN 3 (also called stresscopin) (Vaughan et al., 1995; Reyes et al., 2001; Lewis et al., 2001). Availability of both CRF and UCN 1 can be reduced through interactions with CRF binding protein (CRF-BP), thus providing multiple means of modulating the activity of CRF receptors (Behan et al., 1995; Lewis et al., 2001; Seasholtz et al., 2002).

In rats, infusion of CRF into the BNST was sufficient to induce anxiety-like behavior, while co-administration of a CRF1R antagonist, but not a CRF2R antagonist, could block the CRF-induced increase in anxiety (Sahuque et al., 2006). In agreement with this, deletion of GABA(A)α1 receptors in CRF neurons increases anxiety-like behavior in a manner that can be blocked by CRF1R antagonism in the BNST (Gafford et al., 2012). Similarly, CRF1R is upregulated, while CRF2R is downregulated, in a rat model of PTSD, and lentiviral overexpression of CRF2R in PSTD-like rats is sufficient to blunt PTSD-related fear behavior (Elharrar et al., 2013). However, CRF2R levels were increased in a mouse model of PTSD, while knockdown of CRFR2 in the BNST reduced the susceptibility of PTSD-related behavior (Lebow et al., 2012). CRF receptor expression differences in PTSD models could potentially result from differences in the types of stress exposure used to induce PTSD-like states. Regardless, the results from these studies implicate CRF receptor signaling in the BNST as a contributor to behavior during pathological states.

The mechanistic underpinnings of these differences are complex. Within the BNST, CRF1R facilitates postsynaptic GABAergic signaling while also facilitating presynaptic glutamate release (Kash & Winder, 2006; Silberman et al., 2013). Given the diverse projections of the BNST, the localization of these effects is critical for the potential behavioral impact. CRF-induced enhancement of glutamatergic events in the BNST, for example, has been observed in VTA-projecting neurons (Silberman et al., 2013). This result is intriguing given that BNST projections to the VTA modulate anxiety and ethanol drinking behavior

(Jennings, Sparta, et al., 2013; Rinker et al., 2015). Interestingly, CRF depolarizes BNST neurons categorized as Type II, which are potentially BNST interneurons (Ide et al., 2013; Hammack et al., 2007). Additionally, CRF interacts with other neurotransmitter systems in the BNST as it has been shown that dopamine-induced increases in glutamatergic transmission in the BNST requires CRF1R activation (Kash et al., 2008). The source of CRF for both behavioral and electrophysiological effects remains unclear. As described above, the BNST contains both CRF-expressing cells and receives a dense CRF input from the CeA. Further dissection of local BNST microcircuits is required to fully assess the contributions of local CRF release to both behavior and synaptic events.

Serotonin (5-hydroxytryptamine; 5-HT)

5-HT has long been implicated in emotion regulation, particularly depression, and many pharmaceutical treatments for affective disorders target the 5-HT system (Griebel & Holmes, 2013; Berger et al., 2009; Asan et al., 2013; Graeff, 2002; Jasinska et al., 2012; Wise et al., 1972). Unlike the broad brain-wide distribution of most neurotransmitter and neuropeptide systems, the majority of serotonergic cells are located in the DR nucleus (Fuxe, 1965). DR 5-HT neurons receive diverse inputs from forebrain and brainstem nuclei, thus allowing the 5-HT system to integrate inputs from throughout the brain (Pollak Dorocic et al., 2014). Likewise, DR 5-HT neurons project throughout the brain and regulate an array of biological and neuropsychological functions, including mood, sleep, appetite, and affect (Berger et al., 2009). In agreement with this, acute diet-induced reductions in tryptophan, the precursor for 5-HT, is sufficient to elevate anxiety-related startle in humans (Robinson et al., 2012). In rodents, DR 5-HT neurons are engaged by multiple types of stressful stimuli and can be directly activated by CRF (Hammack et al., 2002; Hammack et al., 2003; Kirby et al., 2000; Lowry et al., 2000). Elevated synaptic 5-HT release is also observed in the amygdala and PFC upon exposure to psychological threats (Kawahara et al., 1993). The cellular effects of 5-HT signaling occur through 5-HT binding of fourteen subtypes of 5-HT receptors (divided into classes of 5-HT_1 – 5-HT_7) that are localized to both pre- and postsynaptic membranes (Roth, 1994; Asan et al., 2013; Hannon & Hoyer, 2008; Barnes & Sharp, 1999). 5-HT receptor subtypes are G protein-coupled receptors that bind various G alpha subunits with the exception of the ionotropic 5-HT_3 receptor. This heterogeneity allows 5-HT to modulate pre- and postsynaptic function through the engagement of an array of G protein-mediated signaling cascades. The

family of 5-HT_1 receptors preferentially bind Gi/o, thereby leading to reductions in cyclic AMP (cAMP) production and a hyperpolarization resulting from activation of inwardly rectifying potassium channels (Polter & Li, 2010). 5-HT1A receptor function can be divided into autoreceptor or heteroreceptor activity. As an autoreceptor, 5-HT1A receptors are located on presynaptic and somatodendritic membranes of serotonergic neurons of the raphe nucleus, ultimately reducing the firing of serotonergic neurons (Polter & Li, 2010). Conversely, postsynaptic localization of 5-HT1A heteroceptors function as the predominant inhibitory postsynaptic 5-HT receptor in the forebrain (Garcia-Garcia et al., 2014). This positions the 5-HT1A receptor as a modulator of both the synaptic levels of 5-HT release and the magnitude of the postsynaptic response. Given this broad role for 5-HT1A receptor signaling, it is not surprising that disruption of 5-HT1A receptor function or expression alters numerous behavioral states. In contrast to the 5-HT1A receptor, the 5-HT2 family of receptors preferentially couple to Gq subunits and have excitatory effects through activation of the phospholipase C (PLC) signaling pathways and inhibition of potassium channels (Polter & Li, 2010; Asan et al., 2013).

Behavioral pharmacology and genetic manipulation studies in rodents have identified 5-HT receptor involvement in mediating anxiety and fear-related behaviors. Numerous studies have identified the 5-HT2C receptor is involved in modulating anxiety-related behavior. Specifically, it was identified that antagonism of 5-HT2 signaling, through oral administration of a 5-HT2 family antagonist, reduced anxiety-like behavior in mice tested on the elevated plus maze (Stutzmann et al., 1991). Similarly, agonism of the 5-HT2C receptor using *meta*-cholorophenylpiperazine (mCPP) or 6-chloro-2[1-piperazinyl] pyrazine (MK-212) induces anxiety-related behavior in rodents (Kennett et al., 1989; De Mello Cruz et al., 2005; Hackler et al., 2007). Antagonism of 5-HT2C receptors induces anxiety and panic-like episodes in both normal healthy subjects and in patients suffering from panic disorder (Charney et al., 1987). Adding to the role of 5-HT in regulating emotional behavior, patients suffering from major depressive disorder (MDD) have reduced blood platelet levels of 5-HT and the 5-HT precursor L-trypotphan (Maurer-Spurej et al., 2007; Ogawa et al., 2014). These results, coupled with the clinical observations that drugs elevating 5-HT levels have remained the most effective treatments for depressive disorders, have contributed to the 5-HT hypothesis of depression disorders (Fakhoury, 2016). Further, the involvement of 5-HT receptors in mediating the effects of anxiety and depression is consistent with high clinical comorbidity of anxiety and

depression (Gorwood, 2004; Ballenger, 1999). It is thus unsurprising that pharmacological targeting of the 5-HT system remains the most common form of clinical treatment for patients suffering emotional disorders.

Selective serotonin reuptake inhibitors (SSRIs) are a first-line treatment for many anxiety and depressive disorders (Griebel & Holmes, 2013). Mechanistically, SSRIs act by elevating synaptic levels of 5-HT through blockade of the serotonin reuptake transporter, which is localized to serotonergic neurons (Austin et al., 1994). While such results are in agreement with data showing 5-HT levels are reduced in patients diagnosed with MDD, this is not without caveats. Therapeutic benefits of SSRIs require multiple weeks of treatment, and acute responses to SSRIs can exacerbate anxiety, fear, and suicidal ideation in human patients (Grillon et al., 2007; Griebel & Holmes, 2013; Gorman et al., 1987; Fergusson et al., 2005). Interestingly, the therapeutic benefits of chronic SSRI treatment are not limited to patients suffering from a psychiatric illness. Chronic SSRI treatment has been sufficient to reduce anxiety-related behavior in healthy patients (Grillon et al., 2009). This study further demonstrated that the therapeutic benefits of SSRI treatment in healthy subjects were limited to context-induced anxiety, and not cue-evoked fear behavior. The dissociation of context- and cue-evoked fear is of particular interest given the complex modulation of anxiety and fear responses within the extended amygdala. As the BNST is largely considered to mediate anxiety-related behaviors, it is possible the therapeutic benefits of SSRI treatment are mediated through changes in BNST function.

Although it may seem counter-intuitive that initial response to SSRIs, and therefore elevated synaptic levels of 5-HT, can worsen symptoms of anxiety and depression, similar results have been widely observed in rodents (Burghardt et al., 2004; Mombereau et al., 2010; Burghardt et al., 2007; Ravinder et al., 2011; Belzung et al., 2001). As the acute aversive effects of SSRI administration increase anxiety and fear behavior, the extended amygdala has been an intriguing structure that could mediate these effects. Both the CeA and BNST receive serotonergic afferents from the DR nucleus (Commons et al., 2003). Of particular interest, serotonergic fibers in the BNST are present near CRF-expressing cells, and some serotonergic cells of the DR also express CRF (Commons et al., 2003; Phelix et al., 1992). In keeping with this, systemic administration of the 5-HT2C receptor agonist mCPP increases anxiety-like behavior and elevates c-fos expression in the BNST (Singewald et al., 2003). To better probe the

underlying circuitry of 5-HT induced effects on anxiety, recent work has used behavioral pharmacology and site-directed infusion of drugs targeting 5-HT receptors to various brain areas.

1.6 Optogenetic and Chemogenetic Tools for Modulating Discrete Neural Circuits

As detailed above, the neural circuits underlying emotional behavior are complex, interconnected, and composed of vastly heterogeneous cell types. We have begun to untangle these circuits through a wealth of behavioral studies employing the use of transgenic rodent lines, pharmacological or electrolytic lesions of discrete brain nuclei, or local pharmacological manipulations that have all provided useful insights into circuits that drive discrete behaviors. A caveat to these approaches, however, is the ability to directly modulate activity of cell types defined by anatomical connectivity or genetic identity within brain nuclei of interest. For example, while pharmacological inhibition of a brain nucleus is possible through cannulation and infusion of drugs targeting endogenous receptors, this approach is unable to selectively target cells that project to another nucleus of interest. This is critical, as recent studies using optogenetic approaches have demonstrated that both anatomical outputs or genetic identities of cell types within a nucleus contribute to the ultimate behavioral effect following activation (Kim et al., 2013; Jennings, Sparta, et al., 2013).

Optogenetics provides a temporally precise way of selectively activating or inhibiting neurons through optical activation of light-sensitive proteins that can directly influence action potential firing (Boyden et al., 2005; Deisseroth, 2011). Channelrhodopsin-2 (ChR2) is a light-sensitive protein naturally found in the algae *Chlamydomanas reinhardtii* that undergoes a conformational change upon stimulation with blue light that results in the influx of cations through the channel (Nagel et al., 2003; Zhang et al., 2011). Similarly, light-sensitive GPCRs have been developed for optical manipulation of intracellular signaling (Airan et al., 2009). While ChR2 remains the most common optogenetic tool for stimulating cells, the optogenetic toolbox has grown to include inhibitory opsins, step-function opsins (SFOs), and an array of optically stimulated cation channels with various kinetic properties (Tye & Deisseroth, 2012; Klapoetke et al., 2014; Lin et al., 2009; Zhang et al., 2007; Chow et al., 2010; Berndt et al., 2009). Pioneering studies demonstrated that optical stimulation of genetically defined cell types in mice could induce action potential firing and alter behavior (Adamantidis et al., 2007; Tsai et al., 2009). Later work identified that implantation of optical fibers above ChR2-expressing axon terminals in downstream brain areas allowed

for *in vivo* stimulation of discrete neural projections (Tye et al., 2011). These landmark optogenetic studies demonstrated how light-sensitive opsins provide a precise way of manipulating discrete cell types and projections *in vivo*.

In contrast to optogenetics, chemogenetics refers to the use of proteins that have been modified to bind previously unassociated compounds (Roth, 2016). In neuroscience, the most common chemogenetic tools are the Designer Receptors Exclusively Activated by Designer Drugs (DREADDs) that are modified G protein-coupled receptors (GPCRs) that are coupled to the canonical G alpha subunits (Gs, Gi, and Gq) (Armbruster et al., 2007; Guettier et al., 2009). The original DREADD constructs are modified muscarinic receptors that are activated by the inert ligand clozapine *n*-oxide (CNO) (Armbruster et al., 2007). However, alternative ligands have also been discovered, including perlapine and compound 21 (Chen et al., 2015). An advantage of these compounds is that they avoid the back-metabolism of CNO to clozapine that occurs in humans (Jann et al., 1994). While the most commonly used DREADD constructs are modified muscarinic receptors, additional DREADD variants exist, such as a modified κ-opioid receptor DREADD (KORD) that is exclusively activated by the inert compound salvinorin B (Vardy et al., 2015). Combination of DREADD constructs that are activated by discrete ligands allows for temporal modification of multiple discrete G protein-coupled signaling pathways, such as combining the use of the CNO activated hM3Dq receptor and the salvinorin B activated KORD (Vardy et al., 2015).

Engagement of G proteins coupled to DREADDs can induce changes in membrane potential and can alter expression of intermediate early genes (Alexander et al., 2009; Nakajima et al., 2016). It is important to note that this approach differs from optogenetic strategies using light-gated ion channels, including ChR2, halorhodopsin, and archaerhodopsin, in that changes in cellular activity are downstream of the receptor manipulation. Light-gated ion channels allow for a direct means of altering ion influx or efflux, thus directly altering membrane potential and action potential firing within milliseconds, while G protein-coupled DREADDs require interaction with endogenous signaling cascades to induce changes in neuronal activity and excitability. However, while used less than chemogenetic tools, light-gated G protein-coupled receptors also exist, such as ChARGe, Rh-CT, and OptoXR (Zemelman et al., 2002; Oh et al., 2010; Airan et al., 2009).

While DREADD technology allows for the modulation of discrete G protein-coupled signaling pathways, it is important to consider the mechanism underlying DREADD-induced effects. Early assessments of hM3Dq DREADD receptor function observed that bath application of CNO induces a depolarization of CA1 pyramidal neurons, which is blocked in the presence of a PLC inhibitor, indicating that the depolarization observed required the canonical Gq-coupled signaling cascade (Alexander et al., 2009). Further, activation of the hM3Dq DREADD induced an increase in action potential firing, verifying that Gq stimulation increases activity and action potential probability. This technology has also been extended to modulate activity of other cell types, including increasing Ca^2 release of astrocytes, smooth muscle cells, and various others (Agulhon et al., 2013; Armbruster et al., 2007; Guettier et al., 2009; Roth, 2016). Stimulation of Gq signaling with hM3Dq increases phosphorylation of ERK-1/2 in smooth muscle cells, highlighting the recruitment of endogenous second messenger systems (Armbruster et al., 2007). The inhibitory effects of the Gi-coupled hM4Di and KORD appear to occur through multiple classic signaling mechanisms. In part, hyperpolarization is mediated through the activation of G protein inward rectifying potassium (GIRK) channels by the Gβγ subunit (Armbruster et al., 2007). The hM4Di-induced hyperpolarization has been observed in multiple brain regions, including within the BNST (Pleil et al., 2015). In addition to hyperpolarization effects, stimulation of Gi-coupled DREADD activity reduces neurotransmitter release probability and the frequency of postsynaptic currents (Stachniak et al., 2014; Vardy et al., 2015). Beyond acute cellular effects, recent evidence has demonstrated that *ex vivo* stimulation of Gi-DREADD expressing CA1 neurons can alter long-term forms of synaptic plasticity (López et al., 2016). It is likely that other mechanisms contribute to the reduction in synaptic release, including inhibition of presynaptic Ca^2 channels and interactions with proteins involved with synaptic vesicle fusion (Gerachshenko et al., 2005; Blackmer et al., 2005).

As with optogenetic approaches, DREADDs can be delivered to target cells using viral vectors that encode DREADD constructs. As DREADDs are activated by exogenous administration of CNO, many routes of administration are available depending on the experimental design. Acute systemic injections of CNO provide a temporally controlled stimulation of DREADDs, while chronic activation can be achieved through inclusion of CNO in home cage drinking water (Urban et al., 2015). CNO can also be locally infused both in somatic regions or at DREADD-expressing axon terminals to directly stimulate

distinct pathways (Rinker et al., 2015). DREADDs have been used to identify distinct GPCR-mediated signaling pathways involved in a number of behaviors, including feeding (Krashes et al., 2014; Krashes et al., 2011; Atasoy et al., 2012), reward (Chang et al., 2015; Ward et al., 2015), fear (Yau & McNally, 2015; López et al., 2016), pain (Peirs et al., 2015; Bourane et al., 2015), and depression (Urban et al., 2015). Further, a recent study identified that Gq- vs Gs-coupled DREADD activation differentially stimulates neurotransmitter and neuropeptide effects on feeding within the arcuate nucleus, respectively (Nakajima et al., 2016). Modulation of neural circuits using DREADDs is not limited to behavioral output. Studies coupling DREADD activation with positron emission tomography (PET) imaging have identified metabolic changes induced by DREADD activation throughout the brain (Michaelides et al., 2013; Anderson et al., 2013; Urban et al., 2015). This combinatorial approach is referred to as DREADD Assisted Metabolic Mapping (DREAMM) (Michaelides et al., 2013). Chemogenetic approaches are particularly valuable given that the majority of pharmaceutical drugs developed target GPCRs, thus identification of these signaling pathways is valuable for future drug discovery (Rogan & Roth, 2011).

1.7 Dissecting Contributions of Signaling within the BNST to Anxiety and Fear-Related Behavior

The heterogeneity of the BNST with respect to both neurotransmitter and neuropeptide content provides a wealth of opportunity for identifying new discrete circuits and signaling mechanisms that drive anxiety and fear behavior. Exciting recent discoveries have highlighted how discrete outputs of the BNST can produce opposing anxiety responses (Kim et al., 2013; Jennings, Sparta, et al., 2013), thus implicating the importance of these smaller projection-defined subpopulations of cells as targets for mediating particular affective states. These landmark studies used a combination of transgenic mouse lines with viral delivery of light-sensitive opsins to drive discrete projections of genetically defined cell types to identify select pathways that mediate the behavioral and autonomic components of anxiety. Interestingly, broad inhibition of the BNST with glutamate receptor antagonists reduced anxiety-like behavior, but optical stimulation and activation of multiple discrete BNST outputs reduced anxiety-like behavior. Further, optical stimulation of the BNST projection to the PBN had no effect on anxiety behavior, but did suppress respiration rate (Kim et al., 2013). Similarly, optical stimulation of GABAergic projections to the LH and VTA reduced anxiety-like behavior (Jennings, Rizzi, et al., 2013; Jennings, Sparta, et al., 2013; Kim et al., 2013). These findings are critical to untangling the behavioral and

emotional components modulated by extended amygdala circuitry. In this dissertation, I used a combination of optogenetic and chemogenetic strategies to identify both anatomical pathways and intracellular G protein-mediated signaling pathways that contribute to anxiety and fear within the BNST.

Discerning the circuits and cell types that drive various types of behavior will hopefully lead to the identification of cell populations to target for therapeutic manipulations. Although efforts are being made to use viral introduction of DREADDs in humans and non-human primates, we can still benefit from identifying endogenous GPCRs coupled to identified signaling pathways of interest. We touch on this approach in Chapter 2 where we used identification of a GPCR pathway in a genetically defined population of cells within the BNST to discern a potential target that may affect anxiety behavior. Further characterization of this cell type yielded endogenous receptors coupled to the same GPCR-mediated signaling pathway that affected anxiety, thus providing novel targets within the BNST for modulation of the anxious state. Building upon this, we also identify brain-wide changes in metabolic activity associated with this signaling pathway, leading to a possible measureable endophenotype that could be a predictor of activity in the brain during anxiety. Manipulations of one aspect of a circuit will produce changes in activity downstream, so we hope that metabolic mapping of network function can produce both a marker of the disease state and a readout of whether treatments are returning a network state to normal levels of activity.

It is important to also consider that modulation of circuits in rodents during the naïve state, by pharmacological, optogenetic, or chemogenetic means, is only one piece of the emotional circuit puzzle. As stress exposure and withdrawal from drugs of abuse is known to change activity of forebrain and limbic structures, we also need to identify how manipulation of circuits and signaling pathways under anxiety- and fear-inducing conditions affects subsequent behavior following stress or withdrawal. We consider this in Chapter 3 in a study in which we identify that activation of Gi-coupled signaling in BNST CRF neurons during fear learning does not affect subsequent fear expression, but is sufficient to block SSRI-induced enhancement of fear. This last point is of particular relevance for the potential therapeutic prevention of disorders such as PTSD, in which a devastatingly stressful event produces long-lasting changes in emotional circuitry that result in debilitating and exaggerated responses to previously innocuous environmental or internal stimuli. Perhaps targeted inhibition of cells identified to be critical in

producing the long-lasting changes in circuit function could blunt or prevent this development. Here we explore and discuss this possibility.

1.8 Figures

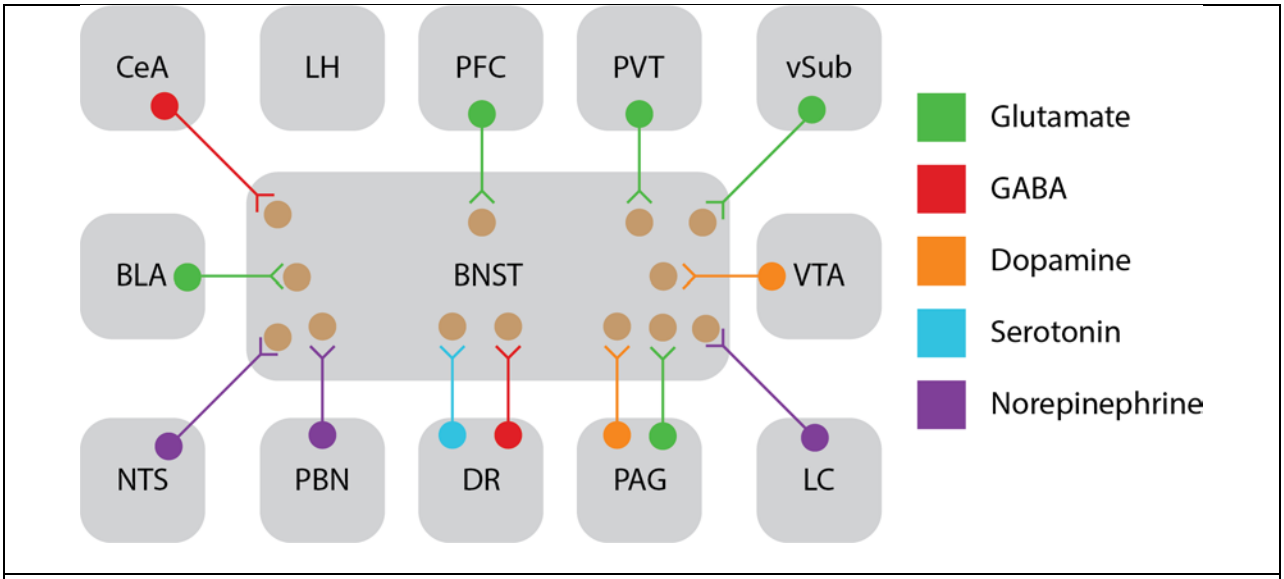

Figure 1.1: Synaptic inputs to the BNST. The BNST receives an array of inputs from the throughout the brain. Colors indicate known types of neurotransmitter inputs. CeA, central nucleus of the amygdala; LH, lateral hypothalamus; PFC, prefrontal cortex; PVT, paraventricular nucleus of the thalamus; VTA, ventral tegmental area; LC, locus coeruleus; PAG, periaqueductal gray; DR, dorsal raphe nucleus; PBN, parabrachial nucleus; NTS, nucleus of the solitary tract; BLA, basolateral amygdala.

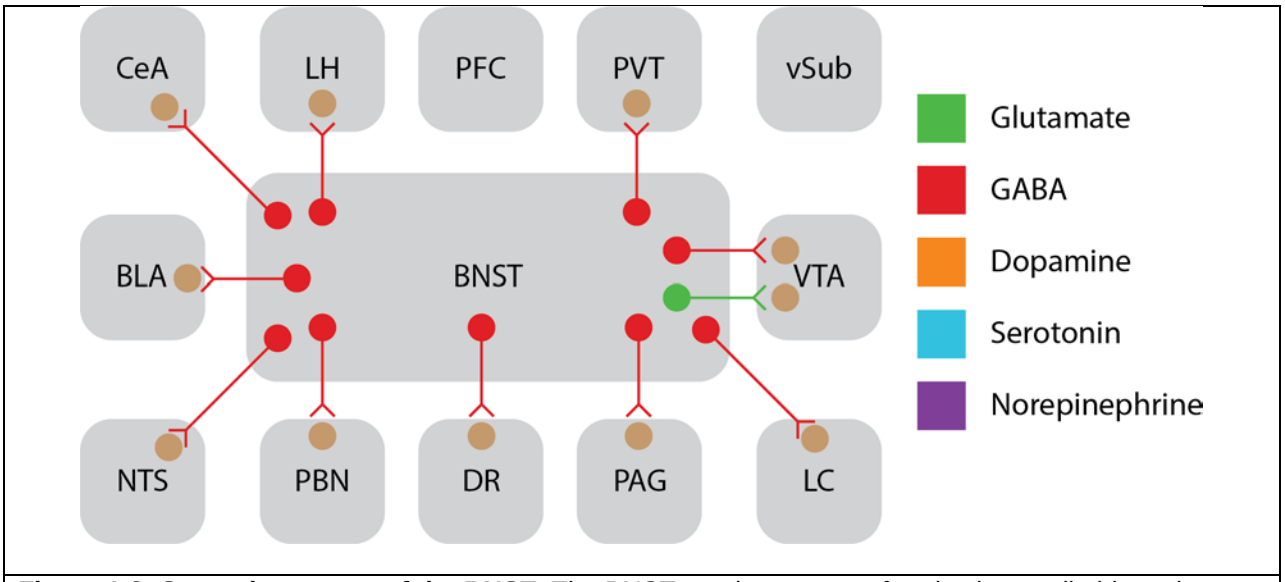

Figure 1.2: Synaptic outputs of the BNST. The BNST sends an array of projections to limbic and hindbrain structures. Colors indicate known types of neurotransmitter output. CeA, central nucleus of the amygdala; LH, lateral hypothalamus; PFC, prefrontal cortex; PVT, paraventricular nucleus of the thalamus; VTA, ventral tegmental area; LC, locus coeruleus; PAG, periaqueductal gray; DR, dorsal raphe nucleus; PBN, parabrachial nucleus; NTS, nucleus of the solitary tract; BLA, basolateral amygdala.

CHAPTER 2 CHEMOGENETIC MODULATION OF Gq-COUPLED GPCR SIGNALING IN THE BNST INDUCES ANXIETY-RELATED BEHAVIOR[1]

2.1 Historical Context

Anxiety disorders, including generalized anxiety disorder (GAD), panic disorder, and social anxiety disorder, are prevalent neuropsychiatric conditions. Despite decades of research and the availability of diverse pharmacological treatment options, few treatments for these disorders remain effective long-term (Griebel & Holmes, 2013; Kessler, 2005; Kessler et al., 2007; Insel, 2012). In order to develop better therapies, it is important to understand the complex neural networks spanning cortical, limbic, and hindbrain nuclei that control both the behavioral and autonomic components of anxiety states (Calhoon & Tye, 2015). One brain region that has long been associated with modulating such states is the bed nucleus of the stria terminalis (BNST; recently reviewed in (Daniel & Rainnie, 2015; Lebow & Chen, 2016)). This ventral forebrain structure has a large population of GABAergic neurons and has reciprocal projections with numerous limbic and hindbrain nuclei (Sun & Cassell, 1993; Dong & Swanson, 2004a; Dong & Swanson, 2006a). Such diverse connectivity allows the BNST to function as a critical relay center for regulating a range of emotional and motivational processes. In humans, the BNST has elevated activity during anticipatory threat, and in rodents, broad inhibition of the BNST reduces anxiety-like behavior (Straube et al., 2007; Mobbs et al., 2010; Dean Mobbs et al., 2013; Somerville et al., 2010; Kim et al., 2013). However, optogenetic activation of discrete BNST outputs can also reduce anxiety-like behavior, highlighting how BNST stimulation can have opposing regulatory processes (Kim et al., 2013; Jennings, Sparta, et al., 2013). Increased activity within the BNST is associated with elevated anxiety states in both humans (Straube et al., 2007; Somerville et al., 2010; Yassa et al., 2012) and non-human primates (A. S. Fox et al., 2008; Kalin et al., 2005), while lesioning or pharmacological inhibition of the BNST reduces anxiety-like behavior (Lee & Davis, 1997; Walker & M Davis, 1997; Waddell et al., 2006;

[1] This chapter was previously published as an article in *Molecular Psychiatry*. Some minor adjustments have been made to accommodate dissertation formatting. The original citation is as follows: Mazzone, CM, et al., "Acute engagement of Gq-mediated signaling in the bed nucleus of the stria terminalis induces anxiety-like behavior." *Molecular Psychiatry*. In press.

Kim et al., 2013). Thus, the BNST is an important nucleus in the regulation of anxiety and studies aimed at better understanding the role of the BNST in anxiety are important for the development of more effective therapeutics.

In addition to complex anatomical connectivity, the BNST expresses an array of ionotropic channels and metabotropic G-protein coupled receptors (GPCRs) for both neurotransmitter and neuropeptidergic systems (Kash, 2012; Kash et al., 2015). Pharmacological and *ex vivo* slice electrophysiology studies have demonstrated that local infusion of GPCR ligands into the BNST can produce changes in anxiety-like behavior and synaptic function, but the broader effects of downstream network activity remain unknown (Khoshbouei et al., 2002; Walker, Miles, et al., 2009; Walker, Yang, et al., 2009; Hammack, Cheung, et al., 2009; Levita et al., 2004; J. H. Fox et al., 2008). Treatment with an α1-receptor antagonist, for example, can blunt stress-induced increases in anxiety, and restraint stress elevates norepinephrine release in the BNST (Khoshbouei et al., 2002). 5-HT_{2c} knockout (KO) mice show blunted anxiety and reduced c-fos induction in corticotropin-releasing factor (CRF)-expressing cells of the BNST following an anxiogenic stimulus (Heisler et al., 2007). While these studies highlight the importance of GPCR-coupled signaling and anxiety within the BNST, they are unable to determine whether the effects are driven by pre- or postsynaptic mechanisms. Here we provide the first characterization of the behavioral and network consequences following activation of G_q-mediated signaling within BNST VGAT-expressing neurons using chemogenetic approaches. Further, we identify endogenous G_q-coupled GPCR expression in BNST VGAT neurons at the single cell level that may provide useful targets for modulating anxiety-like states.

2.2 Methods

Mice: All animals (>8 weeks old) were group housed on a 12 hour light cycle (lights on at 7 a.m.) with *ad libitum* access to rodent chow and water, unless described otherwise. VGAT-*ires*-Cre (VGAT-Cre) mice were provided by Dr. Bradford Lowell (Harvard University) and have been described previously (Vong et al., 2011). To isolate BNST VGAT neurons for single-cell qPCR and whole-cell patch clamp electrophysiology, VGAT-Cre mice were crossed with a *Rosa26*-floxed-stop-L10-GFP reporter line (VGAT-L10)(Krashes et al., 2014). Only male mice were used for behavioral, DREAMM, and single-cell profiling experiments. Male and female mice were used for electrophysiological recordings and *in situ*

hybridization experiments as described below. All procedures were conducted in accordance with the National Institutes of Health guidelines for animal research and with the approval of the Institutional Animal Care and Use Committee at the University of North Carolina at Chapel Hill. For acoustic startle assessment, eight week old, male C57BL/6J mice (n = 16) were obtained from Jackson Laboratories in Bar Harbor, Maine. Mice were housed in groups of four in standard acrylic cages (24 cm (W) × 45cm (D) × 20cm (H)) located in an Association for Assessment and Accreditation of Laboratory Animal Care (AAALAC) approved conventional animal facility. Mice were maintained on a 12 h light/dark cycle (lights on at 07:00 h) with food and water available at all times. All procedures were approved by the University of Vermont Animal Care and Use Committee.

Viruses and tracers: All AAV viruses were produced by the Gene Therapy Center Vector Core at the University of North Carolina at Chapel Hill and had titers of $>10^{12}$ genome copies/mL. For chemogenetic manipulations, mice were bilaterally injected with 0.4-0.5 µl of rAAV8-hsyn-DIO-mCherry, rAAV8-hsyn-DIO-hM3Dq-mCherry, rAAV8-hsyn-DIO-hM4Di-mCherry, or rAAV8-hsyn-DIO-rM3Ds.

Stereotaxic injections: Adult mice (>8 weeks) were deeply anesthetized with 5% isoflurane (vol/vol) in oxygen and placed into a stereotactic frame (Kopf Instruments) while on a heated pad. Sedation was maintained at 1.5-2.5% isoflurane during surgery. Following 3 alternating swabs with betadine and 70% ethanol, an incision was made down the midline of the scalp, a burr hole was drilled above the target regions, and viruses were microinjected using a 1 µl Neuros Hamilton syringe at a rate of 100 nl/min. After infusion, the needle was left in place for at least an additional 5 minutes to allow for diffusion of the virus before being slowly withdrawn. Injection coordinates for the BNST were (in mm: midline, Bregma, dorsal surface): ±0.9 – 1.10, 0.30, -4.35 (Paxinos & Franklin, 2008). Following surgery, all mice were returned to group housing. Mice were allowed to recover for at least 3 weeks prior to the start of experiments.

BNST cannulation: Cannulae were obtained from Plastics One (Roanoke, VA). The cannulae used had a 22 gauge inner diameter and extended 5 mm below the 4mm pedestal. Injection cannulae had an inner diameter of 28 gauge and were 9.5 mm long and projected 0.5 mm beyond the guide cannula. Mice were

anesthetized using 2% Isoflurane and oxygen and then placed into a stereotaxic instrument (Steolting, Wood Dale, Illinois). The scalps of the mice were shaved and then scrubbed in alternate with 9% betadine and 95% ethyl alcohol. The scalp was opened using a cut along the midline and then the skull was lightly scraped with the edge of a scalpel blade to remove fascia. A small burr hole was drilled in the skull where each cannula was lowered. Coordinates were 0.3 mm anterior to Bregma, 2.6 mm lateral, and 4.2 mm ventral. The cannulae were lowered at a 20 degree angle in order to avoid hitting the ventricles that lie dorsal and medial to the BNST. The same procedure was done for both the left and right BNST. After lowering both cannulae, they were affixed to the skull using glue (Loctite 454, Locktite, Westlake, OH) and a glue hardening accelerator (Loctite 7542). Mice were given 0.05mg/kg of buprenorphine prior to being removed from the sterotaxic apparatus. The mice were allowed to recover under a heat lamp prior to being returned to their home cage and the colony room. Mice were monitored daily and received 3 more doses of buprenorphine to help alleviate pain associated with the surgical procedure.

Drugs: Tetrodotoxin (TTX) and picrotoxin were purchased from Abcam, while U73122, SR 141716A, and meta-Chlorophenylpiperazine (mCPP) were purchased from Tocris. Clozapine *N*-oxide (CNO) was generously provided by Dr. Bryan Roth (University of North Carolina).

Electrophysiology: Mice were decapitated following deep isoflurane anesthesia, then brains were extracted and placed in ice-cold sucrose artificial cerebrospinal fluid (aCSF) containing (in mM) 194 sucrose, 20 NaCl, 4.4 KCl, 2 $CaCl_2$, 1 $MgCl_2$, 1.2 NaH_2PO_4, 10.0 glucose, and 26.0 $NaHCO_3$ saturated with 95% O_2/5% CO_2. Coronal sections of the BNST were sliced at 300 µm on a Leica 1200S vibratome at 0.07 mm/s. Slices were incubated in a heated holding chamber containing normal, oxygenated aCSF [(in mM): 124 NaCl, 4.4 KCl, 2 $CaCl_2$, 1.2 $MgSO_4$, 1 NaH_2PO_4, 10.0 glucose, and 26.0 $NaHCO_3$] maintained at 32 ± 1˚C for at least 1 hour before recording. Slices were then transferred to a recording chamber (Warner Instruments), submerged in normal, oxygenated aCSF and maintained at 28-30˚C with a flow rate of 2 ml/min and allowed to incubate for 30 minutes. Female mice were used for recordings validating Gq DREADD function and Long-term depression (LTD) experiments, while male and female mice were used to verify hM4Di-induced hyperpolarization in response to CNO. Neurons of the BNST were visualized using infrared differential interference contrast (DIC) video-enhanced microscopy

(Olympus) and DREADD-expressing cells were identified by mCherry fluorescence. Whole-cell patch clamp recordings were made in current clamp mode with a potassium gluconate-based intracellular solution [(in mM): 135 K-gluconate, 5 NaCl, 2 MgCl2, 10 HEPES, 0.6 EGTA, 4 Na_2ATP, 0.4 Na_2GTP, pH 7.3, 289–292mOsmol]. To record CNO-induced depolarization of G_q-DREADD expressing VGAT neurons in the presence of 0.5 µM TTX, 10 µM CNO was bath applied for 5 minutes after a four-minute baseline. The CNO-induced depolarization was calculated as the difference between the resting membrane potential (RMP) during the last 2 minutes of CNO application and the RMP 2 minutes before CNO reached the bath. To assess the effects of phospholipase C (PLC) inhibition on CNO-induced depolarization, 10 µM U73122 was present in the bath throughout recordings. Similar recordings were obtained in G_i-DREADD expressing cells without TTX present in the bath. In G_i-DREADD-expressing cells, the rheobase, which was defined as the minimal amount of current required to elicit an action potential using a current ramp, was obtained using the potassium gluconate internal described above both before and following 5 minutes of bath application of 10 µM CNO. One cell was identified as an outlier by the Grubbs' test (alpha set to 0.01) and was excluded from the rheobase dataset. To assess the effects of G_q-DREADD activation in BNST VGAT neurons on LTD, whole cell voltage clamp recordings were obtained using a cesium-gluconate internal [(in mM): 117 Cs-gluconate, 20 HEPES, 15.2 EGTA, 83 TEA, 40 MgCl2, 200 Na_2ATP, 20 Na_2GTP, pH 7.31, 292 mOsmol] with the cell clamped at -70 mV throughout the recording period. All experiments were performed with 25 µM picrotoxin, or picrotoxin plus 5 µM SR 141716A, present in the bath. To record evoked excitatory postsynaptic currents (EPSCs), a bipolar Ni-chrome stimulated electrode was placed in the dorsal BNST and dorsal to the recorded neuron. EPSCs were evoked at a frequency of 0.167 Hz using either voltage or current pulses. Evoked experiments were analyzed in Clampfit 10.5 (Molecular Devices Sunnyvale, CA). All evoked responses were normalized to the average EPSC amplitude during the first 50 sweeps (5 mins) before CNO application. Each data point consists of a 60 second (6 sweep) average of evoked responses. In all experiments, signals were digitized at 10-20 kHz and filtered at 3 kHz using a Multiclamp 700B amplifier.

Behavioral Assays: Mice used for behavioral studies were habituated to handling for two days beginning three days prior to the first behavioral test. All behavioral testing was done during the light cycle, and there was at least 48 hours between test sessions. For chemogenetic manipulations, mice were

transported to a holding cabinet adjacent to the behavioral testing room to habituate for at least 30 minutes before being pretreated with CNO (3.0 mg/kg, i.p.) unless stated otherwise. All behavior testing began 30 minutes after CNO treatment. Experimenters were blind to mouse treatment during testing. Equipment was cleaned with a damp cloth between mouse trials. Sessions were video recorded and analyzed using EthoVision software (Noldus Information Technologies). *Elevated Plus Maze:* Mice were placed into the center of an elevated plus maze and allowed to explore for a 5 minute session. Light levels in the open arms were ~14 lux. The probability of an open arm entry was calculated as the number of open arm entries divided by the total number of arm entries (open + closed). *Open Field:* Mice were placed into the corner of a white Plexiglas open field arena (20 x 20 x 10 cm) and allowed to freely explore for 30 minutes. The center of the open field was defined as the central 25% of the arena. Light levels were ~14 lux. In one behavioral cohort, 5 mice were excluded due to a malfunctioning camera in one of the boxes (1 mCherry, 3 G_q, 1 G_i). *Light-Dark:* Mice were placed into the dark side of a two-compartment box containing a dark side (black walls with lid) and a light side (clear Plexiglas walls, no lid) and were allowed to freely explore for 15 minutes. The two sides were connected by a central small opening in the walls of the enclosed side. Light levels in the light side were ~300 lux in the center. *Acoustic startle:* mCPP HCl (Tocris, Ellisville, MO) was mixed fresh on the morning that behavioral testing took place. mCPP was mixed with artificial cerebral spinal fluid (aCSF) at 1 µg/.5 µl. Animals were randomly assigned to receive mCPP or vehicle with the flip of a coin. Mice received either vehicle or mCPP infusions using the injection cannula connected with polyethelene tubing to a 10ul micro syringe (Hamilton, Reno, NV). Infusions were performed with a mechanical infusion pump (KD Scientific, Holliston, MA) at a rate of 0.25ul/minute for 2 minutes for a total volume of .5ul per side. The injector cannulae were left in place for an additional 2 minutes to aid in diffusion of the drug into the target area. Behavioral testing took place immediately after infusion. The startle tests were conducted in eight sound attenuating cubicles measuring 58 cm (W) × 32 cm (D) × 55 cm (H). Each cubicle was lined with black, sound absorbing foam with no internal source of light. Each cubicle contained a stabilimeter device consisting of a load cell platform onto which the behavioral chamber was mounted (MED-ASR-PRO1, Med-Associates, Georgia, VT). The chamber was constructed from clear acrylic, cylindrical in shape, 12.5 cm in length, with an inner diameter of 5 cm. The floor of the chamber consisted of a removable grid

composed of 6 steel rods 3.2 mm in diameter, and spaced 6.4 mm apart. Startle responses were transduced by the load cell, amplified, and digitized over a range of 0–4096 units. Startle amplitude was defined as the largest peak to trough value within 100 ms after the onset of the startle stimulus. After a five-minute acclimation period, mice were presented with the first of 30 startle stimulus alone trials. The startle stimulus was comprised of white noise bursts lasting for 20 milliseconds. Ten stimuli of each intensity level (95, 100, and 105 dB) were presented in a pseudo-random order (the constraint being that each intensity occur within each block of 3 trials) with an inter-trial interval (ITI) of 60 s. Data collection and the control and sequencing of all stimuli were controlled by Med-Associates startle reflex hardware and software. Raw startle scores were converted into a percent change score based on the average startle response in vehicle treated mice.

Placement Verification and Histology: All mice used for behavioral and anatomical tracing experiments were anesthetized with Avertin and transcardially perfused with 30 ml of ice-cold 0.01M PBS followed by 30 ml of ice-cold 4% paraformaldehyde (PFA) in phosphate buffered saline (PBS). Brains were extracted and stored in 4% PFA for 24 hours at 4°C before being rinsed twice with PBS and stored in 30% sucrose/PBS until the brains sank. 45 µm slices were obtained on a Leica VT1000S and stored in 50/50 PBS/Glycerol at -20°C. DREADD-containing sections were mounted on slides, allowed to dry, coverslipped with VectaShield (Vector Labs, Burlingame, CA), and stored in the dark at 4°C. Viral injection sites were verified on either a Zeiss Axio Zoom.V16 microscope or Zeiss 800 confocal microscope. For the acoustic startle study, mice were euthanized using pentobarbital (SleepAway, Fort Dodge Drug Company, Fort Dodge, IA) and were immediately perfused transcardially using 0.9% saline followed by 10% neutral buffered formalin. Brains were saved in 10% neutral buffered formalin and coronal sections were obtained on a cryostat at 50-60um. Slices were stained with cresyl violet for cannula placement verification.

DREADD-Assisted Metabolic Mapping (DREAMM): Male VGAT-Cre mice expressing a DIO-hM3Dq-mCherry in the BNST were fasted overnight. The next morning mice were injected with either vehicle or CNO (3 mg/kg, i.p.) and 5 minutes later were injected with [^{18}F]fluorodeoxyglucose (FDG) (~250 µCi, i.p.) and placed individually in a mouse home cage (each mouse was scanned twice). 35-40 minutes after the

FDG injection mice were anesthetized with 1.5% isoflurane, placed in a prone position on the bed of an Inveon microPET scanner (Siemens Medical Solutions, Malvern, PA) and scanned using a 20 min static acquisition protocol. These time points were chosen to align with those used for behavioral testing. All scans were reconstructed using the *maximum a posteriori* (MAP) algorithm. After reconstruction, images were spatially processed and normalized using the Pixel-wise Modeling software suite (PMOD) (PMOD Inc., Zurich, Switzerland) to a mouse brain MRI template (Michaelides et al., 2010) . Normalized scans were then analyzed using statistical parametric mapping (SPM) as previously described (Urban et al., 2015) . All SPM contrasts consisted of paired t-tests within each group (e.g. VEH>CNO, VEH<CNO) and were evaluated at p=0.01. Only clusters of at least 100 contiguous voxels were reported.

FACS and Single-Cell qPCR: *Single-cell suspension preparation*: On two separate experimental runs, brains from one adult male VGAT-*ires*-Cre:*Rosa26*-floxed-stop-L10-GFP and one adult male mouse lacking either Cre or L10-GFP expression, were extracted following deep isoflurane anesthesia. The brains were blocked on ice to obtain a 1 mm thick coronal section containing BNST. The BNST was then isolated from the rest of the section using razor blades and was then finely minced with razor blades before being transferred to 1 ml of ice-cold Hibernate A (HA-if, Brain Bits). The samples were centrifuged for 2 minutes at 110 x g at 4°C, the supernatant removed, and the pellets resuspended in 1 ml of Accutase (SCR005, Millipore) and triturated up and down 4 times before digesting the tissue for 1 hour at 4°C with end-over-end mixing. Following digestion, the tissue was centrifuged for 2 minutes at 960 x g at 4°C, the supernatant was removed, and the pellets were resuspended in 0.6 ml of ice-cold Hibernate A. The samples then underwent a series of trituration steps using fire-polished glass pipettes with successively smaller diameters (1.3, 0.8, and 0.4 mm) that consisted of triturating up and down 10 times followed by placing the tube on ice for 2 minutes to allow undissociated debris to settle before collecting the supernatants and resuspending the undissociated debris with 0.6 ml of Hibernate A. The supernatants were pooled after each trituration step. Three additional trituration steps were carried out with a 0.4 mm diameter glass pipette resulting in pooled samples of dissociated cells with a volume of ~3.6 ml. These samples were then filtered with 100 µm and 40 µm cell strainers (Falcon brand, BD Biosciences) before being used for FACS. *Single-cell isolation and qPCR:* Cells expressing VGAT-*ires*-Cre:*Rosa26*-floxed-stop-L10a-GFP were isolated by Fluorescence Activated Cell Sorting (FACS) using a

Sony SH800 FACS instrument (Sony Biotechnology, San Jose, CA). Multimers were excluded using a Forward-Scatter Area (FSC-A) versus Forward-Scatter Height (FSC-H) gating strategy. Dead cells were excluded using SYTOX Blue Live/Dead stain (S34857; Thermo-Fisher Scientific, USA). Gating windows were adjusted to only include events present in the GFP+ sample relative to the GFP- control brain. ~8-9,000 VGAT-*ires*-Cre:*Rosa26*-floxed-stop-L10a-GFP cells were sorted into 20 µl of Optimem with the apoptotic inhibitor Y-27632 (Cat. #S1049, Selleck Chemical) diluted to 1:1000. Eight µl of the cell suspension (~4000 cells) was added to 2 µl of C1 resuspension buffer (Fluidigm, South San Francisco). Five µl of this cell suspension was added to a 17-25 µm Fluidigm C1 Integrated Fluidics Chip (IFC). Specific target amplification (STA) was performed on the C1 instrument according to manufacturer's specifications. The STA for each cell was interrogated for target gene (See Table 1 for Taqman probe information) expression levels by qPCR on a 192.24 IFC using the Fluidigm Biomark HD instrument according to that standard Fluidigm protocols.

Double Fluorescence *in situ* hybridization (FISH): For validation of the VGAT-Cre line and comparison of VGAT and GPCR cellular colocalization, mice were anesthetized using isoflurane, rapidly decapitated, and brains rapidly extracted. Female VGAT-Cre mice were used for *Slc32a1/Cre* comparisons, while male C57Bl/6 mice were used for comparisons of *Slc32a1* and GPCR expression. Immediately after removal, brains were placed on a square of aluminum foil on dry ice to freeze. Brains were then placed in a -80°C freezer for no more than 1 week before slicing. 12 µm slices containing the BNST were obtained on a Leica CM3050S cryostat (Germany) and placed directly on coverslips. FISH was performed using the Affymetrix ViewRNA 2-Plex Tissue Assay Kit with custom probes for *Slc32a1* (VGAT), *Grm5*, *Chrm1*, *Htr2c*, *Adra1a*, *Adra1b*, and *Cre* designed by Affymetrix (Santa Clara, CA). Slides were coverslipped with SouthernBiotech DAPI Fluoromount-G. (Birmingham, AL). 3x5 tiled z stack (8 optical sections comprising 10.57 µm total) were obtained on a Zeiss 800 confocal microscope. All images were preprocessed with stitching and maximum intensity projection. For quantification of *Slc32a1* and GPCR probe colocalization, 8-9 BNST images from 3 mice were hand counted using the cell counter plugin in FIJI (ImageJ) by a scorer blinded to the probes used. For validation of the VGAT-Cre line, 3 BNST images from 3 mice were analyzed. For all studies, cells were classified into three groups: probe 1+, probe 2+, or probe 1 and 2 +. Only cells positive for a probe were considered.

Group assignment: No specific method of randomization was used to assign groups. Whenever possible, mice from the same litter were randomly split across treatments to minimize differences in age.

Inclusion/exclusion criteria: Pre-established criteria for excluding mice or cells from analysis included 1) missed injections or a lack of viral expression, 2) equipment failures during testing, 3) statistical outliers as determined by Grubbs' test. Specific instances of exclusion are described above.

Sample size: Sample sizes were based on the expected variances from previous behavioral, electrophysiological, and *in situ* hybridization experiments. For behavioral experiments, we targeted 6-10 mice per group. For electrophysiological experiments, we aimed for 5-10 cells from 3-6 mice. The one exception was 4 cells from 2 mice used for testing G_q-induced depolarization in the presence of the PLC inhibitor U73122.

Statistics: Data are presented as means ± SEM. For comparisons with only two groups, *p* values were calculated using two-tailed paired or unpaired *t*-tests as described in the figure legends, unless specified otherwise. In cases where the data were not normally distributed, a Mann-Whitney test was performed as listed in the figure legends. Comparisons across more than two groups were made using a one-way Analysis of Variance (ANOVA). When an ANOVA was used, data met the assumptions of equality in variance. A Tukey's posttest was performed following significance with an ANOVA. Differences were considered significant at *p* values below 0.05. All data were analyzed with GraphPad Prism 6 software. Figures were assembled using Adobe Illustrator.

2.3 Results

Selectively targeting GABAergic neurons in the BNST

The BNST consists primarily of GABAergic neurons (Sun & Cassell, 1993), but also contains a population of vesicular glutamate transporter 2 (vGlut2)-and vesicular glutamate transporter 3 (vGlut3)-expressing glutamatergic neurons in the ventral BNST (vBNST) (Hur & Zaborszky, 2005; Poulin et al., 2009; Kudo et al., 2012). As prior reports show that stimulation of glutamatergic and GABAergic BNST outputs can evoke opposing behavioral states, we selectively targeted GABAergic BNST neurons using

stereotaxic delivery of adeno-associated viruses (AAVs) encoding Cre-inducible DREADDs to the BNST of VGAT-*ires*-Cre (VGAT-Cre) mice (Jennings, Sparta, et al., 2013) (Figure 2.1a). Injection of these viral constructs encoding a control mCherry fluorophore, hM3Dq-mCherry, or hM4Di-mCherry produced robust expression in both the dorsal and ventral regions of the BNST (Figure 2.1b). Importantly, we did not observe DREADD expression in Cre-negative littermates injected with the Cre-inducible hM3Dq (see Figure 2.5 f). Additionally, we validated that Cre expression was limited to VGAT-expressing cells using *in situ* hybridization and observed that 99.1% of cells expressing *Cre* were positive for *Slc32a1* (VGAT) mRNA (Figure 2.2). These data demonstrate that we were able to anatomically isolate BNST GABAergic cells for chemogenetic manipulations. To confirm functional DREADD expression, we recorded from hM3Dq-expressing BNST neurons using *ex vivo* whole cell slice electrophysiology (Figure 2.1c). Bath application of 10 µM CNO in the presence of TTX produced a 2.12 ± 0.35 mV depolarization in hM3Dq-mCherry expressing BNST VGAT neurons (Figure 2.1 d-e), consistent with previous reports (Krashes et al., 2011; Alexander et al., 2009; Yiu et al., 2014). Bath application of the PLC inhibitor U73122 (10 µM) significantly reduced the CNO-induced depolarization (Figure 2.1 d-e). As PLC is a known downstream target of G_q activation, these data highlight that CNO-induced depolarization following activation of hM3Dq receptors involve canonical G_q-mediated signaling pathways. In the absence of TTX, 50% (3/6) of hM3Dq expressing neurons began firing action potentials within 5 minutes of 10 µM CNO application, while the remaining neurons showed an average depolarization of 1.69 ± 0.24 mV (data not shown). Activation of G_q-coupled receptors can also result in an LTD of postsynaptic excitatory currents (Grueter et al., 2006; McElligott et al., 2010; McElligott & Winder, 2008). To assess if activation of hM3Dq activity within BNST VGAT neurons is sufficient to produce LTD, we recorded electrically evoked EPSCs during and following bath application of 10 µM CNO. There was a rapid and sustained reduction in EPSC amplitude relative to baseline that persisted for at least 25 minutes after washout of CNO, which was not observed in cells from non-DREADD expressing mice (Figure 2.1 f-h). Furthermore, antagonism of the cannabinoid receptor 1 (CB_1R) with SR141716A (5 µM) blocked hM3Dq-induced LTD (Figure 2.1 f-h). In opposition to our observations with hM3Dq activation, stimulation of the hM4Di receptor was sufficient to induce a hyperpolarization and increase the amount of current required to elicit an action potential, thus indicating opposing actions of hM3Dq versus hM4Di signaling events (Figure 2.1 i-l).

Acute chemogenetic activation of BNST VGAT neurons induces anxiety-like behavior

To determine how engagement of G_q-coupled and G_i-coupled signaling in BNST VGAT neurons affects acute anxiety-like behavior, we injected Cre-inducible hM3Dq or hM4Di constructs into the BNST of VGAT-*ires*-Cre mice with a Cre-inducible mCherry used as a control. Mice were treated with CNO (3.0 mg/kg) 30 minutes before testing to allow time for DREADD-induced changes in activity (Figure 2.3 a). In the elevated plus maze (EPM, Figure 2.3 b), DREADD activation did not alter locomotor activity, but hM3Dq-expressing mice spent less time in the open arms and had a significantly reduced likelihood of entering an open arm. In the open field, neither the hM3Dq-expressing nor the hM4Di-expressing group showed changes in distance traveled (Figure 2.3 e, left), time spent in the center of the open field, or latency to enter the center of the open field (Figure 2.3 e, center and right, respectively). In the light-dark test, only the hM3Dq-expressing mice spent less time in the light compartment and made fewer entrances to the light side (Figure 2.3 f). Separately, we observed that acute activation of G_s-coupled signaling using the rM3Ds DREADD construct did not change anxiety in the same assays relative to mCherry controls (Figure 2.4). These results indicate that acute engagement of G_q-coupled, but neither G_i- nor G_s-coupled, signaling in BNST VGAT neurons is sufficient to generate an anxiety-like state in specific contexts.

Metabolic mapping of BNST VGAT hM3Dq-evoked activity reveals broad circuit engagement

The BNST sends projections to many structures involved with reward, anxiety, and the regulation of autonomic function (Dong & Swanson, 2004a; Kim et al., 2013). Injection of a Cre-inducible mCherry to the BNST of a VGAT-Cre mouse (Figure 2.5 a) showed direct projections of BNST VGAT fibers to these established regions, including the ventral tegmental area (VTA), locus coeruleus (LC), or parabrachial nucleus (PBN) (Figure 2.5 b). Given that we observed increases in anxiety-like behavior following the activation of G_q-coupled DREADDs in BNST VGAT neurons, we hypothesized that engagement of G_q-mediated signaling within BNST VGAT neurons could produce extensive changes in network dynamics in these downstream targets. We used DREADD-assisted metabolic mapping (DREAMM) (Michaelides et al., 2013; Anderson et al., 2013) to assess how activation of hM3Dq receptors in BNST VGAT neurons alters network activity. VGAT-Cre mice expressing DIO-hM3Dq in the BNST underwent two imaging

sessions following both vehicle and CNO pre-treatment. Five minutes after this pre-treatment, mice were injected with [^{18}F]fluorodeoxyglucose (FDG) before being anesthetized with isoflurane 25 minutes later and undergoing scanning (Figure 2.5 c). Mice with hM3Dq expression in the BNST (Figure 2.5 d) showed increases in FDG uptake in the BNST, ventral tegmental area (VTA), the locus coeruleus (LC), and the parabrachial nucleus (PBN) (Figure 2.5 e). Interestingly, we also observed elevated FDG uptake in the medial prefrontal cortex (mPFC), somatosensory cortex, and the central nucleus of the amygdala (CeA). Cre-negative littermates injected with a DIO-hM3Dq-mCherry lacked DREADD expression and showed negligible CNO-induced changes in FDG uptake in these regions (Figure 2.5 f-g).

Single-cell profiling of BNST VGAT cells highlights endogenous transcription of G_q-coupled GPCRs

As we observed robust changes in anxiety-like behavior following activation of G_q signaling in hM3Dq-expressing, but neither hM4Di- nor rM3Ds-expressing BNST VGAT neurons, we sought a greater understanding of the range of endogenous G_q-coupled receptors expressed within these cells. To isolate this population, the BNST was dissected from VGAT-Cre mice crossed with a flox-stop L10-EGFP reporter line. After creating a single-cell suspension, we isolated EGFP positive cells using fluorescence-activated cell sorting (FACS), then captured sorted cells using a Fluidigm C1 microfluidics chip. Captured cells were lysed and used for single-cell quantitative polymerase chain reaction (qPCR) with probes targeting Slc32a1 (VGAT), Map2 (a neuronal marker), Gad1 and Gad2 (GABA markers), and an array of G_q-coupled receptors (Figure 2.6 a-b). We were able to capture 163 cells from two samples collected from two individual mice run on two separate chips. Our *a priori* exclusion criteria removed from analysis any cells negative for VGAT (13/163), Map2 (0/163), or both Gad1 and Gad2 (1/163), resulting in 149 remaining cells. Interestingly, none of the excluded cells were positive for *Slc17a6* (vGlut2), and only 1 cell was positive for *Slc17a8* (vGlut3). Of the remaining 149 cells, we observed that greater than 50% of captured cells expressed transcripts for the G_q-coupled receptors *Grm5* (93.3%), *Ntsr2* (85.2%), *Chrm1* (71.1%), *Htr2c* (55.7%), or *Grm1* (50.3%) (Figure 2.6 c). We next used fluorescence *in situ* hybridization (FISH) to validate our qPCR findings by examining colocalization of mRNA for VGAT and various GPCRs (Figure 2.6 d-i). In agreement with the microfluidics approach, we observed a similar distribution of the

probed GPCRs in VGAT mRNA positive cells (Figure 2.6 i). Together, these results reveal an array of endogenous G_q-coupled receptors expressed within a genetically defined cell population in the BNST.

Infusion of a 5-HT_{2C}R agonist in the BNST increases anxiety-like behavior

Of the identified endogenous G_q-coupled receptors identified in BNST VGAT neurons, we selected the 5-HT_{2C}R for further analysis. The 5-HT system is known to be involved in anxiety and other affective-related behaviors, including within the BNST (Burghardt et al., 2004; Ravinder et al., 2013; Marcinkiewcz et al., 2016) . We implanted cannulae over the BNST and locally infused the 5-HT_{2C}R agonist mCPP immediately before testing in an acoustic startle task. Briefly, mice were placed on an accelerometer in a sound-attenuated chamber then presented with short noise burst. The magnitude of the startle served as an index of anxiety-like behavior. Bilateral infusion of mCPP (1 µg) into the BNST reliably increased acoustic startle responding relative to vehicle treated controls, thus indicating that activation of this G_q-coupled receptor leads to an increase in anxiety-like behavior (Figure 2.7).

2.4 Discussion

Existing pharmacological options for anxiety disorders remain ineffective in many patients and are often accompanied by undesirable side effects (Griebel & Holmes, 2013; Insel, 2012). Therapeutic difficulties arise, in part, due to the incomplete understanding of cell populations and brain circuits involved in mediating the desirable effects of drug treatments. Advances in optogenetic and chemogenetic techniques have revealed how stimulation of specific cell types within a structure can drive pathological behavior. However, many of these studies to date have focused on well-known anatomical pathways, and few have capitalized on discovery-based tools to identify novel endogenous modulators of function. Here we use a chemogenetic strategy to probe the role of GPCR signaling within a genetically defined cell population involved in anxiety-like behavior. We show that engagement of G_q-mediated signaling in BNST VGAT-expressing neurons induces anxiety-like behavior, while acute activation of both G_i and G_s signaling is insufficient to change anxiety-like responses in the assays tested. DREAMM imaging analysis following activation of G_q-DREADD signaling in BNST VGAT neurons showed enhanced activity in brain areas including the VTA, LC, and PBN. Furthermore, we used a discovery-based approach to identify potential novel GPCR regulators of this cell population. These results not only provide an anatomical framework for anxiety-like behavior, but a conceptual framework to parse out novel GPCR regulators of circuit function and behavior.

While hM3Dq-treated VGAT-Cre mice showed increased anxiety-like behavior, it is interesting that we did not see reductions in anxiety-like behavior following activation of hM4Di signaling in BNST VGAT neurons, particularly in light of previous work showing that pharmacological or optical inhibition of the BNST reduces anxiety behavior (Kim et al., 2013). At rest, the BNST has low levels of activity, and it is possible that the environment for our assays was not sufficient to engage BNST activity. As the hM4Di DREADD produced a hyperpolarizing inhibitory effect (Figure 2.1), suppressing activity of the BNST in these contexts may be insufficient to further reduce anxiety-like behavior. It would be interesting to repeat these experiments with activation of hM4Di DREADDs during a stressor that is known to increase BNST activity (foot shock, restraint, etc.) immediately before anxiety testing. Alternatively, similar experiments could be performed under brighter lighting conditions, as previous work has shown that open field exposure under bright lights (~600 lux) increases c-fos expression in the BNST (Heisler et al., 2007). We

also did not see changes in anxiety-like behavior following manipulation of G_s-coupled signaling. While both G_q- and G_s-coupled receptors have excitatory effects, a recent study identified that activation of G_q- and G_s-coupled DREADDs in agouti-related peptide (AgRP) neurons of the hypothalamus promoted feeding behavior through independent mechanisms, and that only G_s DREADD activation promoted AgRP release (Nakajima et al., 2016). As the BNST expresses an array of peptides, including corticotropin-releasing factor (CRF) and neuropeptide Y (NPY) that are known to produce opposing behavioral responses, it is possible that potential stimulation of peptide release in BNST VGAT neurons using the G_s-coupled DREADD occludes the effect of activation of these individual peptide receptors alone (Pleil et al., 2015; Kash & Winder, 2006; Valdez & Koob, 2004; Heilig, 2004; Heilig & Koob, 2007).

In addition to observing G_q-induced changes in behavior, our *ex vivo* slice electrophysiology recordings identified that activation of hM3Dq receptors in BNST VGAT neurons produced stimulatory depolarizing effects capable of increasing action potential firing that were accompanied by an LTD-like reduction of evoked EPSCs that persisted at least 25 minutes following washout of CNO. These changes are in agreement with previous studies demonstrating that bath application of agonists for the G_q-coupled α_1-adrenergic receptor or group I metabotropic glutamate receptors induces LTD in the BNST (Grueter et al., 2006; McElligott et al., 2010; McElligott & Winder, 2008). Similarly, in the CA1 region of the hippocampus, stimulation of G_q-coupled DREADDs alters long-term plasticity, including LTD and long-term potentiation (LTP) as assessed by field recordings (López et al., 2016). It is important to note, however, that while G_q-induced LTD has been observed in the BNST, we are currently unable to selectively antagonize the hM3Dq receptor following LTD induction to confirm the observed changes in synaptic plasticity are independent of CNO remaining bound to the DREADD receptor. Interestingly, we observed that the hM3Dq-induced reductions in EPSC amplitude involved CB_1R-dependent activity, in agreement with previous long-term plasticity reports indicating CB_1R-dependent reductions in evoked EPSC amplitude in the BNST (Grueter et al., 2006; Glangetas et al., 2013).

Our results from DREAMM analysis point to changes in metabolic activity throughout brain regions previously associated with anxiety pathology, including the mPFC, CeA, VTA, PBN, and the somatosensory cortex (Calhoon & Tye, 2015; Sehlmeyer et al., 2009; Nagai et al., 2007; Shackman & Fox, 2016; Gungor & Paré, 2016). Of note, we observed no reductions in regional metabolic activity

following CNO treatment. Other studies assessing brain glucose metabolism during periods of anxiety have also observed enhanced metabolic activity in subcortical and limbic regions across species including rats, monkeys, and humans (A. S. Fox et al., 2008; Shackman et al., 2013; Awwad et al., 2015; M. L. Liu et al., 2012). Importantly, FDG uptake represents increased glucose uptake and would therefore also be observed in active presynaptic terminals (Michaelides et al., 2013). Therefore, the exclusive increase in activity may reflect both enhanced presynaptic activity of BNST GABAergic afferents and increased local activity resulting from polysynaptic disinhibition. In agreement with this, previous work has shown that GABAergic BNST projections to the VTA innervate GABAergic VTA neurons (Jennings, Sparta, et al., 2013). However, the BNST to VTA projection is unlikely to account for the anxiogenic phenotype reported here as that study demonstrated that optogenetic stimulation results in anxiolysis. Nonetheless, given that stimulation of G_q-mediated signaling in BNST VGAT neurons was sufficient to induce anxiety, the observed changes in metabolic activity throughout the brain may highlight a potential biomarker for pathological anxiety.

While the results reported here reflect acute activation of BNST VGAT neurons and corresponding increases in anxiety, changes in BNST neuronal activity have been observed under other models of pathological anxiety. For example, we recently found that BNST neurons exhibited increased excitability following chronic alcohol exposure, and that elevated BNST excitability correlated with increased anxiety-like behavior (Pleil et al., 2016). Moreover, we previously found that the increase in excitability was associated with excessive 5-HT_{2C}R mediated signaling (Marcinkiewcz et al., 2015), and here we identify that an agonist of 5-HT_{2C}R in the BNST increases anxiety-like startle responding. The approach outlined in this study provides a framework for identifying GPCRs that may be differentially altered during anxiety states. Additionally, the application of whole brain imaging using these genetic approaches provides a robust and reproducible approach for connecting cellular signaling events to broad patterns of activity. Identification of brain-wide network activity patterns is especially important as this provides a point of translation for human studies. For example, the new Research Domain Criteria (RDoC) system proposed by the National Institute of Mental Health as a means for understanding brain disorders, suggests that identifying the circuit elements associated with specific endophenotypes across multiple disorders can provide insight into treatment. One such RDoC construct is potential threat or

anxiety. Our work highlights a whole brain metabolic map that could potentially serve as a biomarker for heterogeneous populations of patients suffering from conditions co-morbid with anxiety disorders and identifies potential receptor targets that may drive this endophenotype. Our results presented here in the naive state lay the foundation for future work to assess how the development of pathological anxiety states, such as anxiety associated with withdrawal from chronic alcohol exposure, changes GPCR expression patterns in BNST VGAT neuron and correspondingly changes metabolic brain-wide activity patterns.

2.5 Figures

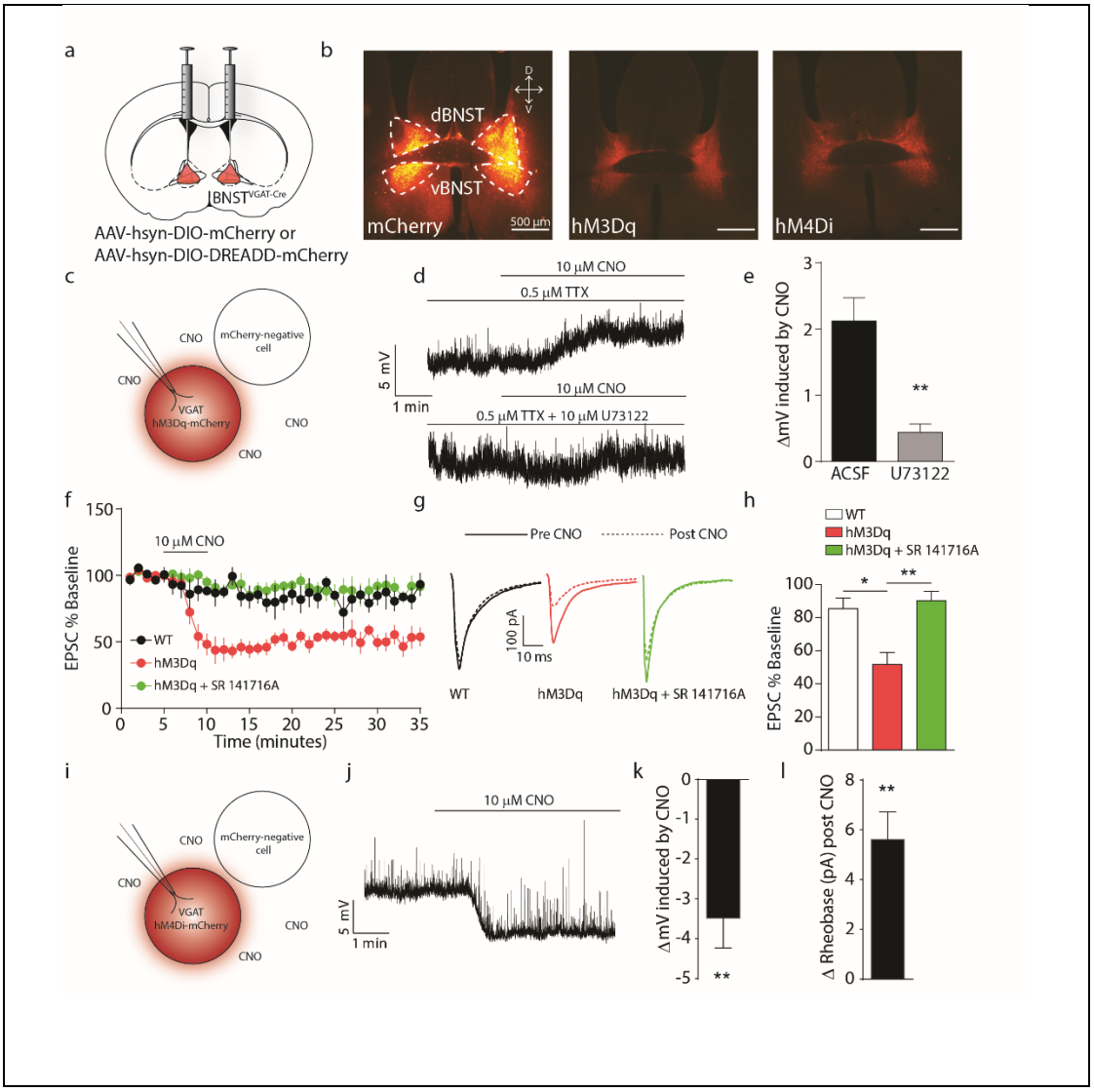
a
BNST
VGAT-Cre
AAV-hsyn-DIO-mCherry or
AAV-hsyn-DIO-DREADD-mCherry
b
dBNST
vBNST
mCherry
500 µm
hM3Dq
hM4Di
c
CNO
mCherry-negative cell
VGAT
hM3Dq-mCherry
d
10 µM CNO
0.5 µM TTX
5 mV
1 min
10 µM CNO
0.5 µM TTX + 10 µM U73122
e
ΔmV induced by CNO
ACSF
U73122
**
f
EPSC % Baseline
10 µM CNO
WT
hM3Dq
hM3Dq + SR 141716A
Time (minutes)
g
Pre CNO
Post CNO
100 pA
10 ms
WT
hM3Dq
hM3Dq + SR 141716A
h
WT
hM3Dq
hM3Dq + SR 141716A
EPSC % Baseline
*
**
i
CNO
mCherry-negative cell
VGAT
hM4Di-mCherry
j
10 µM CNO
5 mV
1 min
k
ΔmV induced by CNO
**
l
Δ Rheobase (pA) post CNO
**

Figure 2.1: Select modulation of BNST VGAT neurons using DREADDs. (**a**) Stereotaxic delivery of viruses encoding a Cre-inducible mCherry or DREADD (hM3Dq or hM4Di) into the BNST of VGAT-Cre mice. (**b**) Representative sections showing expression of a Cre-inducible mCherry (left), hM3Dq (middle), or hM4Di (right). Scale bars indicate 500 µm. (**c**) Schematic of *ex vivo* slice electrophysiology in hM3Dq-mCherry-expressing BNST neurons in the presence of CNO. (**d**) Representative traces from an hM3Dq-expressing BNST VGAT neuron depolarized by bath application of 10 µM CNO in the presence of TTX, but not in the presence of the PLC inhibitor U73122. (**e**) Average change in resting membrane potential during the last 2 minutes of CNO application in ACSF + TTX with and without U73122 (right). *N*: ACSF, 6 cells from 4 mice; ACSF + U73122, 4 cells from two mice. . **, $p<0.01$, Mann Whitney test. Error bars indicate SEM. (**f**) Time course of hM3Dq-induced reduction in evoked EPSCs is blocked by CB_1R antagonist SR 141716A (**g**) Representative superimposed average evoked responses of the five minutes before CNO bath application (solid trace) and 20 to 25 minutes of washout (dotted line). (**h**) Mean evoked EPSC amplitude during minutes 30-35 (20-25 minutes of washout). $F_{(2,10)}=10.36$, $p=0.0037$. *$p<0.05$, Tukey's multiple comparison test; **$p<0.01$ Tukey's multiple comparison test. (**i**) Schematic of *ex vivo* slice electrophysiology in hM4Di-mCherry-expressing BNST neurons in the presence of CNO. (**j**) Representative tracing showing hyperpolarization of hM4Di-mCherry-expressing BNST neuron in the presence of 10 µM CNO. (**k**) Mean hyperpolarization induced by 10 µM CNO. **$p<0.01$, one-sample t-test. *N*: 10 cells from 6 mice. (**l**) Mean change in rheobase following bath CNO application. **$p<0.01$, one-sample t-test. *N*: 5 cells from 4 mice.

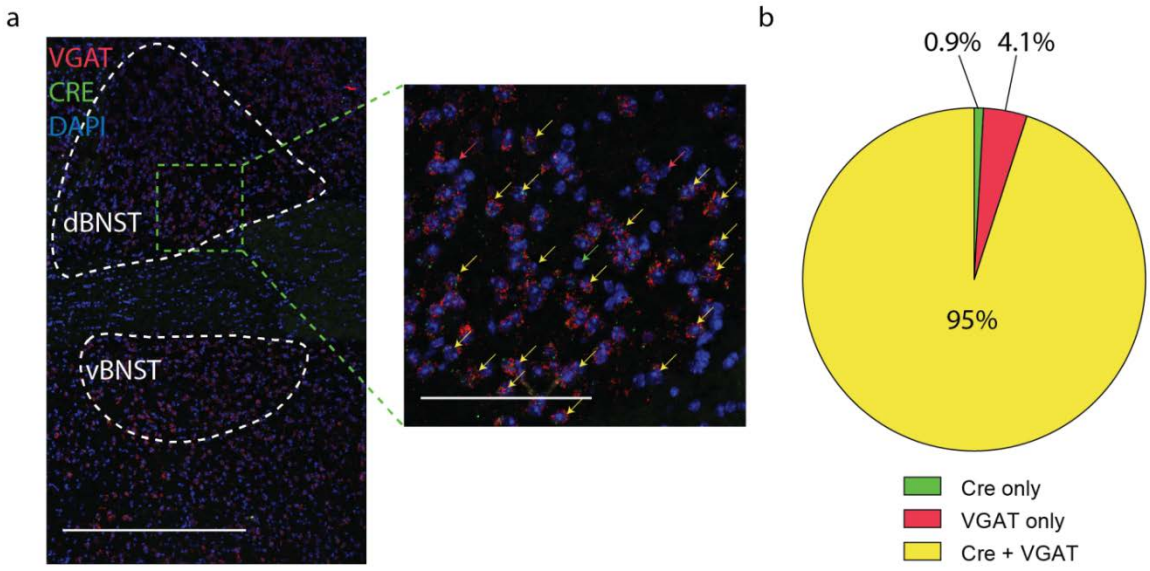

Figure 2.2: Validation of VGAT-Cre mouse in the BNST. (**a**) *In situ* hybridization for *Vgat*, *Cre*, and *Dapi*. Scale bar: 500 µM. Inset shows magnified section with representative cells demonstrating *Cre* only cells (green arrow), *Vgat* only cells (red arrows), and cells positive for both *Cre* and *Vgat* (yellow arrows). Scale bar: 100 µM. (**b**) Percent of BNST cells positive for *Cre* only, *Vgat* only, or both *Cre* and *Vgat*. *N*: 3 images from 3 mice.

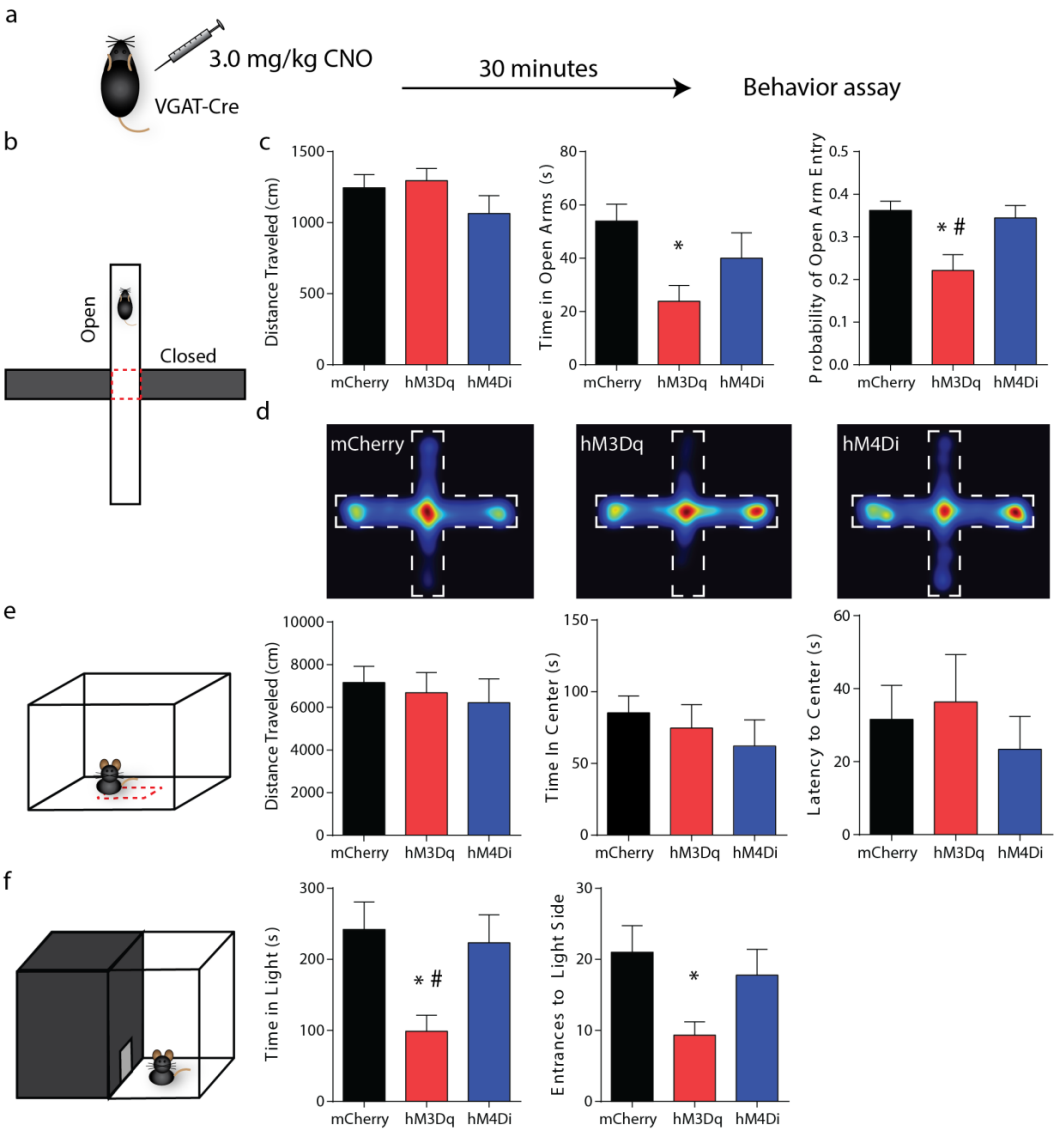

Figure 2.3: Chemogenetic activation of BNST VGAT neurons increases anxiety-like behavior. (**a**) Behavioral assay design. VGAT-Cre mice expressing DIO-mCherry, DIO-hM3Dq, or DIO-hM4Di in the BNST were injected with 3.0 mg/kg CNO 30 minutes before being tested in exploratory assays. (**b**) Elevated plus maze (EPM). (**c**) Distance traveled (left; $F_{(2,23)}$=1.413, p=0.26), time in open arms (middle; $F_{(2,23)}$=3.894, p<0.05, One-Way ANOVA and Tukey's *post-hoc* test) and probability of an open arm entry (right; $F_{(2,23)}$=6.305, p<0.01, One-Way ANOVA, p<0.05, Tukey's *post-hoc* test) during a 5 minute EPM session. *N*: 8 mcherry, 9 hM3Dq, 9 hM4Di). (**d**) Averaged heat maps showing time spent in open and closed arms for mCherry (left), hM3Dq (center), and hM4Di (right) expressing mice. (**e**) Open field. Distance traveled (left; $F_{(2,18)}$=0.2503, p=0.78, One-Way ANOVA. *N:* 7 mCherry, 6 hM3Dq, 8 hM4Di), time in the center (middle; $F_{(2,18)}$=0.5538, p=0.58. *N:* 7 mCherry, 6 hM3Dq, 8 hM4Di), and latency to enter the center (right; $F_{(2,22)}$ = 0.3674, p=0.6967. *N*: 8 mCherry, 9 hM3Dq, 8 hM4Di) during a 30 minute open field session. (**f**) Light-dark box. Time in (left; $F_{(2,23)}$=5.266, p<0.05, One-Way ANOVA, p<0.05, Tukey's *post-hoc* test) and entrances to (right; $F_{(2,23)}$=3.629, p<0.05), One-Way ANOVA, p<0.05, Tukey's *post-hoc* test) the light compartment during a 15 minute session. *N*: 8 mCherry, 9 hM3Dq, 9 hM4Di. *p <0.05 relative to mCherry, # p<0.05 relative to hM4Di, Tukey's post hoc test. Error bars indicate SEM.

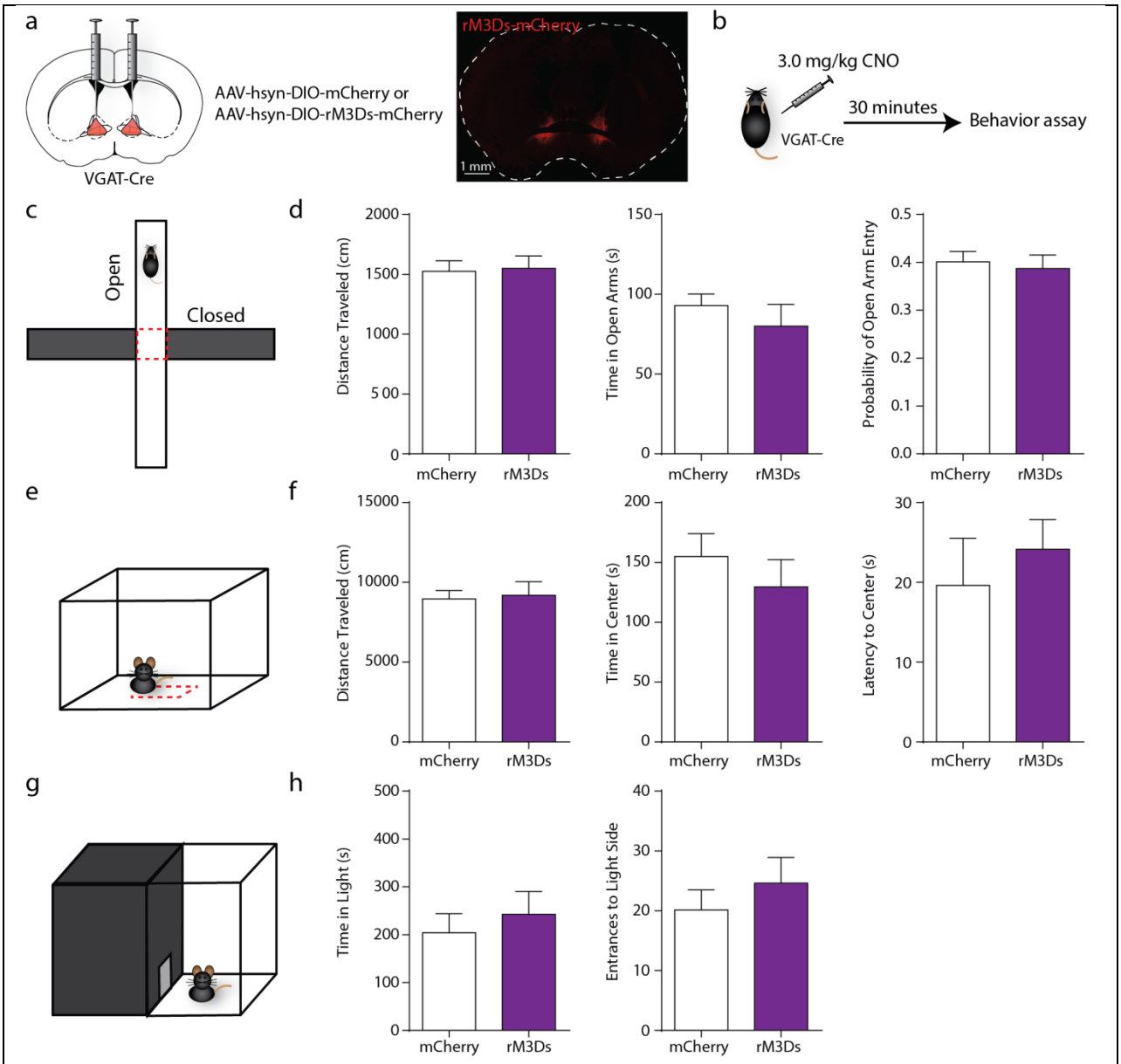

Figure 2.4: Chemogenetic activation of Gs signaling in BNST VGAT neurons does not alter anxiety-like behavior. (**a**) Schematic of viral injection (left) and representative expression of rM3Ds in the BNST of a VGAT-Cre mouse (right). (**b**) VGAT-Cre mice expressing DIO-mCherry or DIO-rM3Ds in the BNST were injected with 3.0 mg/kg CNO 30 minutes before being tested in exploratory assays. (**c**) Elevated plus maze. (**d**) Distance traveled (left; p=0.8551, unpaired t-test), time in open arms (middle; p=0.4393, unpaired t-test) and probability of an open arm entry (right; p=0.7082, unpaired-test) during a 5 minute EPM session. (**e**) Open field. (**f**) Distance traveled (left; p=0.8289, unpaired t-test), time in the center (middle; p=0.4136, unpaired t-test), and latency to enter the center (right; p=0.5161, unpaired t-test) during a 30 minute open field session. (**g**) Light-dark box. (**h**) Time in (left; p=0.5552, unpaired t-test) and entrances to (right; p=0.4332, unpaired t-test) the light compartment during a 15 minute session. N: 7 mCherry, 8 rM3Ds. Error bars indicate SEM.

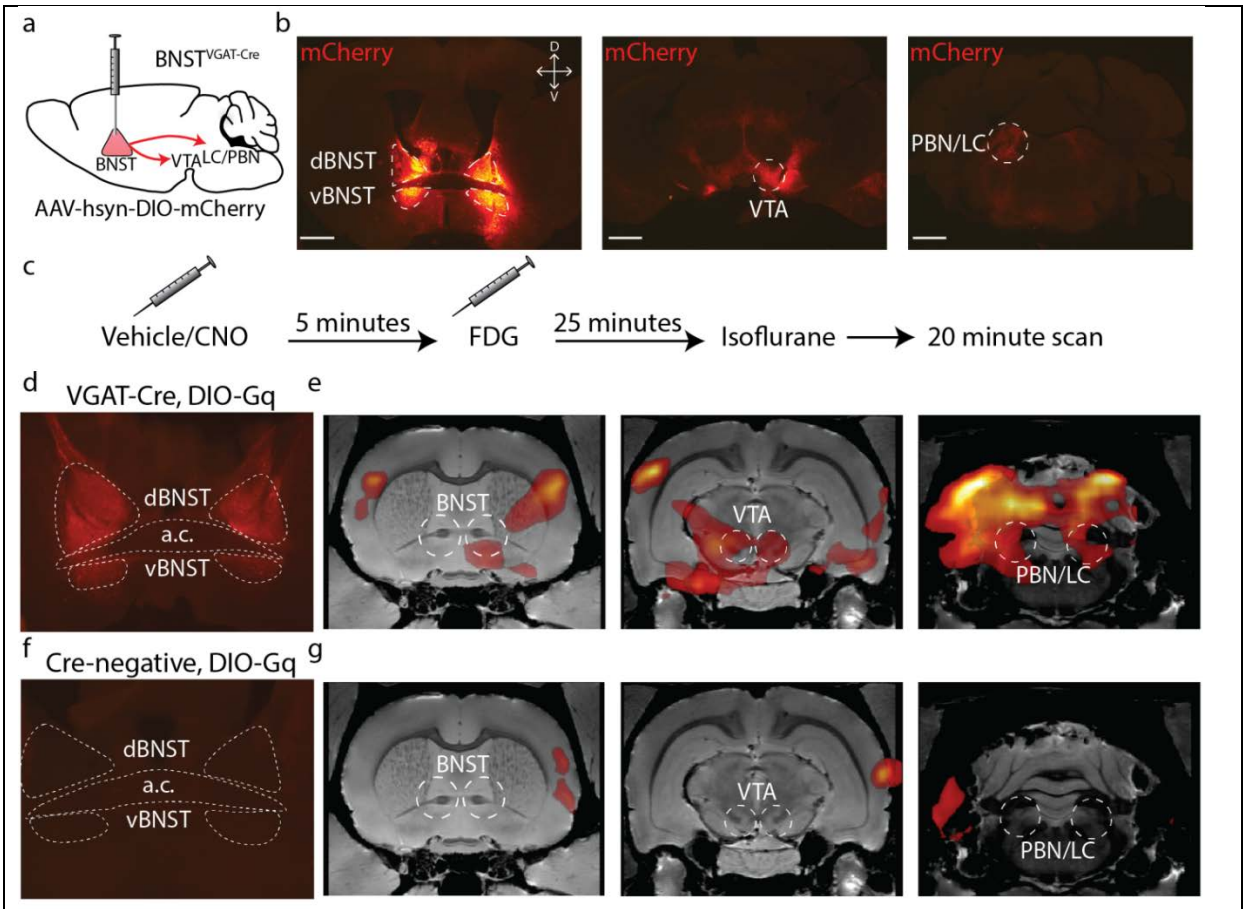

Figure 2.5: Metabolic mapping of downstream activity following CNO-induced activation of hM3Dq in BNST VGAT neurons. (**a**) Injection of a DIO-mCherry to the BNST of a VGAT-Cre to label projection fibers. (**b**) mCherry fluorescence observed in the BNST injection site (left) and fluorescent fibers in the VTA (middle) and PBN/LC (right). Scale bars: 1 mm. (c) µPET imaging timeline. Mice were injected with vehicle or CNO and five minutes later injected with FDG. 25 minutes later mice were anesthetized with isoflurane and placed on the scanning bed for a 20 minute scanning session. (**d**) Representative image of a DIO-hM3Dq-mCherry BNST injection site. (**e**) Increased FDG uptake in areas corresponding to the BNST (left) VTA (middle) and PBN/LC (right) following activation of hM3Dq in BNST VGAT neurons. (**f**) Representative injection of a DIO-hM3Dq-mCherry to a Cre-negative control mouse. (**g**) No change in FDG uptake in the BNST (left), VTA (middle), or PBN/LC (right) from Cre-negative mice injected with a DIO-hM3Dq-mCherry to the BNST. *N*: 4 mice per group. A.c.: anterior commissure.

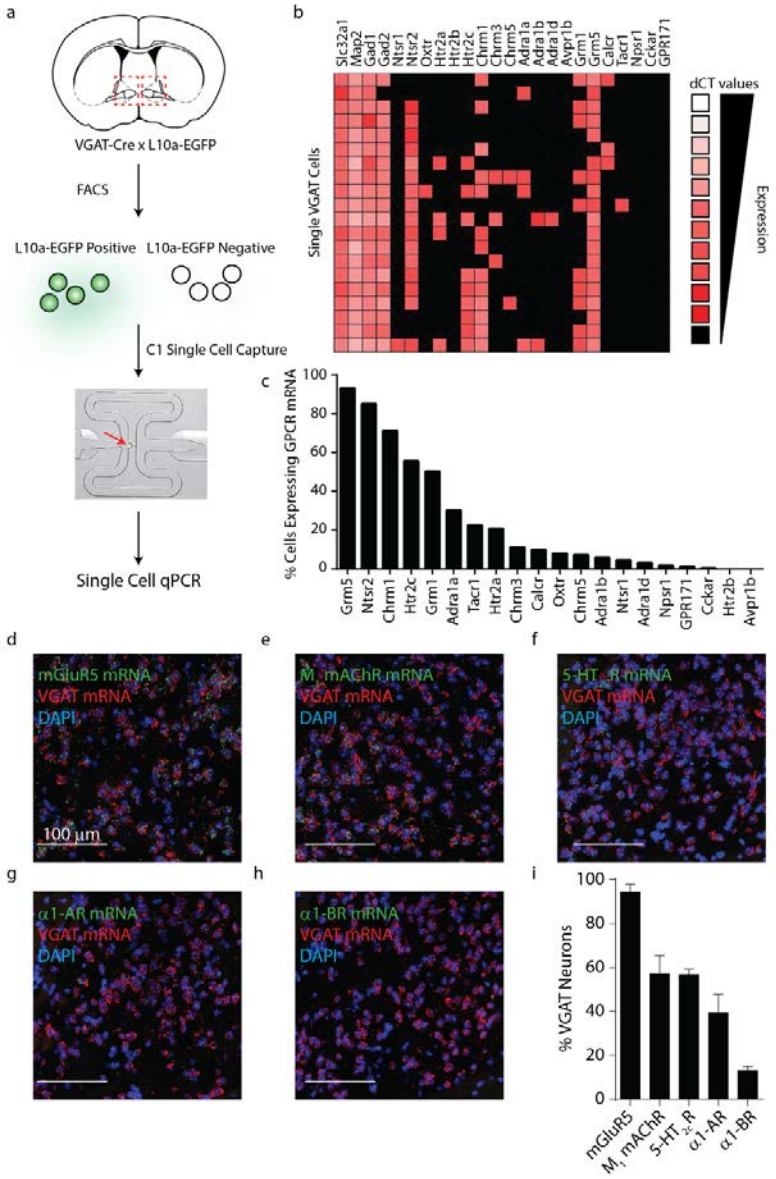

Figure 2.6: Single-cell qPCR analysis reveals Gq-coupled GPCRs in BNST VGAT cells. (**a**) BNST tissue was dissected from a VGAT-Cre x L10-EGFP mouse and dissociated to create a single-cell suspension. Following FACS, individual EGFP-positive cells were captured on a C1 chip and used for single-cell qPCR with probes targeting G_q-coupled receptors. (**b**) Heat map depicting delta Ct values of individual probes from 149 cells positive for Slc32a1, Map2, and Gad1 and/or Gad2. Values are normalized to RN18S. (**c**) Percent of cells expressing transcripts for each G_q-coupled GPCR. (**d-h**) Representative fluorescent *in situ* hybridization sections for assessing colocalization of VGAT mRNA and mRNA for mGluR5 (d), M_1mAchR (e), 5-HT_{2C}R (f), α1-AR (g), α1-BR (h). Scale bar: 100 µm. (**i**) Percent of VGAT mRNA positive cells expressing various GPCR transcripts. Error bars indicate SEM. *Gene* (Protein): *Grm5* (MGLUR5), *Ntsr2* (NTSR2), *Chrm1* (CHRM1), *Htr2c* (HTR2C), *Grm1* (mGluR1), *Adra1a* (α1-AR), *Tacr1* (TACR1), *Htr2a* (5-HT_{2A}R), *Chrm3* (M_3 mAChR), *Calcr* (CT), *Oxtr* (OXTR), *Chrm5* (M_5 mAChR), *Adra1b* (α1-BR), *Ntsr1* (NTSR1), *Adra1d* (α1-DR), *Npsr1* (NPSR1), *Gpr171*(GPR171), *Cckar* (CCKAR), *Htr2b* (5-HT_{2B}R), *Avpr1b* (AVPR1B).

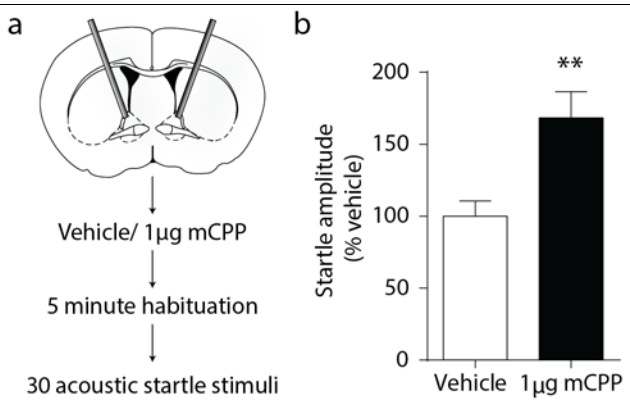

Figure 2.7: Local infusion of mCPP to the BNST increases acoustic startle. (**a**) Mice with cannulae inserted over the BNST received an infusion of 1 µg mCPP and were immediately placed in the acoustic startle chamber. Following a 5 minute habituation period, mice were presented with 30 startle stimuli. (**b**) Mice treated with mCPP showed an exacerbated acoustic startle response ($t(14) = 3.015$, $p = 0.0093$). *N*: 7 vehicle, 9 mCPP. ***p*<0.01, unpaired t-test. Error bars indicate SEM.

Table 1: Taqman probes used for single-cell qPCR	
Gene name	**Taqman Probe Number**
Slc32a	Mm00494138_m1
Map2	Mm00485231_m1
Gad1	Mm00725661_s1
Gad2	Mm00484623_m1
RN18S	Mm04277571_s1
Grm5	Mm00690332_m1
Ntsr2	Mm00435426_m1
Chrm1	Mm00432509_s1
Htr2c	Mm00434127_m1
Grm1	Mm00810231_s1
Adra1a	Mm00442668_m1
Tacr1	Mm00436892_m1
Htr2a	Mm00555764_m1
Chrm3	Mm00446300_s1
Calcr	Mm00432282_m1
Oxtr	Mm01182684_m1
Chrm5	Mm01701883_s1
Adra1b	Mm00431685_m1
Ntsr1	Mm00444459_m1
Adra1d	Mm01328600_m1
Npsr1	Mm00558817_m1
GPR171	Mm02620738_s1
Cckar	Mm00438060_m1
Htr2b	Mm00434123_m1

Avpr1b	Mm01700416_m1
Slc17a6	Mm00499876_m1
Slc17a8	Mm00805413_m1

CHAPTER 3 SEROTONIN SYSTEM INVOLVEMENT IN ANXIETY AND FEAR RELATED BEHAVIOR IN THE EXTENDED AMYGDALA[1]

3.1 Overview of findings

Serotonin (also known as 5-hydroxytryptamine; 5-HT) is a neurotransmitter that has an essential role in the regulation of emotion. However, the precise circuits have not yet been defined through which aversive states are orchestrated by 5-HT. Here we show that 5-HT from the dorsal raphe nucleus (5-HT^{DRN}) enhances fear and anxiety and activates a subpopulation of corticotropin-releasing factor (CRF) neurons in the bed nucleus of the stria terminalis (CRF^{BNST}) in mice. Specifically, 5-HT^{DRN} projections to the BNST, via actions at 5-HT_{2C} receptors (5-HT_{2C}Rs), engage a CRF^{BNST} inhibitory microcircuit that silences anxiolytic BNST outputs to the ventral tegmental area (VTA) and lateral hypothalamus (LH). Furthermore, we demonstrate that this CRF^{BNST} inhibitory circuit underlies aversive behavior following acute exposure to selective serotonin reuptake inhibitors (SSRIs). This early aversive effect is mediated via the corticotrophin releasing factor type 1 receptor (CRF_1R, also known as CRHR1), given that CRF_1R antagonism is sufficient to prevent acute SSRI-induced enhancements in aversive learning. These results reveal an essential 5-HT^{DRN} →CRF^{BNST} circuit governing fear and anxiety, and provide a potential mechanistic explanation for the clinical observation of early adverse events to SSRI treatment in some patients with anxiety disorders(Gorman et al., 1987; Westenberg & den Boer, 1989).

3.2 Methods

Mice: Mice were used in all experiments. For experiments involving Cre lines, mice were crossed for several generations to C57 mice before using. All wild-type mice were C57BL/6 mice obtained from The Jackson Laboratory (Bar Harbor, ME). For all behavior experiments except those involving *Htr2c*^{Cre} mice, male mice ranging in age from 8-16 weeks were used. Female *Htr2c*^{Cre} mice were used in chemogenetic

[1] This chapter was previously published as an article in *Nature*. Some minor adjustments have been made to accommodate dissertation formatting. The original citation is as follows: Marcinkiewcz*, C. A., Mazzone*, C. M., et al. (2016). Serotonin engages an anxiety and fear-promoting circuit in the extended amygdala. *Nature*, *537* (7618), 97–101. * denotes co-first authorship.

manipulations. Both male and female mice aged 6-20 weeks were used for slice electrophysiology and anatomical tracing experiments. All behavioral studies or tissue collection for *ex vivo* slice electrophysiology were performed during the light cycle.

All behavioral experiments in *Htr2c*^{cre} mice were conducted at the University of Aberdeen and in accordance with the United Kingdom Animals (Scientific Procedures) Act of 1986. All *in vivo* electrophysiology experiments were conducted in accordance with all rules and regulations at the National Institute for Alcohol Abuse and Alcoholism at the National Institutes of Health. All other procedures were conducted in accordance with the National Institutes of Health guidelines for animal research and with the approval of the Institutional Animal Care and Use Committee at the University of North Carolina at Chapel Hill.

All animals were group housed on a 12 hour light cycle (lights on at 7 a.m.) with *ad libitum* access to rodent chow and water, unless described otherwise. CRF-*ires*-Cre (*Crf*^{cre}) were provided by Dr. Bradford Lowell (Harvard University) and were previously described(Krashes et al., 2014). C57BL/6J mice were obtained from the Jackson Laboratory (Bar Harbor, ME). To visualize CRF-expressing neurons, *Crf*^{Cre} mice were crossed with either an Ai9 or a cre-inducible L10-GFP reporter line (Jackson Laboratory)(Clarke, 1993) to produce CRF-Ai9 or CRF-L10GFP progeny, referred to throughout the manuscript as CRF-reporters. *Sert*^{Cre} mice (from GENSAT) were a generous gift from Dr. Bryan Roth. *Htr2c*^{Cre} mice were supplied by Dr. Lora Heisler and are described in detail elsewhere(Burke et al., 2016).

Male mice were used for *in vivo* optogenetic behavioral experiments and for assessing the involvement of BNST CRF neurons on fluoxetine-induced enhancement of fear. Female 5-HT$_{2C}$-Cre mice were used in chemogenetic manipulations. Both male and female mice were used for slice electrophysiology and anatomical tracing experiments. All behavioral studies or tissue collection for *ex vivo* slice electrophysiology were performed during the light cycle.

Viruses and tracers: All AAV viruses except INTRSECT constructs were produced by the Gene Therapy Center Vector Core at the University of North Carolina at Chapel Hill and had titers of >10^{12} genome copies/mL. For *ex vivo* and *in vivo* optical experiments, mice were injected with rAAV5-ef1α-DIO-hChR2(H134R)-eYFP or rAAV5-ef1α-DIO-eYFP as a control. Red IX retrobeads (Lumafluor) were used to fluorescently label LH - and VTA-projecting BNST neurons during *ex vivo* slice electrophysiology

recordings. The retrograde tracer Fluoro-Gold (Fluorochrome) was used for anatomical mapping. Choleratoxin B (CTB) 555 and CTB 657 retrograde tracers (Invitrogen; C34776, and C34778, respectively) diluted to 0.5% (w/v) in sterile PBS were used per injection site for anatomical mapping of collateral projections from BNST to LH and VTA. For chemogenetic manipulations, mice were injected with 400 nl of rAAV8-hsyn-DIO-hM3D(Gq)-mCherry, rAAV8-hsyn-DIO-hM4D(Gi)-mCherry, or rAAV8-hsyn-DIO-mCherry bilaterally. HSV-hEF1α-mCherry, HSV-ef1α-LSL1-mCherry-IRES-flpo, and HSV-ef1α-IRES-Cre (supplied by Rachel Neve at the McGovern Institute for Brain Research at MIT) were injected bilaterally into the VTA and LH at a volume of 500500 nL per sitesite. The INTRSECT construct AAVdj-hSyn-Con/Foff-hChR2(H134R)-EYFP was infused at 500 nl per side into the BNST. All AAV constructs had viral titers $>10^{12}$ genome particles/ml.

Stereotaxic injections: All surgeries were conducted using aseptic technique. Adult mice (2-5 months) were deeply anesthetized with 5% isoflurane (vol/vol) in oxygen and placed into a stereotactic frame (Kopf Instruments) while on a heated pad. Sedation was maintained at 1.5-2.5% isoflurane during surgery. An incision was made down the midline of the scalp and a craniotomy was performed above the target regions and viruses and fluorescent tracers were microinjected using a Neuros Hamilton syringe at a rate of 100 nl/min. After infusion, the needle was left in place for 10 minutes to allow for diffusion of the virus before the needle was slowly withdrawn. Injection coordinates (in mm, midline, Bregma, dorsal surface): BNST (±1.00, 0.30, -4.35), LH (±0.9 to 1.10, -1.7, -5.00 to -5.2), VTA (-0.3, -2.9, -4.6), DR (0.0, -4.65, -3.2 with a 23^{o} angle of approach). When using retrobeads, injection volumes into the LH and VTA were 300 nl and 400 nl, respectively. Fluorogold injection volumes were 200 nl per target site. CTB volumes were 200200 nL per target site. An optical fiber was implanted in the BNST (±1.00, 0.20, -4.15) at a 10^{o} angle for *in vivo* photostimulation studies. After fiber implantation, dental cement was used to adhere the ferrule to the skull. Following surgery, all mice returned to group housing. Mice were allowed to recover for at least 3 weeks before being used for chemogenetic behavioral studies, or 6 weeks for *in vivo* optogenetic studies.

Drugs: RS 102221, 5-HT and mCPP were from Tocris (Bristol, UK). For electrophysiology experiments, RS 102221 was made up to 100 mM in DMSO and then diluted to a final concentration of 5 µM in aCSF.

5-HT and mCPP were stocked at 10 and 20 mM, respectively, in ddH_2O and diluted to their final concentations in aCSF. For electrophysiology experiments, clozapine-N-oxide (CNO; from Dr. Bryan Roth) was stocked at 100 mM in DMSO and diluted to 10 µM in aCSF. For behavior experiments, CNO was dissolved in 0.5% DMSO (in 0.9% saline) to a concentration of 0.1 mg/ml or 0.3 mg/ml and injected at 10 ml/kg for a final concentration of 1 or 3 mg/kg, i.p. Fluoxetine (Sigma) was made up in 0.9% NaCl to a concentration of 1 mg/ml and then injected at 10 ml/kg for a final concentration of 10 mg/kg, i.p.

***In vivo* Electrophysiological Procedures**

Surgical Procedures: Mice were anesthetized with 2% Isoflurane (Baxter Healthcare, Deerfield, IL) and implanted with 2x8 electrode (35um tungsten) micro-arrays (Innovative Neurophysiology Inc, Durham, NC) targeted at the BNST (ML: 0.8 mm, AP: ± 0.5 mm , and DV: -4.15 mm relative to Bregma). Following surgery, mice were singly housed and allowed at least one week to recover prior to behavioral testing.

Fear Conditioning: Fear conditioning took place in 27 × 27 × 11cm conditioning chambers (Med Associates, St. Albans, VT), with a metal-rod floor (Context A) and scented with 1% vanilla. Mice received 5 parings of a pure tone CS with a .6mA foot shock. 24 h following conditioning, mice underwent a CS recall test (10 presentations of the CS alone, 5 sec ITI), which was conducted in a Plexiglas cylinder (20cm diameter) and scented with 1% acetic acid (Context B). Stimulus presentations for both tests were controlled by MedPC (Med Associates Inc, St. Albans, VT). Cameras were mounted overhead for recording freezing behavior, which was scored automatically using CinePlex Behavioral Research System software (Plexon Inc, Dallas, TX).

Electrophysiological recording and single unit analysis: Electrophysiological recording took place during both fear conditioning and CS recall tests. Individual units were identified and recorded using Omniplex Neural Data Acquisition System (Plexon Inc, Dallas, TX). Neural data was sorted using Offline Sorter (Plexon Inc, Dallas, TX). Waveforms were isolated manually, using principal component analysis. To be included in the analyses, spikes had to exhibit a refractory period of at least 1 ms. Autocorrelograms from simultaneously recorded units were examined to ensure that no cell was counted twice. Single units were analyzed by generating perievent histograms (3 sec bins) of firing rates from 30 sec prior to CS onset

until 30 sec after CS offset (NeuroExplorer 5.0, Nex Technologies, Madison, AL). Firing rates were normalized to baseline (30 sec prior to CS onset) using z-score transformation. Analysis included a total of 139 cells over three days of recording. Data reported for raw firing rates include only putative principal neurons (<10Hz). The formula for computing the suppression ratio was (average freezing rate) / (average freezing rate + average movement rate). Each cell was calculated individually. A value of .5 = no change in rate).

***Ex vivo* Slice Electrophysiology:** Brains were sectioned at 0.07 (mm/s) on a Leica 1200S vibratome to obtain 300 µm coronal slices of the BNST, which were incubated in a heated holding chamber containing normal, oxygenated aCSF (in mM:124 NaCl, 4.4 KCl, 2 $CaCl_2$, 1.2 $MgSO_4$, 1 NaH_2PO_4, 10.0 glucose, and 26.0 $NaHCO_3$) maintained at 30 ± 1˚C for at least 1 hour before recording. Slices were transferred to a recording chamber (Warner Instruments) submerged in normal, oxygenated aCSF maintained at 28-30˚C at a flow rate of 2 ml/min. Neurons of the BNST were visualized using infrared differential interference contrast (DIC) video-enhanced microscopy (Olympus). Borosilicate electrodes were pulled with a Flaming-Brown micropipette puller (Sutter Instruments) and had a pipette resistance between 3-6 MΩ. Signals were acquired via a Multiclamp 700B amplifier, digitized at 10 kHz and analyzed with Clampfit 10.3 software (Molecular Devices, Sunnyvale, CA, USA).

Light-evoked action potentials: In $Sert^{Cre}$ or Crf^{Cre} mice, fluorescently labeled neurons expressing ChR2 were visualized and stimulated with a blue (470 nm) LED using a 1 Hz, 2 Hz, 5 Hz, 10 Hz, and 20 Hz stimulation protocol with a pulse width of 0.5 ms. Evoked action potentials were recorded in current clamp mode using a potassium gluconate based internal solution (in mM: 135 K+ gluconate, 5 NaCl, 2 $MgCl_2$, 10 HEPES, 0.6 EGTA, 4 Na_2ATP, 0.4 Na_2GTP, pH 7.3, 285–290 mOsmol).

Light-evoked synaptic transmission: In Crf^{Cre} mice with ChR2 in the BNST and retrograde tracer beads in the VTA or LH, we visualized non-ChR2-expressing, beaded neurons using green (532 nm) LED. Recordings were conducted in voltage clamp mode using a cesium-methansulfonate (Cs-Meth) based internal solution (in mM: 135 cesium methanesulfonate, 10 KCl, 1 $MgCl_2$, 0.2 EGTA, 2 QX-314, 4 MgATP, 0.3 GTP, 20 phosphocreatine, pH 7.3, 285–290 mOsmol) so that we could detect EPSCs (-55 mV) and IPSCs (+10 mV) in the same neuron. After confirming the absence of a light-evoked EPSC signal, we

measured light-evoked IPSCs during a single, 5 ms light pulse of 470 nm. In a subset of these experiments, SR95531 (GABAzine, 10 µM) was bath applied for 10 minutes to block IPSCs.

Drug effects in CRF^{BNST} neurons: Crf-reporter mice were injected with retrograde tracer beads into the VTA (ML -0.5, AP -2.9, DV -4.6). We then recorded from beaded (VTA-projecting) and non-beaded (non-projecting) CRF neurons in the BNST. Acute drug effects were determined in current clamp mode in the presence of TTX using a potassium gluconate-based internal solution. After a 5-minute stable baseline was established, 5HT (10 µM) or mCPP (20 µM) was bath applied for 10 minutes while recording changes in membrane potential. The difference in membrane potential between baseline and drug application at peak effect (delta or Δ MP) was later determined. In a subset of mCPP experiments, slices were incubated with RS 102221 (5 µM) for at least 20 minutes before experiments began.

Synaptic transmission: Spontaneous inhibitory postsynaptic currents (sIPSCs) were assessed in voltage clamp using a potassium-chloride gluconate-based intracellular solution (in mM: 70 KCl, 65 K^+-gluconate, 5 NaCl, 10 HEPES, 0.5 EGTA, 4 ATP, 0.4 GTP, pH 7.2, 285–290 mOsmol). IPSCs were pharmacologically isolated by adding kynurenic acid (3 mM) to the aCSF to block AMPA and NMDA receptor-dependent postsynaptic currents. The amplitude and frequency of sIPSCs were determined from 2 minute recording episodes at -70 mV. The baseline was averaged from the 4 minutes preceding the application of 5-HT (10 µM) or mCPP (10 µM) for 10 minutes. In a subset of these experiments, RS 102221 (5 µM) was added to the aCSF and slices were incubated in this drug solution for at least 20 minutes before experiments began. For miniature IPSCs (mIPSCs), TTX was included in the aCSF to block network activity.

In *Sert^{Cre}*::ChR2^{BNST} mice with retrograde tracer beads in the VTA, sIPSCs were recorded as described above. After achieving a stable baseline, a 10 s, 20 Hz photostimulation was applied.

For assessment of spontaneous excitatory postsynaptic currents (sEPSCs), a cesium gluconate-based intracellular solution was used (in mM: 135 Cs^+-gluconate, 5 NaCl, 10 HEPES,

0.6 EGTA, 4 ATP, 0.4 GTP, pH 7.2, 290–295 mOsmol). $AMPA_R$-mediated EPSCs were pharmacologically isolated by adding 25 µM picrotoxin to the aCSF. sEPSC recordings were acquired in 2 minute recording blocks at -70 mV.

Fast-scan cyclic voltammetry (FSCV): Electrodes were fabricated as previously described and cut to 50-100 um in length(Bath et al., 2000). Animal and slice preparation were as described above for electrophysiology and slices were perfused on the rig in ACSF. Using a custom built potentiostat (University of Washington Seattle), 5-HT recordings were made in the BNST using TarHeel CV written in lab view (National Instruments). Briefly a triangular waveform (-0.1 V to 1.3 V with a 10% phase shift at 1000 V/s, vs. Ag/AgCl) was applied to the carbon fiber electrode at a rate of 10 Hz. Slices were optically stimulated with 20 5-ms blue (490 nm) light pulses at a rate of 20 Hz down the submerged 40x objective. 10 cyclic voltammograms were averaged prior to optical stimulation for background subtraction. Voltammograms were digitally smoothed one time with a fast Fourier transform following data collection and analyzed with HDCV (UNC Chapel Hill). Fluoxetine (10 µM) was bath applied following a stable baseline (20 minutes).

Behavioral Assays:

For chemogenetic manipulations, mice were transported to a holding cabinet adjacent to the behavioral testing room to habituate for at least 30 minutes before being pretreated with CNO (3 mg/kg, i.p. for Crf^{Cre} mice and 1 mg/kg, i.p. for $Htr_{2C}{}^{Cre}$ mice). All behavior testing began 45 minutes following CNO treatment, with the exception of fear conditioning training, which occurred 30 minutes after a CNO injection. When assessing the effect of fluoxetine on fear conditioning, fluoxetine (10 mg/kg, i.p.), or vehicle, was administered 1 hour before training (30 minutes before CNO treatment). For optogenetic manipulations, mice received bilateral stimulation (473 nm, ~10 mW, 5 ms pulses, 20 Hz) when specified. Unless specified, all equipment was cleaned with a damp cloth between mouse trials. All sessions were video recorded and analyzed using EthoVision software (Noldus Information Technologies) except where noted.

Elevated Plus Maze: Mice were placed in the center of an elevated plus maze and allowed to explore during a 5 minute session. Light levels in the open arms were ~14 lux. During optogenetic manipulations mice received bilateral stimulation during the entire 5 minute session. Mice that left the maze were excluded from analysis (n= 2 control, 1 ChR2 from optogenetic experiments).

Open Field: Mice were placed into the corner of a white Plexiglas open field arena (25 x 25 x 25 cm) and allowed to freely explore for 30 minutes. The center of the open field was defined as the central 25% of the arena. For optogenetic studies the 30 minute session was divided into three 10-minute epochs consisting of stimulation off, stimulation on, and stimulation off periods.

Novelty-Induced Suppression of Feeding: 48 hours prior to testing mice were provided with access to a single piece of Froot Loops cereal (Kellogg's) in their home cage. 24 hours prior to testing, home cage chow was removed and mouse body weights were recorded. Water remained available *ad lib*. Beginning at least one hour before testing mice transferred to new clean cages so they were singly housed for the test session and body weights were recorded. During the test session mice were placed into an arena (25x25x25 cm) that contained a single Froot Loop on top of a piece of circular filter paper. Mice were monitored by a live observer and the latency for the mouse to begin eating the pellet was measured, allowing up to 10 minutes. All mice began eating within this time. Following the initiation of feeding, mice were removed from the arena and placed back into their home cages. Mice were then provided with 10 minutes of access to a pre-weighed amount of Froot Loops™ for a post-test feeding session. After this 10 minute post-test, the remaining Froot Loops were weighed and mice were returned to *ad lib* home cage chow. Mice were returned to group housing at the end of this session. For optogenetic experiments, mice received constant 20 Hz optical stimulation during both the latency to feed assay and the 10 minute post-test. During optogenetic experiments, one control mouse did not feed during the 10 minute NSF session and was excluded from the results.

Home cage feeding: Sert^{Cre} mice were food deprived for 24 hours. On the day of the experiment, mice were acclimated to the behavior room for 1 hour. A single preweighed food pellet was placed in the home cage and the mice were allowed to eat for 10 minutes during optogenetic stimulation. At the end of the experimental session, the pellet was removed and weighed and mice were given *ad lib* access to food.

Htr$_{2C}^{Cre}$ mice were acclimated in metabolic chambers (TSE Systems, Germany) for 2 days before the start of the recordings. After acclimation, mice were food deprived for 24 hours. Following fasting, mice received an IP injection of CNO 30 minutes before food presented again. Mice were recorded for 12 hours with the following measurements being taken every 30 minutes: water intake, food intake, ambulatory activity (in X and Z axes), and gas exchange (O_2 and CO_2) (using the TSE LabMaster system, Germany). Energy expenditure was calculated according to the manufacturer's guidelines (PhenoMaster Software, TSE Systems).

Fear Conditioning: We used a three day protocol to assess both cued and contextual fear recall. On the first day, mice were placed into a fear conditioning chamber (Med Associates) that contained a grid floor and was cleaned with a scented paper towel (19.5% EtOH, 79.5% H2O, 1% vanilla). After a 3 minute baseline period, mice were exposed to a 30 second tone (3 KHz, 80 dB) that co-terminated with a 2 second scrambled foot shock (0.6 mA). A total of 5 tone-shock pairings were delivered with a random inter-tone interval (ITI) of 60-120 seconds. For optogenetic studies, light stimulation occurred only during the 30-second tones of this session. Following delivery of the last foot shock, mice remained in the conditioning chamber for a two minute consolidation period. 24 hours later, mice were placed into a separate conditioning box (Med Associates) that contained a white Plexiglas floor, a striped pattern on the walls, and was cleaned and scented with a 70% EtOH solution. After a 3 minute baseline period, mice were presented with 10 tones (30 seconds, 3 KHz, 80 dB) with a 5 second ITI. Mice remained in the chamber after the last tone for a two-minute consolidation period. 24 hours later (48 hours after training), mice were returned to the original training chamber for 5 minutes. For each session, freezing behavior was hand-scored every 5 seconds by a trained observer blinded to experimental treatment as described previously(Hefner et al., 2008). Freezing was defined as a lack of movement except as required for respiration.

Immunohistochemistry and histology: All mice used for behavioral and anatomical tracing experiments were anesthetized with Avertin and transcardially perfused with 30 ml of ice-cold 0.01M PBS followed by 30 ml of ice-cold 4% paraformaldehyde (PFA) in PBS. Brains were extracted and stored in 4% PFA for 24 hours at 4°C before being rinsed twice with PBS and stored in 30% sucrose/PBS until the brains sank. 45

µm slices were obtained on a Leica VT100S and stored in 50/50 PBS/Glycerol at -20°C. DREADD or ChR2-containing sections were mounted on slides, allowed to dry, coverslipped with VectaShield (Vector Labs, Burlingame, CA), and stored in the dark at 4°C.

Tryptophan hydroxylase/Fluorogold/cfos triple labeling We stained free-floating dorsal raphe sections using indirect immunofluorescence sequentially for first tryptophan hydroxylase (TPH) and Fluoro-Gold(FG) and then c-*fos*. For TPH/FG, we washed sections 3X for 5 min with 0.01 M PBS, permeabilized them for 30 min in 0.5% Triton/0.01 M PBS, and washed the sections again 2X with 0.01 M PBS. We blocked the sections for 1 hour in 0.1% Triton/0.01 M PBS containing 10%(v/v) Normal Donkey Serum and 1%(w/v) Bovine Serum Albumin (BSA). We then added primary antibodies (1:500 Mouse anti-TPH [Sigma Aldrich T0678] and 1:3000 Guinea Pig anti-Fluoro Gold [Protos Biotech NM101]) to blocking buffer and incubated the sections overnight at 4 degrees C. The next day, we washed the sections 3X for 5 min with 0.01 M PBS, then incubated them with 1:500 with Alexa Fluor 647-conjugated Donkey anti-mouse and Alexa Fluor 488-conjugated Donkey anti-guinea pig secondary antibodies for 2 hr at RT, and washed the sections 4X for 5 min with 0.01 M PBS. We then proceeded directly to the c-*fos* tyramide signal amplification based immunofluorescent staining. We permeabilized the sections in 50% methanol for 30 min, then quenched endogenous peroxidase activity in 3% hydrogen peroxide for 5 min. Followed by two 10 min washes in 0.01 M PBS, we blocked the sections in PBS containing 0.3% Triton X-100 and 1.0 % BSA for 1 hour. *c-fos* primary antibody (Santa Cruz Biotechnology - sc-52) was added to sections at 1:3000 and sections were incubated for 48 hours at 4 degrees. On day 3, we washed the sections in TNT buffer (0.1 M Tris-HCl pH 7.5, 0.15 M NaCl, 0.05% Tween-20) for 10 min, blocked in TNB buffer (0.1 M Tris-HCl pH 7.5, 0.15 M NaCl, 0.5% Blocking reagent – PerkinElmer FP1020) buffer for 30 min. We then incubated the sections in secondary antibody (Goat anti-rabbit HRP-conjugated- PerkinElmer) 1:200 in TNB buffer for 30 min., washed the sections in TNT buffer 4X for 5 min, and then incubated the sections in Cy3 dye diluted in TSA amplification diluents for 10 min. We washed the sections 2X in TNT buffer, mounted them on microscope slides. We coverslipped the slides using Vectashield mounting medium. We acquired 4-5 2x4 tiled z-stack(5 optical slices comprising 7 µm total) images of the dorsal raphe from each naïve and shock mouse on a Zeiss 800 Upright confocal microscope. Scanning parameters and laser power were matched between groups. Images were preprocessed using stitching

and maximum intensity projection and then analyzed using an advanced processing module in Zeiss Zen Blue that allows nested analysis of multiple segmented fluorescent channels within parent classes. Double and triple-labeled cells were validated in a semi-automated fashion. At least 4 sections per mouse were counted in this way. One mouse was identified as a significant outlier in the Shock group and was excluded from further analysis.

Sert^{Cre}::ChR2*, and Crf*^{Intrsect}-ChR2 validation: To verify expression of ChR2-expressing fibers in the BNST originating from DR serotonergic neurons, 300 µm slices used for *ex vivo* electrophysiological recordings containing the DR and BNST were stored in 4% paraformaldehyde at 4°C for 24 hours before being rinsed with PBS, mounted, and coverslipped with Vectashield mounting medium. Images showing eYFP fluorescence from the DR and BNST were obtained on a Zeiss 800 upright confocal microscope using a 10x objective and tiled z stacks. To validate the INTRSECT construct, mice received injections of HSV-hEF1α-mCherry or HSV-ef1α-LSL1-mCherry-IRES-flpo to both the LH and VTA bilaterally (N=4 and 5, respectively). Both groups received AAVDJ-hSyn-Cre-on/Flp-off-hChR2(H134R)-EYFP to the BNST bilaterally. Six weeks following injection, mice were perfused and tissue was collected as described above. To visualize YFP expression in the BNST of *Crf*^{Cre}::Intrsect^{BNST} mice, free floating slices containing the BNST were rinsed three times with PBS for 5 minutes each. Slices were then incubated in 50% methanol for 30 minutes then incubated in 3% hydrogen peroxide for 5 minutes. Following three 10-minute washes in PBS, slices were incubated in 0.5% Triton X-100 for 30 minutes followed by a 10 minute PBS wash. Slices were blocked in 10% normal donkey serum/0.1% Triton X-100 for 1 hour, and then they were incubated overnight at 4°C with a primary chicken anti-GFP antibody (GFP-1020, Aves) at 1:500 in blocking solution. Following primary incubation, slices were rinsed three times with 0.01M PBS for 10 minutes each and incubated with a fluorescent secondary antibody (AlexaFluor 488 Donkey anti-chicken) at 1:200 in PBS for 2 hours at room temperature. Slices were then rinsed with four 10-minute PBS washes before being mounted onto glass slides and coverslipped with Vectashield with DAPI. A 3x4 tiled z stack (7 optical sections comprising 35 µm total) image from both the left and right hemispheres of the BNST was obtained at 20x magnification using a Zeiss 800 upright confocal microscope. Scanning parameters and laser power were matched between groups. Images were preprocessed using stitching and maximum intensity projection. The number of fluorescent cells in the dorsal and ventral aspects of

the BNST were counted by a blinded scorer using the cell counter plug-in in FIJI (ImageJ). Each hemisphere was considered independently per mouse. One mouse in the flp-expressing group was a significant outlier for number of cells expressed in a ventral BNST hemisphere (ROUT, Q=0.1%) and all data from that mouse were excluded.

Choleratoxin retrograde tracer studies in CRF reporter mice: 3 male CRF-L10a reporter mice were injected with 200 nl of CTB 555 and CTB 647 bilaterally to the LH and VTA, respectively, as described above. 5 days following injection, mice were perfused as described above, the brains were extracted, and were stored in 4% paraformaldehyde for 24 hours at 4°C before being rinsed with PBS and transferred to 30% sucrose until the brains sank. 45 µm sections containing the BNST were collected as described above. Sections containing the BNST were mounted on glass slides and coverslipped using Vectashield. An image from the left and right hemispheres of a medial section of the BNST was obtained on a Zeiss 800 upright microscope using a 20x objective and 3x5 tiled z stacks (5 optical slices comprising 7 µm total). Images were preprocessed using stitching and maximum intensity projection, and were then analyzed using the cell counter function in FIJI (ImageJ). Only cells positive for GFP (putative CRF neurons) were considered. Cells were scored exclusively as either 555+ only (LH-projecting), 647+ only (VTA-projecting), 555+ and 647+ (projecting to both LH and VTA), or 555- and 647- (unlabeled; neither LH- nor VTA- projecting). The total number of CRF neurons scored was calculated as the sum of all four groups, and percentages of each type were calculated from this value. Each hemisphere was scored and plotted independently (N=6 images from 3 mice), and the dorsal and ventral BNST were considered separately. The average values were plotted as pie charts (ED 9).

Double Fluorescence *in situ* hybridization (FISH): For validation of 2C-cre line and comparison of CRF/2C mRNA cellular colocalization, mice were anesthetized using isoflurane, rapidly decapitated, and brains rapidly extracted. Immediately after removal, the brains were placed on a square of aluminum foil on dry ice to freeze. Brains were then placed in a -80°C freezer for no more than 1 week before slicing. 12 µm slices were made of the BNST on a Leica CM3050S cryostat (Germany) and placed directly on coverslips. FISH was performed using the Affymetrix ViewRNA 2-Plex Tissue Assay Kit with custom probes for CRF, 5-HT2C, and Cre designed by Affymetrix (Santa Clara, CA). Slides were coverslipped

with SouthernBiotech DAPI Fluoromount-G. (Birmingham, AL). 3x5 tiled z stack (15 optical sections comprising 14 µm total) images of the entire 12 µm slice were obtained on a Zeiss 780 confocal microscope for assessment of CRF/2C colocalization. A single-plane 40x tiled image of a CRF/2C slice was obtained on a Zeiss 800 upright confocal microscope for the magnified image shown in Extended Data 6b, right. 3x5 tiled z stack (7 optical sections comprising 18 µm) images of 2C/Cre slices were obtained on a Zeiss 800 upright confocal microscope for the 2C/Cre validation. All images were preprocessed with stitching and maximum intensity projection. An image of the BNST from 3 mice in each condition was hand counted for each study using the cell counter plugin in FIJI (ImageJ). Cells were classified into three groups: probe 1+, probe 2+, or probe 1 and 2 +. Only cells positive for a probe were considered. Results are plotted as average classified percentages across the three images.

Group assignment: No specific method of randomization was used to assign groups. Animals were assigned to experimental groups so as to minimize the influence of other variables such as age or sex on the outcome.

Inclusion/exclusion criteria: Pre-established criteria for excluding mice from behavioral analysis included 1) missed injections, 2) anomalies during behavioral testing, such as mice falling off the elevated plus maze, 3) damage to or loss of optical fibers, 4) statistical outliers, as determined by the Grubb's test.

Sample size: A power analysis was used to determine the ideal sample size for behavior experiments**.** Assuming a normal distribution, a 20% change in mean and 15% variation, we determined that we would need 8 mice per group. In some cases, mice were excluded due to missed injections or lost optical fibers resulting in fewer than 8 mice per group. For electrophysiology experiments, we aimed for 5-7 cells from 3-4 mice.

Statistics: Data are presented as means ± SEM. For comparisons with only two groups, *p* values were calculated using paired or unpaired t-tests as described in the figure legends. Comparisons across more than two groups were made using a one-way ANOVA, and a two-way ANOVA was used when there was more than one independent variable. A Bonferonni posttest was used following significance with an ANOVA. In cases in which ANOVA was used, the data met the assumptions of equality of variance and

independence of cases. If the condition of equal variances was not met, Welch's correction was used. Some of the sample groups were too small to detect normality (<8 samples) but parametric tests were used because nonparametric tests lack sufficient power to detect differences in small samples (Graphpad Statistics Guide – www.graphpad.com). The standard error of the mean is indicated by error bars for each group of data. Differences were considered significant at *p* values below 0.05. All data were analyzed with GraphPad Prism software.

3.3 Results

Electrophysiological interrogation of 5-HT inputs from the DR to the BNST

In view of multiple converging lines of evidence pinpointing 5-HT as a critical neuromodulator of pathological fear learning (Burghardt et al., 2007; Ravinder et al., 2013), we first interrogated the endogenous recruitment of the 5-HT$^{DRN\rightarrow BNST}$ circuit by an aversive footshock stimulus. Using fluorogold to retrogradely label BNST-projecting 5-HT neurons in the DRN, we found that c-fos, an immediate early gene indicative of *in vivo* neuronal activation, was significantly elevated in 5-HT$^{DRN\rightarrow BNST}$ neurons after footshock (Figure 3.1a-f). Using *in vivo* electrophysiology, we then probed the neuronal dynamics of the BNST during fear conditioning and recall and found evidence for engagement during both conditioning and recall (Figure 3.2).

To decipher the role of this 5-HT$^{DRN\rightarrow BNST}$ circuit in aversive behavior, Channelrhodopsin2 (ChR2)-eYFP was selectively expressed in 5-HT^{DRN} neurons through the delivery of a Cre-inducible viral vector in mice expressing Cre recombinase under the control of a serotonin transporter promoter (*Sert^{Cre}*) for both *in vivo* and *ex vivo* analysis. We observed eYFP+ (5-HT) cell bodies in the DRN and eYFP+ fibers in both the dorsal and ventral aspects of the BNST (*Sert^{Cre}*::ChR2$^{DRN\rightarrow BNST}$), confirming a direct projection of 5-HT neurons originating in the DRN to the BNST (Figure 3.1g-h)(Phelix et al., 1992). Optical stimulation of these fibers in BNST slices evoked 5-HT release, as measured by fast-scan cyclic voltammetry (FSCV) (Figure 3.1i-j). Furthermore, bath application of the SSRI fluoxetine reliably decreased the rate of 5-HT reuptake, confirming that photostimulation of SERT+ terminals in the BNST originating from the DRN induces 5-HT release (Figure 3.1k-l).

Stimulation of 5-HT inputs to the BNST increases anxiety and fear learning

We next examined whether this 5-HT$^{DRN→BNST}$ circuit is functionally relevant for fear and anxiety-like behavior. To investigate this, *Sert^{Cre}*::ChR2$^{DRN→BNST}$ mice were implanted with bilateral optical fibers and photostimulated in the BNST (473 nm, 20 Hz) using a standard tone-shock fear conditioning paradigm. Optogenetic stimulation of this pathway was paired with a tone that co-terminated with a scrambled footshock. Cued fear was assessed 24 hours after, and contextual fear 48 hours after, the initial fear acquisition session (Figure 3.1m-n). While no changes were observed during fear acquisition, both cued and contextual fear recall were significantly heightened in photostimulated *Sert^{Cre}*::ChR2$^{DRN→BNST}$ mice (Figure 3.1o-q). We next assessed anxiety-like behavior using well-characterized assays, the elevated plus maze (EPM) and novelty-suppressed feeding (NSF) tests. Upon stimulation with light, *Sert^{Cre}*::ChR2$^{DRN→BNST}$ mice exhibited enhanced anxiety-like behavior in both the EPM and NSF (Figure 3.1r-s and Figure 3.3a-b). Importantly, photostimulation did not induce hypolocomotion in the EPM or open field tests nor did it alter home-cage feeding, thus confirming that hypophagia in the NSF assay was due to anxiety and not a reduction in appetitive drive (Figure 3.3c-e). One potential explanation of these results is that terminal stimulation in the BNST produces antidromic spikes in DRN cell bodies that release 5-HT in other brain regions, which could be also be driving these behaviors. In light of this, we probed the mechanism more deeply using converging approaches.

Characterization of 5-HT actions on BNST CRF neurons and contributions of the 5-HT2C receptor to anxiety

To determine a receptor target through which 5-HT is signaling in the BNST, we then examined the impact of optogenetically evoked 5-HT^{DRN} release on postsynaptic neuronal excitability and found a 3.05 ± 0.59 mV depolarization that was blocked by a 5-HT$_{2C}$R antagonist (Figure 3.1t-u). In contrast to previous reports demonstrating co-release of 5-HT and glutamate from DRN projections to the nucleus accumbens(Liu et al., 2014), we did not observe any time-locked light-evoked EPSCs in the BNST (data not shown). These results indicate that 5-HT$^{DRN→BNST}$ projections have a predominantly excitatory effect that is dependent on 5-HT$_{2C}$R signaling. To examine the role of 5-HT$_{2C}$R containing neurons in anxiety-like behavior, we next took advantage of a *Htr2c^{Cre}* mouse line (Figure 3.4a-b)(Burke et al., 2016). Using Designer Receptors Exclusively Activated by Designer Drugs (DREADDs)(Armbruster et al., 2007), we

found that activation of G_q signaling in 5-HT_{2C}R-expressing neurons in the BNST significantly delayed the onset of feeding in the NSF assay without impacting home cage feeding behavior (Figure 3.4c-g), thus phenocopying the effect observed with 5-$HT^{DRN\rightarrow BNST}$ fiber stimulation during NSF. Taken together, these results provide converging evidence that activation of 5-$HT^{DRN\rightarrow BNST}$ inputs elicits anxiety-like behavior via 5-HT_{2C}R signaling.

We then considered the neurochemical phenotype of these target 5-$HT^{DRN\rightarrow}$5-$HT_{2C}R^{BNST}$ neurons and hypothesized that 5-HT via 5-HT_{2C}R modulates the activity of neurons expressing the neuropeptide CRF. This hypothesis was based upon a previous analysis of 5-HT_{2C}R knockout mice, which exhibit an anxiolytic phenotype associated with a reduction of c-fos in CRF^{BNST} neurons(Heisler et al., 2007). Initially, using CRF reporter mice to *a priori* select CRF neurons for recordings, we found a heterogeneous 5HT-induced response of CRF^{BNST} (Figure 3.5a), with only a subset demonstrating a depolarization. Consistent with this, double fluorescence *in situ* hybridization revealed that only a subset of CRF neurons within the dorsal BNST (~70%) and ventral BNST (~43%%) express 5-HT_{2C}Rs (Figure 3.5b-d).

Dissection of BNST CRF neuron projections to the LH and VTA

While CRF signaling within the BNST is classically associated with anxiety-like behavior(Olive et al., 2002; Huang et al., 2010), more recent studies using circuit-based tools have found that optogenetic stimulation of GABAergic projections (which include CRF^{BNST} neurons) to the VTA are anxiolytic(Jennings, Sparta, et al., 2013). This led us to hypothesize the existence of functionally distinct subsets of CRF^{BNST} neurons that gate different behaviors and are differentially sensitive to 5HT. We used fluorescent retrograde tracer beads to label CRF^{BNST} neurons as VTA-projecting or non-VTA-projecting (Figure 3.6a) and found that VTA-projecting CRF neurons ($CRF^{BNST\rightarrow VTA}$ neurons) were hyperpolarized by an average of 5.73 ± 1.24 mV and non-VTA-projecting CRF neurons were depolarized by an average of 2.74 ± 0.39 mV during 5-HT bath application. Moreover, the excitatory response to 5-HT in non-VTA-projecting CRF neurons was reversed in the presence of a 5-HT_{2C} receptor antagonist (Figure 3.6b). Furthermore, all $CRF^{BNST\rightarrow VTA}$ neurons were non-responsive to the 5-HT_2R agonist meta-Chlorophenylpiperazine (mCPP), while all non-VTA projecting CRF neurons were depolarized by mCPP by an average of 3.78 ± 1.17 mV (Figure 3.5e-h). These findings suggest an anatomically distinct

response to 5-HT by different subsets of CRF^{BNST} neurons. The subset of CRF^{BNST} neurons expressing 5-HT_{2C}Rs do not project to the VTA and are depolarized by 5-HT, whereas the $CRF^{BNST\rightarrow VTA}$ neurons are hyperpolarized by 5-HT, via actions at another 5-HT receptor.

To determine if this 5-HT-dependent mechanism extended to other anxiolytic efferents, we injected retrograde tracer beads into the lateral hypothalamus (LH) of CRF reporter mice and found 5-HT had similar bidirectional effects on non-LH and LH projecting CRF^{BNST} neurons (Figure 3.7a-c). Noting the functional similarities between these two populations, we used retrograde tracing to determine that roughly ~58% of CRF^{BNST} neurons have projections to the LH or VTA (Figure 3.7d-f). Notably, ~20-31% of these CRF^{BNST} output neurons form parallel projections to these structures.

In light of recent reports that CRF^{BNST} neurons are exclusively GABAergic(Dabrowska et al., 2011), we hypothesized that non-VTA-projecting CRF^{BNST} neurons may locally inhibit BNST→VTA neurons to promote fear and anxiety. To test this hypothesis, we injected Crf^{Cre} mice with a Cre-inducible ChR2 into the BNST and retrograde tracer beads into the VTA. We then recorded light-evoked IPSCs from non-ChR2 (ChR2-negative, retrograde tracer-positive) VTA-projecting BNST neurons (Figure 3.6c). Photostimulation produced action potentials in CRF^{BNST} neurons and light-evoked IPSCs in non-ChR2 VTA-projecting neurons, indicating that CRF^{BNST} neurons form local GABAergic synapses with BNST neurons that project to the VTA. Repeating these same experiments in Crf^{CRE}::$ChR2^{BNST}$ mice with retrograde tracer beads in the LH, we found that we could light-evoke GABA currents in LH projecting neurons as well (Figure 3.7g-i). Moreover, we observed that 5-HT increased GABAergic transmission on to BNST→VTA projecting neurons in a tetrodotoxin and 5-HT_{2C}R antagonist dependent manner (Figure 3.6d-f and Figure 3.7j-n). Similar effects of 5-HT on GABAergic transmission were found in BNST→LH projecting neurons (Figure 3.7o-v). Furthermore, slice recordings in a CRF reporter line indicates that 5-HT does not increase GABAergic transmission on to the general population of CRF^{BNST} neurons nor does it directly excite non-CRF VTA projecting neurons (Figure 3.8). The 5-HT_2R agonist mCPP also increased GABAergic but not glutamatergic transmission in the BNST (Figure 3.9). Finally, to test if optically evoked 5-HT can inhibit BNST outputs to the VTA, we performed slice recordings in the BNST of $Sert^{Cre}$::$ChR2^{DRN\rightarrow BNST}$ mice and found that brief photostimulation of 5-HT terminals in the BNST increased sIPSCs on to VTA projecting BNST neurons in a manner similar to bath applied 5-HT (Figure 3.10a-c).

Together, these experiments indicate that CRF^{BNST} neurons inhibit at least two major BNST outputs to the VTA and LH that are reported to be anxiolytic (Kim et al., 2013; Jennings, Sparta, et al., 2013), providing mechanistic insight into the aversive actions of 5-HT signaling in the BNST.

We next took advantage of an intersectional strategy for direct visualization of these non projecting, putatively local CRF^{BNST} neurons(Fenno et al., 2014). By coupling retrograde Cre-dependence flpases (HSV-LSL1-mCherry-IRES-flpo) in the VTA and LH with INTRSECT(Cre_{on}/flp_{off})-Chr2-eYFP in the BNST of *Crf*^{cre} mice (*Crf*^{Cre}::Intrsect-$ChR2^{BNST}$ mice), we were able to genetically isolate non-VTA/LH projecting CRF neurons in the BNST. We also infused Cre-dependent HSV-mCherry vector in a subset of *Crf*^{Cre}::Intrsect-$ChR2^{BNST}$ mice as a control. In HSV-flp infused *Crf*^{Cre}::Intrsect-$ChR2^{BNST}$ mice, we observed a significant reduction in YFP+ cells in the ventral BNST (Figure 3.10d-f), indicating that a large proportion of VTA and LH-projecting CRF^{BNST} neurons are located in the ventral BNST. We also found that 5-HT robustly depolarized these *Crf*^{Cre}::Intrsect-$ChR2^{BNST}$ neurons compared to CRF neurons at large (Figure 3.6g-i). Furthermore, we observed light evoked IPSCs in the BNST of *Crf*^{Cre}::Intrsect-$ChR2^{BNST}$ mice, confirming local GABA release from these neurons (Figure 3.10g). These results support the existence of a separate population of local CRF^{BNST} neurons that is excited by 5-HT and increases local GABAergic transmission in the BNST, distinct from a population of CRF^{BNST} neurons that project to and release GABA in the VTA or the LH (Figure 3.10h-j).

BNST CRF neurons contribute to SSRI-induced increases in fear

To probe the translational relevance of these BNST microcircuits, we adopted a pharmacological approach using SSRIs. SSRIs represent one of the most widely used classes of drugs for psychiatric disorders. One limitation of SSRIs is that acute administration can lead to negative behavioral states(Gorman et al., 1987; Westenberg & den Boer, 1989), a finding that is recapitulated in rodent models(Burghardt et al., 2007; Dekeyne et al., 2000; Belzung et al., 2001; Javelot et al., 2011; Liu et al., 2010; Mombereau et al., 2010). Importantly, the BNST has been demonstrated to be an anatomical site of action for some of the aversive actions of SSRIs in rodents(Ravinder et al., 2013). This provided the opportunity to test our model that 5-HT in the BNST drives aversive behavior through inhibition of BNST outputs to the VTA. We observed that an acute systemic injection of the SSRI fluoxetine increased GABAergic transmission on to VTA projecting neurons in the BNST (Figure 3.11a-d). We then

interrogated the role of CRF^{BNST} neurons in acute fluoxetine-enhanced anxiety using *Crf*^{CRE} mice transduced in the BNST with the Cre-inducible Gi-coupled DREADD. We found that acute fluoxetine potentiated anxiety-like behavior, and this effect was blocked by chemogenetic inhibition of CRF^{BNST} neurons (Figure 3.11e-h).

To evaluate directly whether endogenous 5-HT acts on CRF^{BNST} neurons to enhance cued fear memory, we used the same chemogenetic approach to silence CRF^{BNST} neurons during fluoxetine treatment and subsequent fear conditioning (Figure 3.11i). Chemogenetic inhibition of CRF^{BNST} neurons also significantly attenuated fluoxetine-induced enhancement of cued fear recall, providing proof of concept that augmentation of 5-HT via acute SSRI treatment recruits CRF^{BNST} neurons to enhance fear-related behavior (Figure 3.11j-k). Next, using connectivity based chemogenetic approaches; we tested whether inhibition of BNST outputs to the VTA and LH is a critical component of 5-HT→BNST-induced aversive states. We observed that activation of G_q signaling in VTA- and LH-projecting BNST neurons, targeted by HSV-Cre-eYFP infused in the VTA and LH and Cre-dependent Gq-coupled DREADD infused in the BNST (HSV^{Cre}::$hM3Dq^{BNST}$), significantly attenuated fluoxetine enhancement of cued fear recall (Figure 3.11l-o). Together, these data provide compelling evidence that acute fluoxetine engenders aversive behavior by recruiting CRF neurons in the BNST that in turn inhibit putative GABAergic (anxiolytic and stress buffering) outputs from the BNST to the VTA and LH. Pharmacological interventions that target this circuit may improve adverse symptoms during the initial weeks of SSRI treatment. Based on the critical role for CRF^{BNST} neurons in fluoxetine induced aversive behavior, we examined the impact of a systemic CRF_1R antagonist on SSRI enhancement of cued fear recall. Notably, blocking the CRF system reduced this aversive state and abolished the increase in sIPSCs in LH-projecting neurons in the BNST during bath application of 5-HT (Figure 3.12). This provides translational evidence that CRF_1R antagonists given in concert with SSRIs could be a promising treatment for anxiety disorders.

Taken together, these data reveal a discrete 5-HT responsive circuit in the BNST that underlies pathological anxiety and fear associated with a hyperserotonergic state (Figure 3.13). SSRIs are currently a first-line treatment for anxiety and panic disorders but can acutely exacerbate symptoms, resulting in poor therapeutic compliance. Our results strongly implicate 5-HT engagement of a local BNST inhibitory microcircuit in acute SSRI induced aversive behaviors in rodents, and could potentially be involved in the

early adverse events seen in clinical populations, emphasizing the need to identify compounds that selectively target both genetically-defined and pathway-specific cell populations.

3.4 Figures

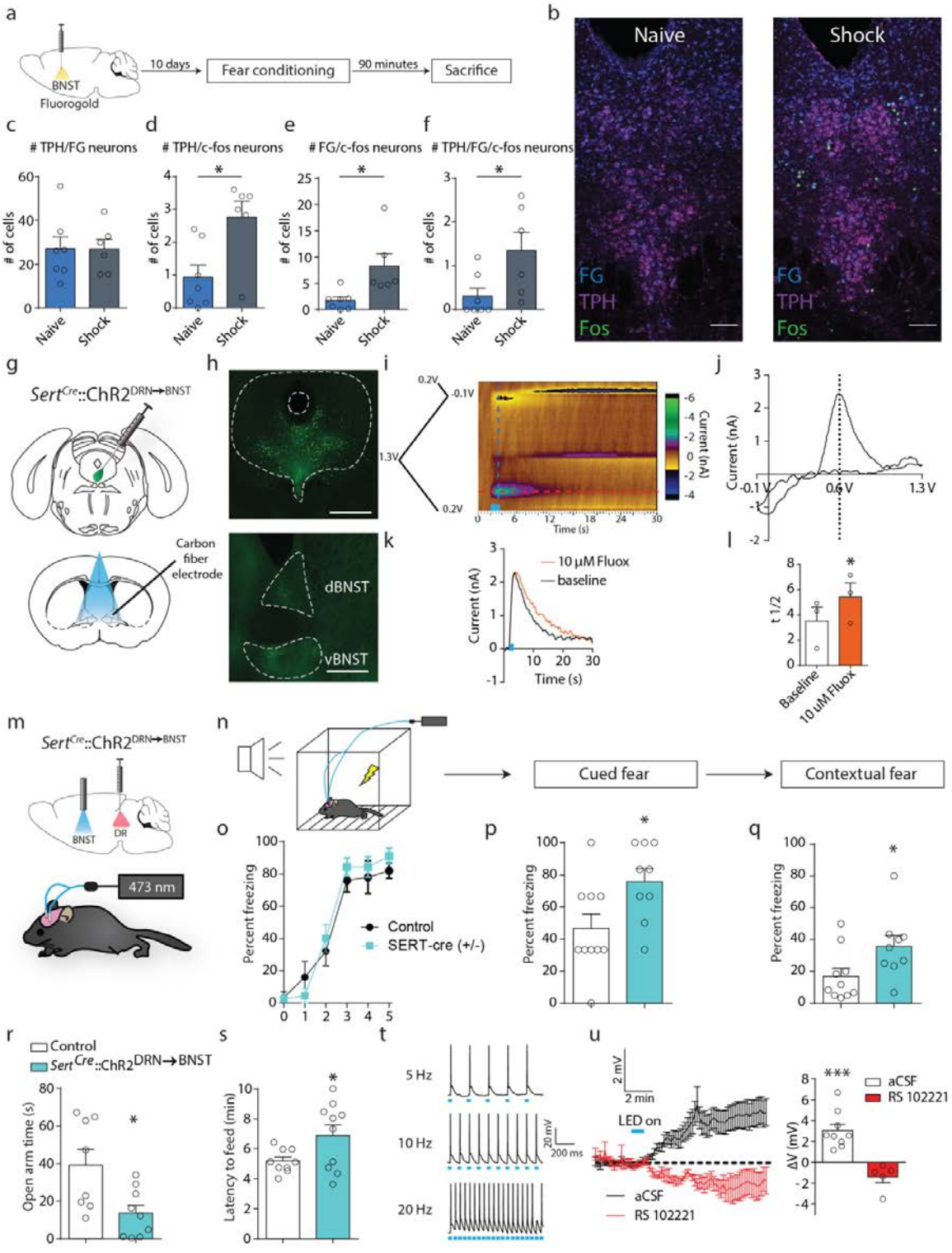
a
BNST
Fluorogold
10 days
Fear conditioning
90 minutes
Sacrifice
b
Naive
Shock
FG
TPH
Fos
c
TPH/FG neurons
d
TPH/c-fos neurons
e
FG/c-fos neurons
f
TPH/FG/c-fos neurons
of cells
Naive
Shock
g
Sert^Cre::ChR2^DRN→BNST
Carbon fiber electrode
h
i
0.2V
-0.1V
1.3V
0.2V
Current (nA)
Time (s)
j
Current (nA)
-0.1 V
0.6 V
1.3 V
k
10 μM Fluox
baseline
Current (nA)
Time (s)
l
t 1/2
Baseline
10 uM Fluox
m
Sert^Cre::ChR2^DRN→BNST
BNST
DR
473 nm
n
Cued fear
Contextual fear
o
Percent freezing
Control
SERT-cre (+/-)
p
Percent freezing
q
Percent freezing
r
Control
Sert^Cre::ChR2^DRN→BNST
Open arm time (s)
s
Latency to feed (min)
t
5 Hz
10 Hz
20 Hz
20 mV
200 ms
u
2 mV
2 min
LED on
aCSF
RS 102221
ΔV (mV)
aCSF
RS 102221

Figure 3.1: Optogenetic identification of a 5-HT DRN→BNST projection that elicits anxiety and fear-related behavior. (a) Experimental timeline for c-fos labeling of 5-HT$^{DRN→BNST}$ neurons following an aversive footshock stimulus. (b) Representative images of fluorogold (blue), tryptophan hydroxylase (violet), and c-fos (green) staining in the DRN for 13 mice. Scale bars: 100 µm. (c-f) Histograms depicting the number of double and triple labeled neurons in the DRN of naïve and shocked mice. (c) There were no significant differences in the number of BNST projecting 5-HT^{DRN} neurons between groups. (d-f) Footshock lead to significant elevations in the number of c-fos+ ("activated") 5-HT neurons (t_{11}=2.975, p<0.05, Student's unpaired two-tailed t-test, n=7 naïve and n=6 shock mice), c-fos+, fluorogold labeled neurons (t_{11}=2.836, p<0.05, Student's unpaired two-tailed t-test, n=7 naïve and n=6 shock mice), and triple labeled neurons (t_{11}=2.374, p<0.05, Student's unpaired two-tailed t-test, n=7 naïve and n=6 shock mice). (g) Experimental configuration for light-evoked FSCV experiments in *Sert^{Cre}*::ChR2$^{DRN→BNST}$ mice (h) Coronal images showing ChR2-YFP expression in soma of the DRN and axons of the BNST. Scale bars: 500 µm. (i) Representative color plot of 5-HT release to optical stimulation (blue bar, 20 Hz 20 pulses) for 3 mice (j) Representative cyclic voltammogram at peak 5-HT (blue dashed line panel E) for 3 mice. (k) Representative Current vs. Time trace at baseline (black) and following 10 µM fluoxetine (red) for 3 mice. (l) Clearance half-life of 5-HT at baseline (white bar) and following 10 µM fluoxetine (red bar). (t_2=8.43, p<0.05, Student's paired two-tailed t-test, n = 3 slices from 3 mice) (m) *Sert^{Cre}* mice were transduced in the DRN and implanted with bilateral optical fibers in the BNST. (n) Schematic of fear conditioning procedures in *Sert^{Cre}*::ChR2$^{DRN→BNST}$ mice. (o-q) Photostimulation during fear acquisition had no effect on freezing behavior during fear learning but increased freezing during cued (t_{17}=2.436, p<0.05, Student's unpaired two-tailed t-test, n=10 control, n=9 ChR2) and contextual fear recall (t_{17}=2.271, p<0.05, Student's unpaired two-tailed t-test, n=10 control, n=9 ChR2). (r) Light delivery to the BNST reduced open arm time in the EPM (t_{15}=2.79, p<0.05, Student's unpaired two-tailed t-test, n=8 control, n=9 ChR2) and (s) increased latency to feed in the NSF (t_{17}=2.19, p<0.05, Student's unpaired two-tailed t-test, n=9 control, n=10 ChR2). (t) Action potentials generated by photostimulation in the DRN (5 Hz (top), 10 Hz (middle), 20 Hz (bottom), 473 nm). (u) Depolarization in cells (t_8=5.20, p<0.01, One-sample t-test, n=9 cells from 4 mice) after photostimulation in the BNST (5 Hz, 10 s, 473 nm) and blockade of this response by 5 µM RS 102221 (t_4=2.5, p>0.05, One-sample t-test, n=5 cells from 2 mice). Data are mean ± s.e.m. *P<0.05; **P<0.01; ***P<0.001.

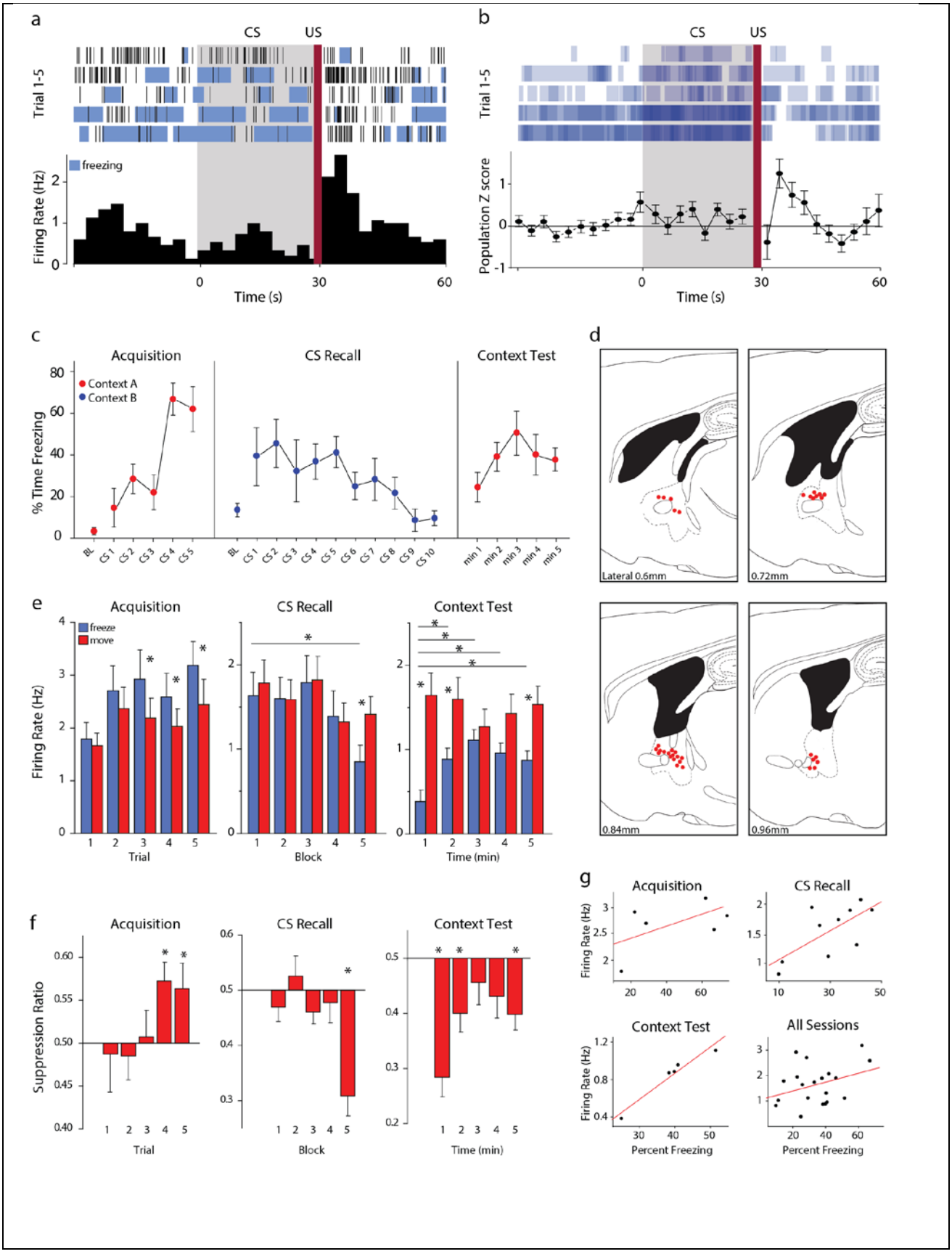
a
CS
US
Trial 1-5
freezing
Firing Rate (Hz)
Time (s)
b
Population Z score
c
Acquisition
CS Recall
Context Test
Context A
Context B
% Time Freezing
d
Lateral 0.6mm
0.72mm
0.84mm
0.96mm
e
freeze
move
Trial
Block
Time (min)
f
Suppression Ratio
g
Percent Freezing
All Sessions

Figure 3.2: In vivo recordings in BNST neurons during fear conditioning reveal opposite patterns of activation during acquisition and recall. (a) Representative neuron firing rate and (b) population Z score of the firing rate for BNST neurons (n=45 cells from 7 mice) 30 s before conditioned stimulus (tone), during the conditioned stimulus, and 30 seconds after the unconditioned stimulus. (c) Percentage time spent freezing during fear acquisition, cued fear recall and contextual fear recall. (d) Electrode placements for BNST recordings. (e) Raw firing rates during freezing (blue) versus movement (red) epochs were averaged across all putative principal neurons (firing rate <10Hz). Acquisition: Cells in BNST exhibited greater average firing rates during freezing epochs compared to movement epochs during CS3 (t_{44}=2.88, p<0.01, Student's unpaired two-tailed t-test), 4 (t_{44}=3.14, p<0.01, Student's unpaired two-tailed t-test), and 5 (t_{44}=4.4, p<0.001, Student's unpaired two-tailed t-test) (n=45 cells from 7 mice). CS Recall: Average firing rates during freezing epochs decreased over CS presentations such that firing during block 5 was significantly less than block 1 (t_{41}=3.44, p=0.001, Student's unpaired two-tailed t-test). Freezing firing rates during block 5 were also significantly less than movement epochs during block 5 (t_{41}=4.03, p<0.001, Student's unpaired two-tailed t-test) (n=42 cells from 7 mice). CX test: Average firing rate was significantly greater during movement versus freezing epochs during minutes 1 (t_{44}=4.83, p<0.001, Student's unpaired two-tailed t-test), 2 (t_{44}=3.17, p<0.01, Student's unpaired two-tailed t-test), and 5 (t_{44}=4.36, p<0.001, Student's unpaired two-tailed t-test) (n=45 cells from 7 mice). (f) Freezing-related changes in firing rates during the CS were determined by measuring the ratio of average firing rates during freezing versus movement epochs for each session. Acquisition: Activity during freezing epochs increased significantly relative to movement epochs during CS4 (t_{45}=3.26, p<0.01, Student's unpaired two-tailed t-test) and CS5 (t_{45}=2.17, p<0.05, Student's unpaired two-tailed t-test) (n=46 cells from 7 mice). CS Recall: Freezing significantly suppressed activity relative to movement epochs during the last two CS presentations (t_{47}=5.29, p=<0.001, Student's unpaired two-tailed t-test) (n=48 cells from 7 mice) CX test: Freezing significantly suppressed activity during minutes 1 (t_{44}=6.06, p<0.001, Student's unpaired two-tailed t-test), 2 (t_{44}=2.92, p<0.01, Student's unpaired two-tailed t-test), and 5 (t_{44}=3.55, p=.001, Student's unpaired two-tailed t-test) (n=45 cells from 7 mice). (g) Plots showing correlation between freezing behavior and firing rate of BNST neurons across sessions and for all sessions. Data are mean ± s.e.m. *P<0.05 **P<0.01; ***P<0.001. Scale bar = 100 µm.

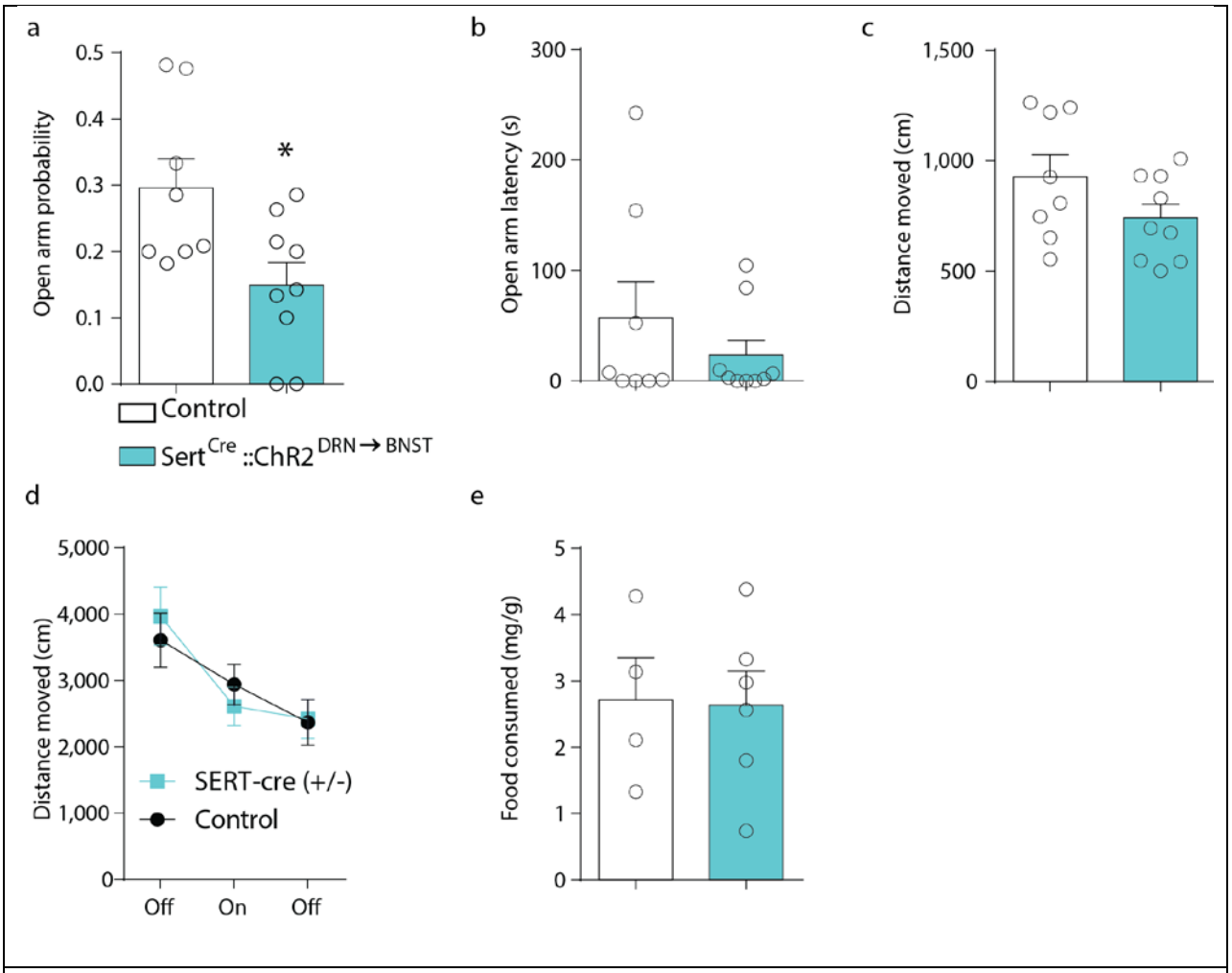

Figure 3.3: Effects of optogenetic stimulation of 5HT inputs to the BNST on feeding, anxiety and locomotion. (a-c) *Sert*^{Cre}::ChR2$^{DRN→BNST}$ mice exhibited reduced probability (t_{15}=2.67, p<0.05, Student's unpaired two-tailed t-test, n=8 control, n=9 ChR2) and latency (t_{15}=1.003, p>0.05, Student's unpaired two-tailed t-test, n=8 control, n=9 ChR2) to enter the open arms of the EPM without exhibiting locomotor deficits. (d) Photostimulation of 5-HT$^{DRN→BNST}$ terminals had no effect on locomotor activity in the open field (n=9 control, n=11 ChR2) or (e) home cage feeding (n=4 control, n=6 ChR2). Data are mean ± s.e.m. *P<0.05.

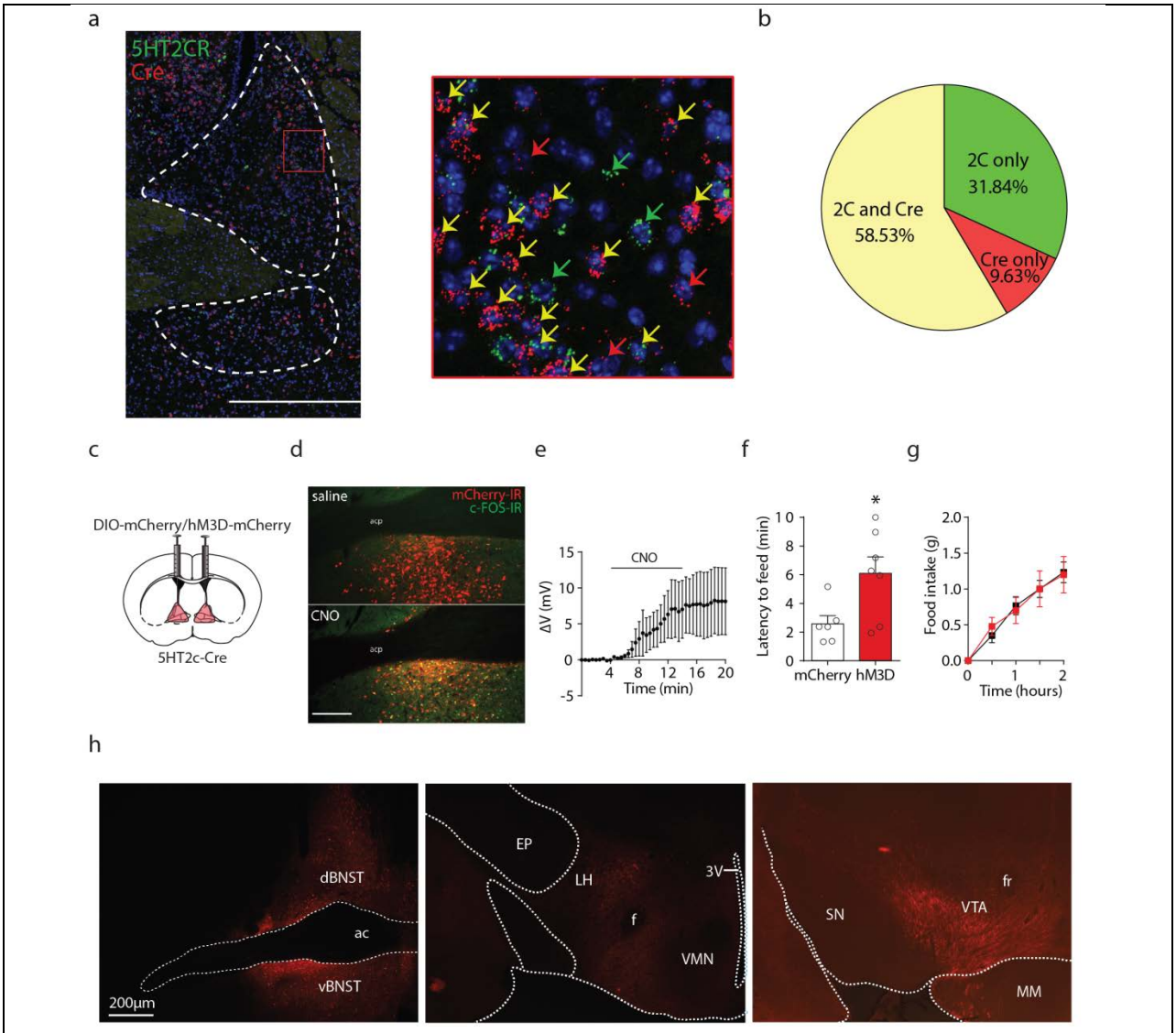

Figure 3.4: Chemogenetic activation of 5-HT2CR expressing neurons in the BNST increases anxiety-like behavior. (a) Confocal images of coronal BNST slices obtained from *htr2c*^{Cre} mice following double fluorescence in situ hybridization for 5-HT$_{2C}$R and cre. Yellow arrows indicate cells in which there is colocalization, red arrows indicate cells in which only Cre is expressed and green arrows indicate cells in which only 5-HT$_{2C}$R is expressed. (b) Pie chart representing the distribution of genetic markers in BNST neurons. (c) Experimental configuration in *Htr2c*^{cre}::hM3Dq^{BNST} mice. (d) Coronal images showing cfos induction in 5-HT$_{2C}$R expressing neurons in the BNST of *Htr2c*^{Cre}::hM3Dq^{BNST} or *Htr2c*^{Cre}::mCherry^{BNST} mice following CNO injection. (e) Bath application of CNO depolarized 5HT$_{2C}$R-expressing neurons expressing hM3Dq in slice (n=3 cells from 3 mice). (f) Chemogenetic stimulation of 5-HT$_{2C}$R expressing neurons in BNST increased latency to feed in the NSF (t_{11}=2.591, p<0.05, Student's unpaired two-tailed t-test, n=6; mCherry, n=7 hM3Dq). (g) Chemogenetic activation of 5-HT$_{2C}$R-expressing BNST neurons had no effect on home cage feeding (n=5 mCherry, n=6 hM3Dq). (h) Confocal images from *Htr2c*^{Cre}::mCherry^{BNST} mice showing mCherry expression in 5-HT$_{2C}$R-expressing soma in the BNST and fibers in the LH and VTA. Data are mean ± s.e.m. *P<0.05. Scale bar = 100 µm.

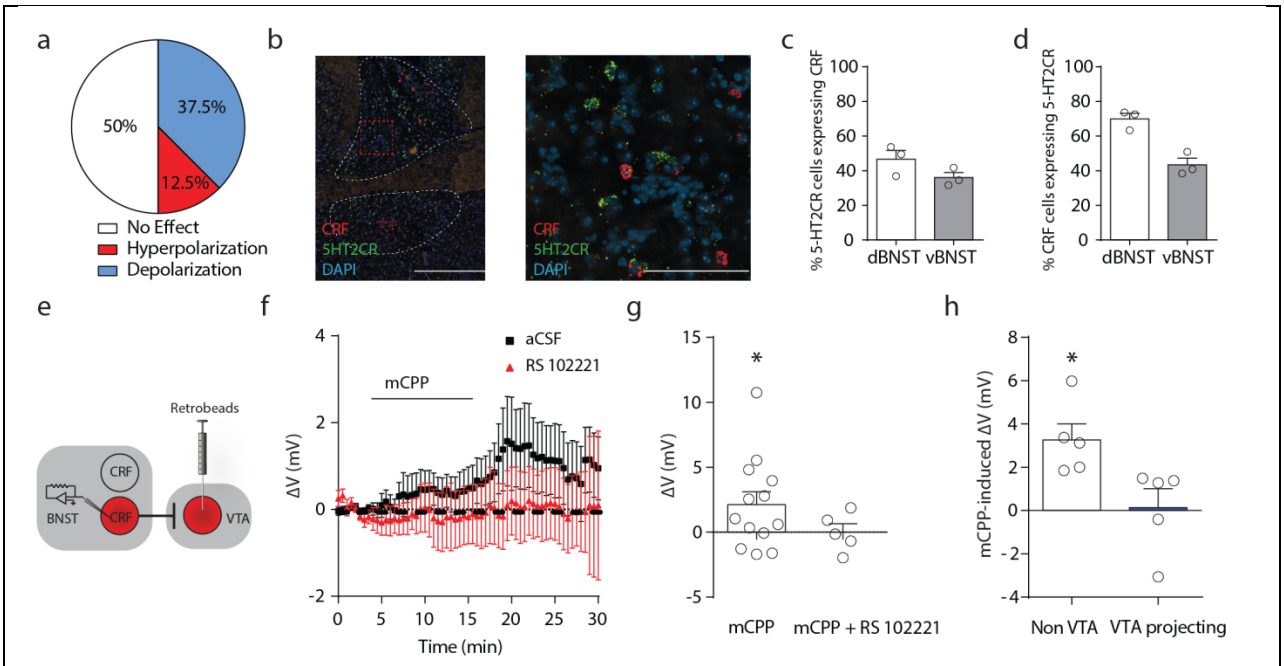

Figure 3.5: Electrophysiological characterization of 5-HT responses and 5-HT receptor expression in BNST CRF neurons (a) A pie chart showing the distribution of CRF^{BNST} neurons that were depolarized, hyperpolarized, or had no response to 5-HT (n=8 cells from 4 mice). (b) Coronal images of the BNST showing colocalization of $5\text{-}HT_{2C}$Rs with CRF mRNA using double fluorescence *in situ* hybridization and (c-d) histograms showing the % of $5\text{-}HT_{2C}$ neurons that express CRF and the % of CRF neurons that express $5\text{-}HT_{2C}$Rs in the BNST (n=3 slices from 3 mice). (e) Recording configuration in CRF^{BNST} neurons. (f) Slice electrophysiology in BNST of *Crf* reporter mice showing depolarization of all (VTA-projecting and non-projecting) CRF neurons following bath application of the $5\text{-}HT_2$ receptor agonist mCPP (n=12 cells from 6 mice) and blockade of this response by the $5\text{-}HT_{2C}$ receptor antagonist RS 102221 (n=5 cells from 3 mice). (g) Change in membrane potential induced by mCPP (t_{12}=2.18, p<0.05, One-sample t-test, n=12 cells from 6 mice) is blocked by a $5\text{-}HT_{2C}$R antagonist (n=5 cells from 3 mice). (h) mCPP selectively depolarizes non-VTA projecting CRF^{BNST} neurons (n=3 cells from 2 mice non VTA-projecting CRF, n=5 cells from 4 mice VTA-projecting CRF). Data are mean ± s.e.m. *P<0.05.

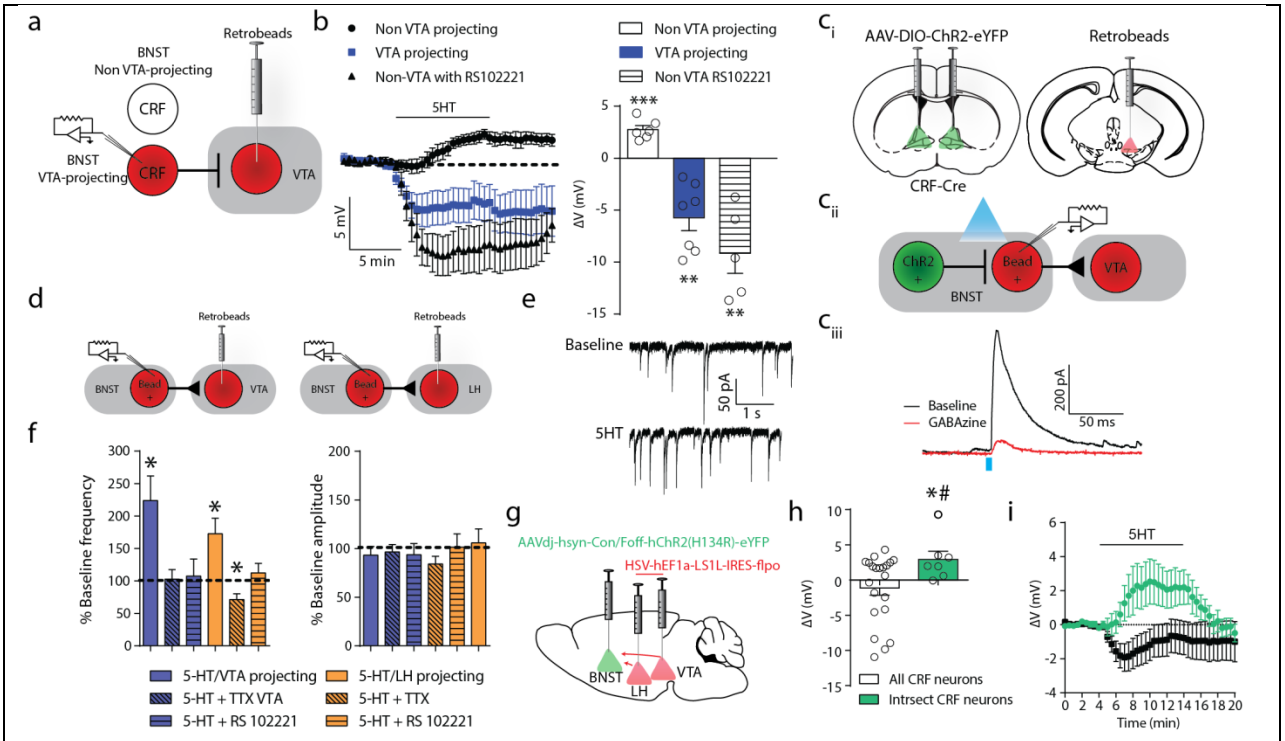

Figure 3.6: Serotonin activates a local population of BNST CRF neurons that inhibits outputs to the midbrain. (a) Recording scheme for CRF reporter mice injected with retrograde tracer beads in the VTA. (b) 5-HT depolarizes local CRF neurons (t_5=7.06 , p<0.001, One-sample t-test, n=6 cells from 4 mice) in the BNST while hyperpolarizing $CRF^{BNST \rightarrow VTA}$ neurons (t_6=4.64, p<0.01, One-sample t-test, n=7 cells from 6 mice). Non VTA projecting CRF neurons are hyperpolarized by 5-HT in the presence of the 5-HT_{2C}R antagonist RS102221 (t_4=4.74, p<0.01, One-sample t-test, n=5 cells from 3 mice) (c_{i-ii}) Schematic depicting infusions and recording configuration for Crf^{Cre}::$ChR2^{BNST}$ mice injected with retrograde tracer beads in the VTA. (c_{iii}) Representative trace of light-evoked IPSC in beaded (i.e. VTA projecting), non-ChR2 expressing neurons in the BNST of Crf^{Cre}::ChR2 mice with retrograde tracer beads in the VTA (n=8 cells from 3 mice) and blockade of this response by GABAzine ($F_{11,33}$=53.16, p<0.001, Repeated Measures One-way ANOVA, n=4 cells from 3 mice). (d) Recording scheme for C57BL/6 mice with retrograde tracer beads in the VTA or LH (e) Representative traces of sIPSCs in BNST neurons that project to the VTA before and after 5-HT application for 5 cells from 4 mice (f) Bar graphs showing magnitude of 5-HT effect on average sIPSC frequency in BNST neurons that project to the VTA (t_4=3.257, p<0.05, One-sample t-test, n=5 cells from 4 mice) and in BNST neurons that project to the LH (t_5=3.027, p<0.05, One-sample t-test, n=6 cells from 3 mice) and blockade of these responses by TTX and RS 102221. Effects on amplitude were non-significant. (g) Experimental scheme for experiments with Crf^{Cre}::Intrsect-$ChR2^{BNST}$mice. (h-i,) 5-HT significantly depolarizes non-projecting CRF ("Intrsect") neurons in the BNST (t_6=2.501, p < 0.05, One-sample t-test, n=7 cells from 5 mice) and produces a significant change in membrane potential in CRF Intrsect neurons compared to all CRF neurons (t_{26}=2.08, p<0.05, Student's unpaired two-tailed t-test, n=21 cells from 14 mice for experiments in all CRF neurons and n=7 cells from 5 mice for Crf^{Cre}::Intrsect-$ChR2^{BNST}$ experiments). Data are mean ± s.e.m. *P<0.05; **P<0.01; ***P<0.001. # donates P<0.05 for the Student's unpaired two-tailed t-test between all CRF neurons and CRF Intrsect neurons in panel 2h.

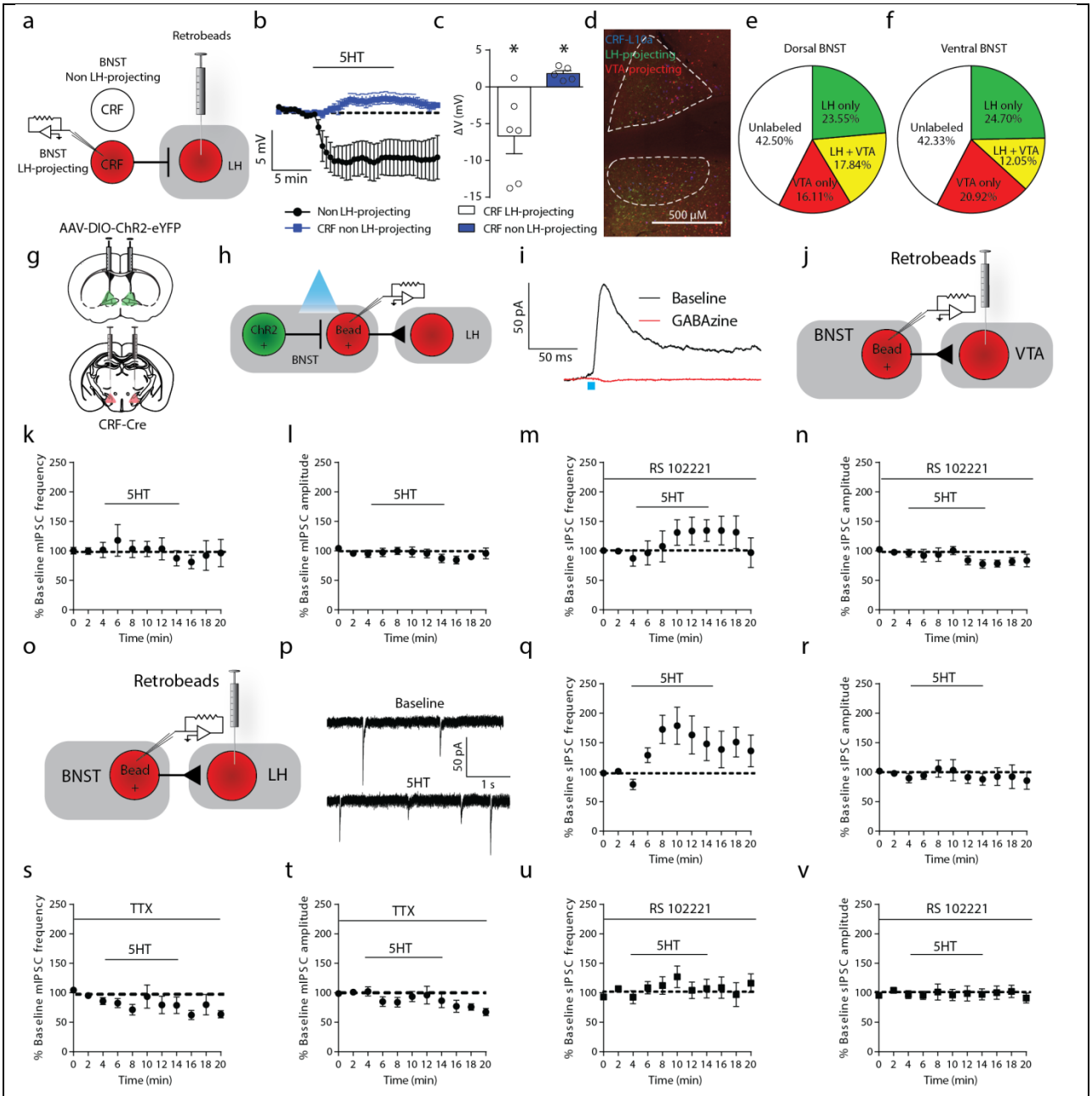

Figure 3.7: 5-HT activates inhibitory microcircuits in the BNST that modulate outputs to the LH. (a) Recording configuration in CRF reporter mice infused with retrograde tracer beads in the LH. (b) Average traces of 5-HT induced depolarization in LH projecting vs non-projecting neurons (c) Histograms showing 5-HT induced depolarization in non-LH projecting BNST neurons (t_4=4.425, p<0.05, One-sample t-test, n=5 cells from 3 mice) and hyperpolarization in LH-projecting neurons (t_5=2.789, p<0.05, One-sample t-test, n=6 cells from 3 mice). (d) Confocal image of retrogradely CTB-labeled VTA (red) and LH (green) outputs in a *CRF-L10a* reporter (blue). (e-f) Pie charts depicting the percentage of LH-projecting only, VTA-projecting only, collateralizing, and CTB-negative (unlabeled) CRF in neurons in the dorsal and ventral aspects of the BNST (n=6 hemispheres from 3 mice). (g) Experimental schematic depicting viral infusions into the BNST and retrograde tracer bead infusions into the LH of Crf^{Cre}::$ChR2^{BNST}$ mice. (h) Recording configuration in Crf^{Cre}::$ChR2^{BNST}$ mice with LH tracer beads (i) Representative trace of light

evoked IPSCs in LH projecting neurons (n=7 cells from 4 mice) and blockade of this light evoked response by GABAzine (n=2 cells from 2 mice). (j) Recording configuration in VTA projecting neurons in the BNST of C57BL/6 mice. (k-l) 5-HT has no effect on miniature IPSC frequency or amplitude in BNST→VTA projecting neurons (n=7 from 4 mice). (m-n) 5-HT has no effect on sIPSC frequency or amplitude in the presence of the 5-HT_{2C}R antagonist RS102221 (n=5 cells from 4 mice). (o) Recording configuration in LH projecting neurons in the BNST of C57BL/6 mice (p) Representative traces showing an increase in sIPSC frequency in the presence of 5-HT for 6 cells from 3 mice (q-r) 5-HT increases sIPSC frequency but not amplitude in BNST→LH projecting neurons ($F_{11,55}$=11.65, p<0.01, Repeated measures one-way ANOVA, n=6 cells from 3 mice). (s-t) 5-HT has no effect on miniature IPSC frequency or amplitude (n=5 cells from 3 mice). (u-v) 5-HT has no effect on sIPSC frequency or amplitude in the presence of RS102221 (n=6 cells from 4 mice). Data are mean ± s.e.m. *P<0.05.

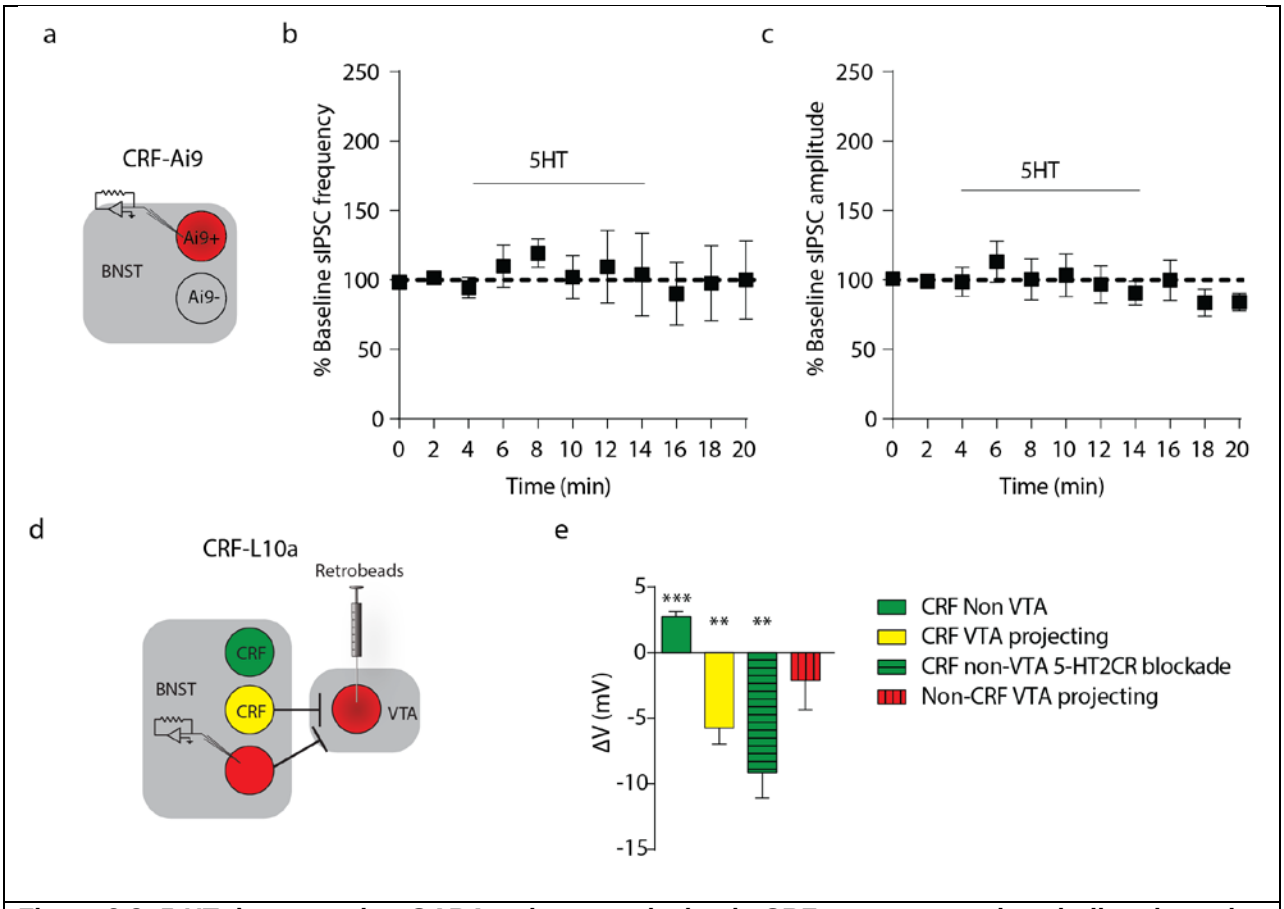

Figure 3.8: 5-HT does not alter GABAergic transmission in CRF neurons nor does it directly excite non-CRF VTA projecting neurons in the BNST. (a) Recording configuration in CRF^{BNST} neurons in a CRF reporter. (b-c) 5-HT has no effect on sIPSC frequency or amplitude in the total population of CRF neurons (n=5 cells from 3 mice). (d) Recording configuration in non-CRF, VTA projecting neurons in the BNST and average trace of 5-HT effect on membrane potential in non-CRF, VTA projecting neurons in the presence of TTX. (e) Histogram summarizing 5-HT effects on membrane potential in local and VTA projecting CRF neurons and local CRF neurons in the presence of the $5\text{-}HT_{2C}$ receptor antagonist RS102221 (same data shown in Figure 3.6b) juxtaposed with the lack of effect of 5-HT on membrane potential in non-CRF, VTA projecting neurons (t_4=0.9381, ns, One-sample t-test, n=5 cells from 3 mice). Data are mean ± s.e.m. **P<0.01; ***P<0.001.

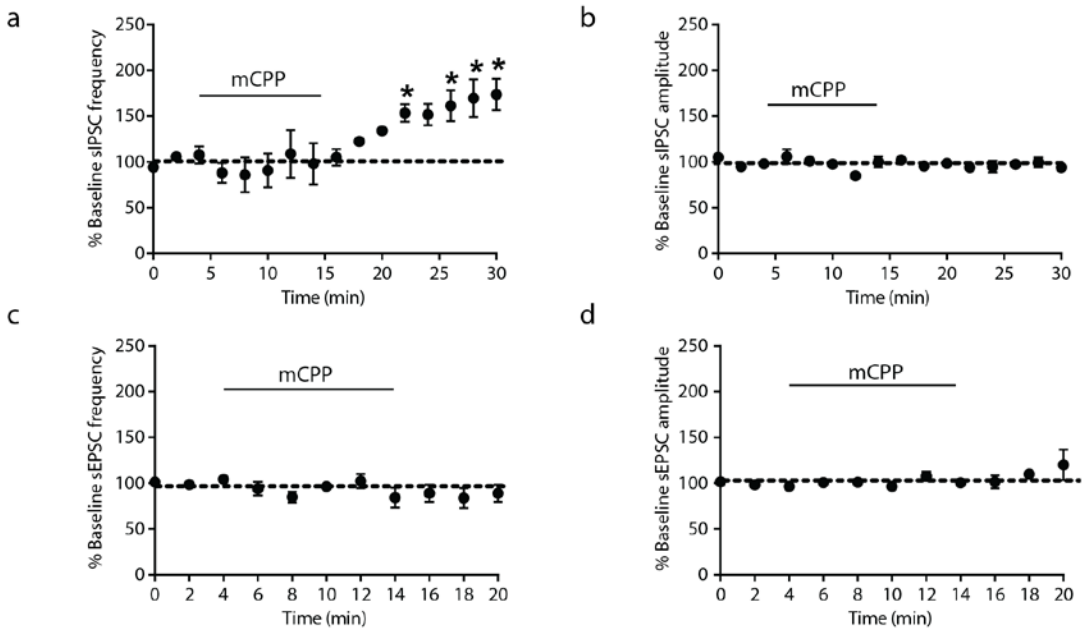

Figure 3.9: The 5-HT2 agonist mCPP increases GABAergic but not glutamatergic transmission in the BNST. (a-b) mCPP increases sIPSC frequency ($F_{15,30}$=1.863, p<0.001, Repeated measures one-way ANOVA, n=3 cells from 3 mice) but not amplitude in the BNST of C57BL/6 mice. (c-d) mCPP has no effect on sEPSC frequency or amplitude in the BNST of C57BL/6 mice (n=5 cells from 3 mice). Data are mean ± s.e.m. *P<0.05.

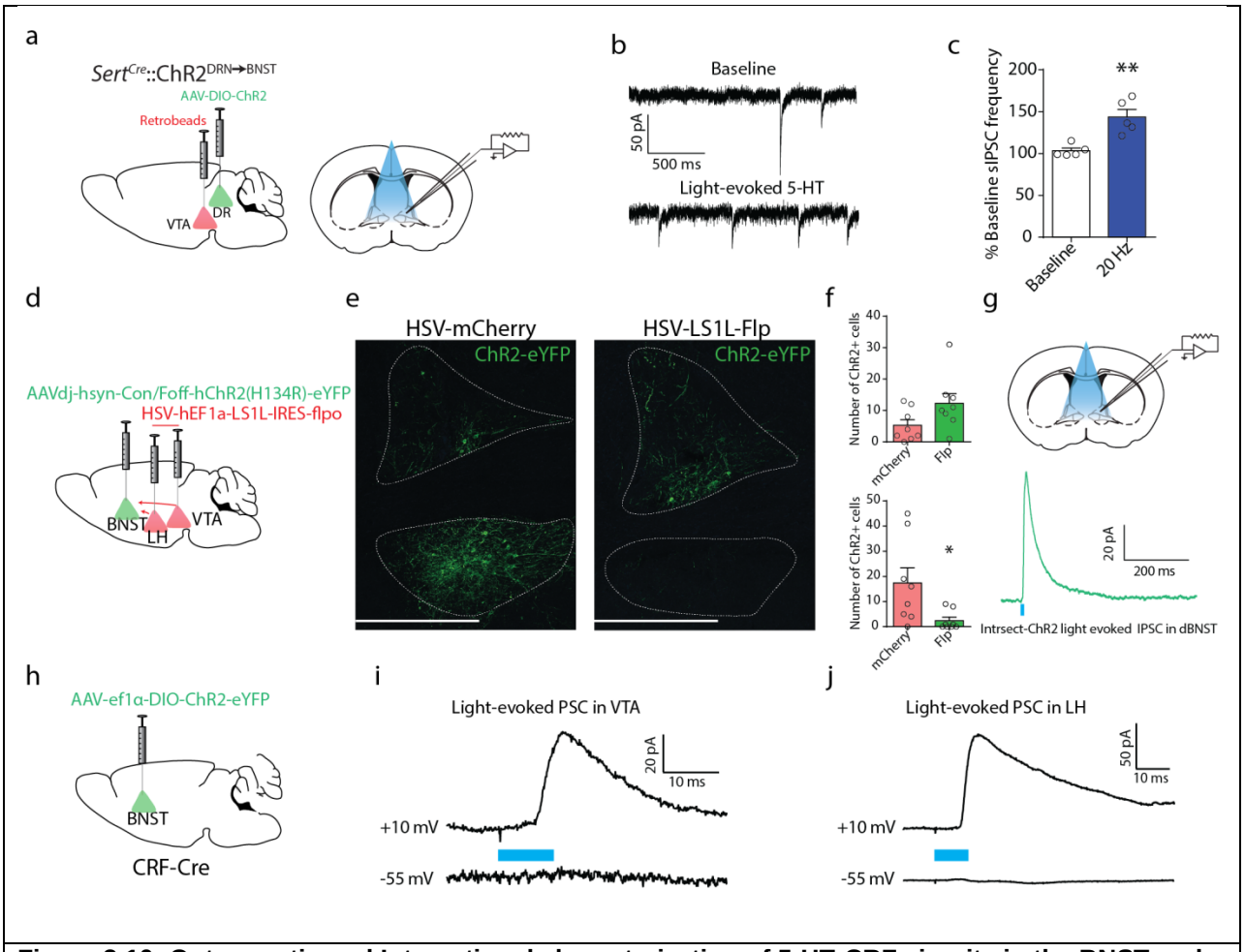

Figure 3.10: Optogenetic and Intrsectional characterization of 5-HT-CRF circuits in the BNST and outputs to the midbrain (a) Experimental design and recording configuration from *Sert*^{Cre}::ChR2$^{DRN\rightarrow BNST}$ mouse with retrograde tracer beads in the VTA. (b) Representative traces for 5 cells from 3 mice depicting the increase in sIPSCs in VTA projecting neurons in the BNST following light-evoked 5-HT release (c) Histogram summarizing the effect of light evoked 5-HT release on sIPSC frequency in VTA projecting neurons (t_4=4.890, p<0.01, One-sample t-test, n=5 cells from 3 mice). (d) Experimental configuration in *Crf*^{Cre}::Intrsect-ChR2^{BNST} mice. (e) Representative images from 4 *Crf*^{Cre}::HSV-LSL1-mCherry-flpo$^{VTA/LH}$ mice and 4 *Crf*^{Cre}::HSV-LSL1-mCherry$^{VTA/LH}$ mice injected with Intrsect-ChR2-eYFP in the BNST. (f) Cell counts of eYFP+ neurons from HSV-LSL1-flpo and HSV-LSL1-mCherry injected *Crf*^{Cre}::Intrsect-ChR2^{BNST} mice indicating the number of non-projecting CRF neurons compared to the total CRF population in the dorsal (top panel; t_{14}=1.959, ns, Student's unpaired two-tailed t-test, n=4 mice, 8 hemispheres per group) and ventral aspects of the BNST (bottom panel; t_7=2.431, p<0.05, Student's unpaired Welch's corrected two-tailed t-test, n=4 mice, 8 hemispheres per group) (g) Recording configuration and light evoked IPSC showing local GABA release from non-projecting CRF neurons in the BNST. (h) Sterotaxic injection of ChR2 in *Crf*^{cre} mouse (i-j) Light evoked IPSCs in the VTA and LH indicating that CRF projections to these regions are GABAergic. Data are mean ± s.e.m. *P<0.05; **P<0.01.

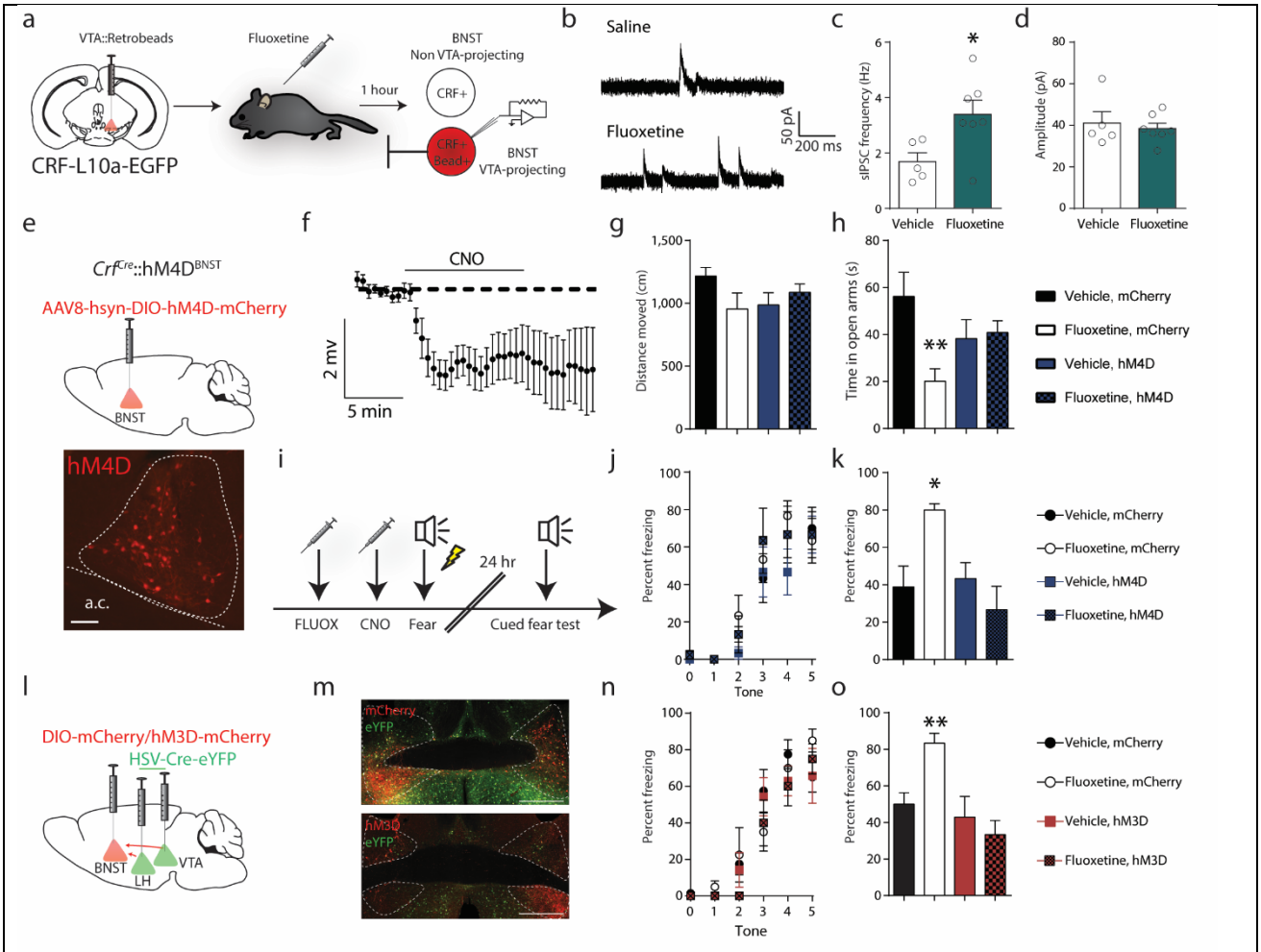

Figure 3.11: Acute fluoxetine elicits aversive behavior by engaging inhibitory CRF circuits in the BNST. (a) Schematic of recording for *in vivo* fluoxetine experiments in CRF reporter mice. (b) Representative traces of sIPSCs in VTA projecting neurons in the BNST for 5 experiments in 2 saline-treated mice and 7 experiments in 2 fluoxetine-treated mice. (c-d) Bar graphs showing that fluoxetine increases in sIPSC frequency (t_{10}=2.55, p<0.05, Student's unpaired two-tailed t-test, n=5 cells from 2 saline-treated mice, n=7 cells from 2 fluoxetine-treated mice), but not amplitude (t_{10}=0.4752, p>0.05, Student's unpaired two-tailed t-test, n=5 cells from 2 saline mice, n=7 cells from 2 fluoxetine mice) in VTA projecting neurons in the BNST. (e) Experimental configuration for assessment of anxiety in fluoxetine-treated *Crf*^{Cre}::hM4Di^{BNST} mice and a coronal slice of the BNST expressing hM4Di-mCherry. Scale bar: 100 µm. (f) Confirmatory electrophysiology in the BNST showing hyperpolarization of hM4Di-mCherry-expressing cells following bath application of CNO (t_5=4.32, p<0.01, One-sample t-test, n=6 cells from 4 mice) (g-h) Chemogenetic silencing of CRF neurons attenuates fluoxetine-induced anxiety like behavior on the elevated zero maze ($F_{1,30}$=7.086, p<0.05, Two-way ANOVA, n=10 fluoxetine/hM4Di and n=8 for all other groups) without any concomitant locomotor effects. (i) Experimental configuration for fear conditioning experiments in *Crf*^{Cre}::hM4Di^{BNST} mice. (j-k) Chemogenetic silencing of CRF^{BNST} neurons had no effect on freezing behavior during fear learning but prevented fluoxetine enhancement of cued fear recall ($F_{1,17}$=8.73, p<0.01, Two-way ANOVA, n=6 mCherry/vehicle and n=5 per group for all other groups). (l) Experimental configuration for assessment of the role of BNST outputs to the VTA and LH in fluoxetine-induced aversive behavior. (m) Confocal image of the BNST from HSV^{Cre}::hM3Dq^{BNST} mice. Scale bars: 500 µm.. (n-o) Chemogenetic activation of BNST neurons that project to the midbrain did not impact fear acquisition but attenuated fluoxetine induced enhancement of cued fear recall ($F_{1,27}$=7.541, p<0.05, Two-way ANOVA, n=7 vehicle/hM3D and n=8 for all other groups). Data are mean ± s.e.m. *P<0.05; **P<0.01; ***P<0.001.

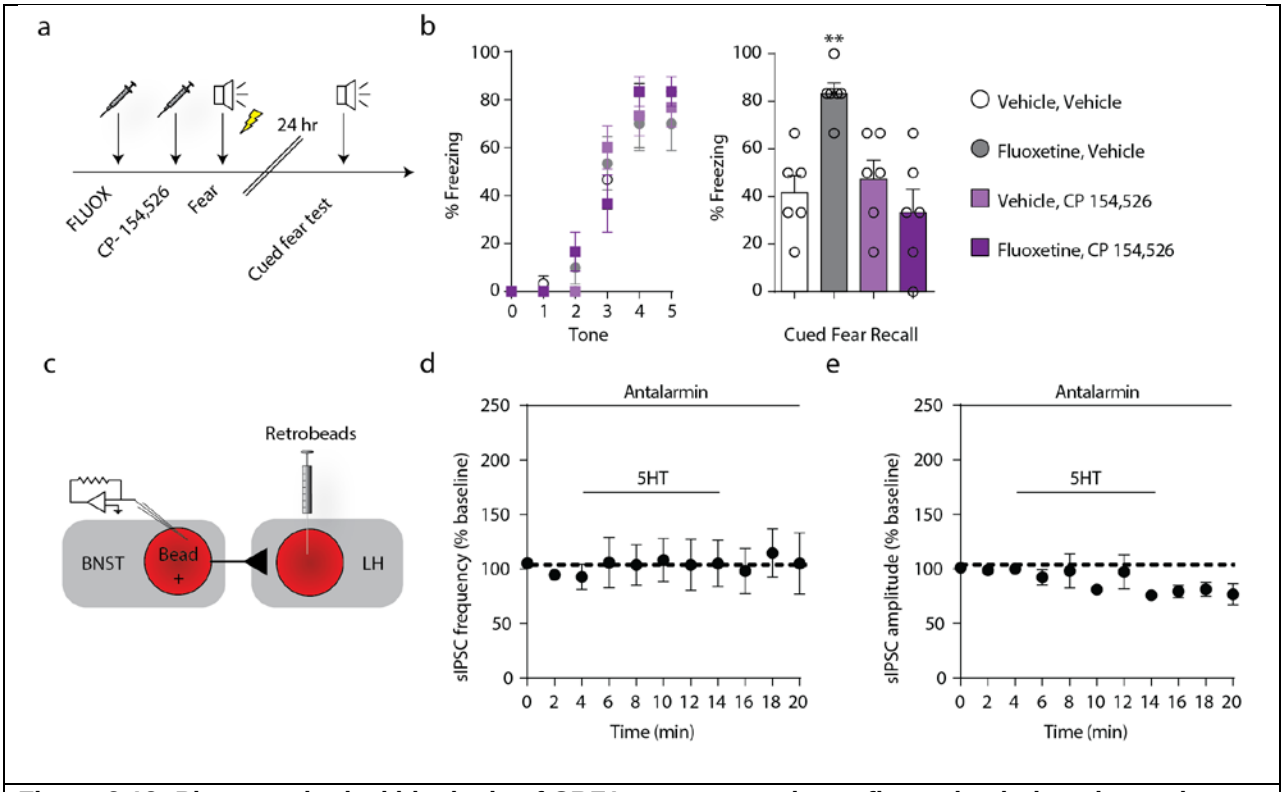

Figure 3.12: Pharmacological blockade of CRF1 receptors reduces fluoxetine induced aversive behavior and 5-HT enhancement of GABAergic transmission in the BNST. (a) Experimental schedule of injections and behavior. (b) CRF_1R antagonist does not modify fear acquisition but reduces fluoxetine enhancement of cued fear recall ($F_{1,20}$=13.70, p<0.01, Two-way ANOVA, n=6 per group). (c) Recording configuration in BNST neurons that project to the LH in C57BL/6 mice. (d) Bath application of a CRF_1R antagonist blocks the 5-HT induced increase in sIPSC frequency in LH projecting neurons in the BNST ($F_{10,30}$=0.2213, ns, Repeated measures one-way ANOVA, n=4 cells from 2 mice). (e) There was a reduction in sIPSC amplitude during 5-HT bath application and CRF_1R blockade ($F_{10,30}$=2.941, p<0.05, Repeated measures one-way ANOVA, n=4 cells from 2 mice). Data are mean ± s.e.m. **P<0.01.

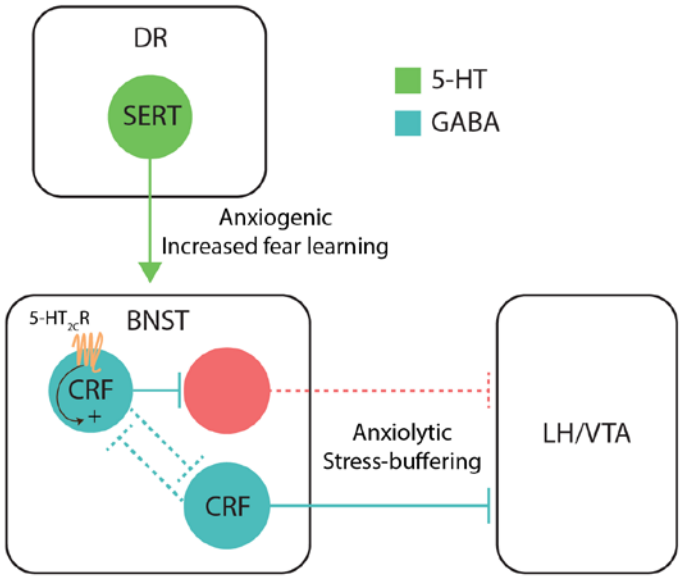

Figure 3.13: Model of a serotonin-sensitive inhibitory microcircuit in the BNST that modulates anxiety and aversive learning. Serotonin inputs to the BNST activate 5-HT$_{2C}$Rs expressed in non-projecting "local" CRF neurons. These "local" CRF neurons promote anxiety and fear by inhibiting anxiolytic outputs to the VTA and LH that are putatively GABAergic. Another discrete subset of CRF neurons, which are inhibited by 5-HT, send direct, inhibitory projections to the VTA and LH. These CRF^{BNST} output neurons are GABAergic and putatively anxiolytic and stress buffering. Blue dashed lines indicate hypothesized additional synapses between CRF^{BNST} neurons. Dashed red line indicates a putatively GABAergic synapse.

CHAPTER 4: DISCUSSION

4.1 Potential interactions accounting for GPCR-mediated effects on anxiety

Recent neurobiological technology advances have provided an unprecedented toolbox for untangling the complex neurocircuitry involved in generating emotional behavior. Here, we used transgenic mouse lines and combinatorial chemogenetic and optogenetic approaches to identify discrete cell populations and projections involved in the expression of anxiety-like behavior. The work presented here focused on circuits within the BNST, as its chemical and anatomical heterogeneity make it a prime candidate for using these innovative tools to dissociate the specific contributions of cells and circuits to anxiety. Our findings revealed GPCR-mediated signaling pathways that are sufficient to drive anxiety-related behavior, and alter the expression of a learned fear. Ultimately, identification of endogenous GPCRs located within these circuits will yield more effective pharmacological targets to alleviate pathological anxiety.

Results presented in Chapter 2 demonstrate that activation of Gq-coupled signaling within GABAergic neurons of the BNST induces anxiety-like behavior in the elevated plus maze and light-dark box. We did not see changes in the amount of time spent in the center of the open field box, another measure of anxiety, indicating that there may be context-specificity to the effects. It would be interesting to parse how Gq-coupled signaling in BNST VGAT neurons also alters anxiety-like behavior in assays independent of novelty-induced exploration. For example, data from other groups show the involvement of the BNST in other emotion and novelty-related behaviors, such as social interaction. Further, projections from the BNST to the lateral hypothalamus (LH) can directly drive feeding-related behavior, and this result is driven by GABAergic neurons of the ventral BNST (Jennings, Rizzi, et al., 2013). As the BNST has direct projections to hindbrain nuclei known to be involved in the regulation of autonomic function, such as the parabrachial nucleus (PBN) and locus coeruleus (LC), it would be useful to see how activation of discrete signaling cascades contribute to the non-emotional aspects of anxiety. Previous reports indicate that manipulations of the BNST can alter autonomic activity, including respiration rate and heart rate, though there appears to be topographical differences to the direction of these effects (Kim et

al., 2013; Crestani et al., 2013). Our studies did not assess how broad stimulation of Gq-induced anxiety behavior alters the autonomic components of anxiety. This would be of interest given that recent work has demonstrated that direct stimulation of BNST outputs can drive anxiety-like behavior in a manner that is independent of the associated changes in autonomic activity (Kim et al., 2013).

In BNST VGAT neurons, DREADD-induced changes in anxiety were selective to the Gq-coupled DREADD, as neither Gi-coupled nor Gs-coupled DREADD receptor activation in the BNST evoked acute changes in anxiety-like behavior. This is particularly interesting, given that previous research using pharmacological inhibition of the BNST, or optogenetic inhibition of the dorsolateral BNST, can reduce anxiety-like behavior in exploratory-based assays (Kim et al., 2013). However, it is known that stress exposure increases c-fos expression in the BNST, and I presented in Chapter 3 elevated BNST activity during shock exposure, so it remains possible that our assays were not stressful enough to engage BNST function. If this were the case, suppression of low BNST activity may be insufficient to observe changes in anxiety-like behavior. Similar results were previously observed with respect to BNST-induced effects on heart rate. Inhibition of BNST synaptic activity using $CoCl_2$ had no effect on baseline heart rate, but pretreatment with $CoCl_2$ blocked increases in heart rate induced by intravenuous injection of phenylephrine (Crestani et al., 2010). Interestingly, these data suggest an inhibitory role of broad BNST activation on cardiac activity, but nonetheless represent that baseline inhibition of the BNST was insufficient to alter a cardiovascular phenotype. Given this, I suspect that inhibition of BNST VGAT neuron activity using a Gi-coupled DREADD during a stress-inducing stimulus may blunt subsequent increases in anxiety-like behavior.

Critically, the effects we observed in our experiments using DREADD-based approaches rely on activation of postsynaptic GPCR signaling. This does not suggest that any peptide bound to a Gi-coupled receptor located within the BNST will be sufficient to reduce anxiety-like behavior. Heterogeneity in localization of receptors is important to take into account. For example, the canonically anti-stress peptide neuropeptide Y (NPY) binds to a family of Gi-coupled receptors (Y1-Y5), some of which are located within the BNST. However, genetic deletion of Y2 receptors in various nuclei associated with stress can reduce anxiety-like behavior (Tasan et al., 2011). While Y2 receptor deletion in the BNST does not alter anxiety, Y2 receptor deletion in the CeA reduces anxiety, which could be mediated by alterations in presynaptic

activity in CeA afferents to the BNST (Tasan et al., 2011). NPY in the BNST suppresses GABA release through activity at presynaptic Y2 receptors (Kash & Winder, 2006). Thus, while Y2 receptors are present within the BNST and are coupled to Gi signaling pathways, activation of Y2 receptors could produce a disinhibition of the BNST through a reduction in inhibitory signaling. Further, NPY interacts with CRF-expressing cells of the BNST to suppress alcohol intake in mice (Pleil et al., 2015). These results highlight the importance of identifying postsynaptic signaling pathways and endogenous receptors that can be targeted to manipulate these defined pathways.

The opposing functions of CRF and NPY in the BNST could partially explain the lack of changes in anxiety-related behavior following stimulation of Gs-coupled DREADDs in the BNST. In particular, CRF and NPY signaling can produce opposing effects on inhibitory transmission in the BNST and interactions between these two peptide systems modulate alcohol consumption in rodents and non-human primates (Kash & Winder, 2006; Pleil et al., 2015). In a study assessing the activity of agouti-related peptide (AgRP) neurons of the hypothalamus, activation of the Gq-coupled DREADD induced behavioral changes in feeding were mediated by the release of neurotransmitters, while behavioral effects elicited with the Gs-coupled DREADD were mediated by the release of neuropeptides (Nakajima et al., 2016). Thus, discrete GPCR-mediated signaling pathways contribute to the regulation of neuronal signaling mechanisms that ultimately lead to neuropeptide and neurotransmitter release. Beyond CRF and NPY, BNST neurons express other neuropeptides, including dynorphin, nociceptin, PACAP, and cholecystokinin (CCK). It is possible that broad stimulation of BNST VGAT neurons results in the release of multiple neuropeptides that could occlude effects that would be seen by stimulation of neuropeptide populations individually. However, given that the bulk of BNST neurons are GABAergic, broad expression of hM3Dq in our study may have biased signaling towards GABA release. Future experiments assessing the contribution of Gs-coupled signaling in discrete neuropeptide defined subpopulations of BNST neurons to anxiety-related behavior will better dissect the unique involvement of peptide systems. In addition to targeting G protein signaling pathways in discrete neuropeptide populations, it would be useful to use the single-cell characterization described in Chapter 2, or an RNA sequencing approach, to identify the overlap of peptide-expressing cell populations in the BNST. While the numerous genetic and pharmacological behavioral studies described above demonstrate the importance of receptors and

peptide expression in the BNST contributing to an array of behaviors, it is unclear of the degree of overlap of the peptide expressing populations themselves. A rigorous characterization of single-cell expression profiles in the BNST will yield valuable insights into the complexities of peptide expressing populations, and could also determine how peptide expression profiles are altered by multiple types of stress-inducing stimuli.

In Chapter 3 we demonstrated that chemogenetic inhibition of CRF-expressing cells of the BNST disrupts SSRI-induced increases in fear, but we did not assess the contributions of Gq or Gs-induced effects on acute anxiety in CRF neurons. However, a recent paper observed that chemogenetic inhibition of BNST CRF-expressing neurons with the Gi DREADD following repeated cycles of drinking in the dark (DID) reduces anxiety-like behavior in the elevated plus maze, while stimulation with the Gs DREADD does not alter anxiety (Pleil et al., 2015). It is important to note, however, that these experiments were conducted following chronic alcohol exposure and not under naïve conditions. Chronic exposure to alcohol is known to produce an array of changes in excitability and receptor expression of neurons within the extended amygdala, which has been extensively characterized in both the CeA and BNST. These stress-induced changes in receptor expression could ultimately affect the behavioral consequences of G protein-mediated activity. For example, a study demonstrated that while the actions of CRF1R and CRF2R binding in the nucleus accumbens are initially rewarding, exposure to severe stress reverses the response such that local infusion of CRF receptor agonists to the nucleus accumbens is aversive (Lemos et al., 2012).

CRF-expressing neurons of the BNST have recently been demonstrated to be directly involved in alcohol drinking behaviors. The reduction in alcohol drinking induced by BNST CRF neuron inhibition may be mediated through BNST CRF projections to the VTA (Rinker et al., 2015). In this study, antagonism of the CRF1 receptors in the VTA reduced alcohol intake, which could be recapitulated with agonism of the CRF2 receptor in the BNST. Simultaneous antagonism of CRFR1 and CRFR2 did not affect alcohol intake, suggesting that intact signaling through CRFR2 is required for CRFR1-induced effects on alcohol consumption. Chemogenetic inhibition of CRF-expressing VTA neurons did not suppress alcohol intake. However, chemogenetic inhibition of CRF terminals originating from the BNST through infusion of CNO to the VTA was sufficient to blunt alcohol drinking. This study identified a discrete output of BNST CRF

neurons to the VTA that may be sufficient to drive alcohol drinking (Rinker et al., 2015). This finding is important, as we show in Chapter 3 that BNST CRF neurons have GABAergic projections to the VTA, and previous research identified that optogenetic activation of GABAergic projections from the BNST to the VTA reduces anxiety-like behavior (Jennings, Sparta, et al., 2013). Given the wealth of literature demonstrating stress- or anxiety-induced increases in alcohol intake, one may suspect that stimulation of an anxiolytic pathway would suppress alcohol consumption. It is important to consider, however, that BNST CRF neurons are only a subset of the GABAergic BNST projections to the VTA, so it remains possible the CRF projection subset may alter anxiety-related behavior differently than the GABAergic population as a whole. Heterogeneity in the anterior and posterior VTA contributions to alcohol drinking further complicate the effects of GABAergic signaling in the VTA on alcohol consumption (Melón & Boehm, 2011). Regardless, future work assessing the contributions of GABA or CRF release from BNST CRF neurons in driving alcohol drinking or anxiety-like behavior using the Gq and Gs DREADD variants will yield better information in the involvement of transmitter and peptide systems in behavioral outcomes. Further, as we observe that local CRF neurons can inhibit VTA-projecting neurons in the dorsal BNST, which are primarily GABAergic, it is possible that CRF neurons with local inhibitory synapses will differentially affect behavior relative to stimulation of CRF neurons that project beyond the BNST. It will be interesting to use an intersectional strategy to selectively label CRF neurons using either DREADDs or light-gated opsins to target the behavioral contributions of these projection-defined subpopulations.

It is important to consider that the investigative approaches described thus far have relied on a pre-determined transmitter or peptide to define a neural population of interest. While the selection of the transmitter, peptide, or receptor is guided by knowledge of that marker's function, defining a neural population entirely by any one marker provides both benefits and drawbacks. For example, in some cases, such as AgRP and pro-opiomelanocortin (POMC) neurons of the arcuate nucleus, peptide defined populations can be largely non-overlapping and can drive opposing behavioral effects (Aponte et al., 2011; Krashes et al., 2011). In this situation, AgRP and POMC expression serves as a good molecular marker for targeting molecularly and behaviorally discrete cell populations. A drawback to this approach, however, is that stimulation of the entire peptide population may not represent how the neural population is activated by the appropriate stimulus. Heterogeneity within a peptide-specific population may still exist.

In agreement with this, we observed in Chapter 3 that CRF neurons of the BNST can be differentially activated or inhibited by 5-HT, and differences in circuit connectivity suggests that these connections may differentially affect behavioral output in a manner that may not be captured by stimulation of the entire population. Further, as described above, neurons may express numerous neuropeptides, so defining a cellular population by any one peptide may not truly capture the peptide or transmitter that is driving a potentially observed behavioral effect. Nonetheless, if stimulation or inhibition of a peptide-defined cell type is sufficient to drive a behavior, then targeting a receptor enriched in this population to selectively modulate neuronal activity may prove to be a useful therapeutic target. In contrast to defining cells by peptide identity, neurons can also be defined by activity-dependent identity through the use of intermediate early genes (IEGs). Such an approach has commonly been used in the identification of an engram, or neural ensemble that encodes a particular memory (X. Liu et al., 2012; Trouche et al., 2016; Ramirez et al., 2015).

4.2 Gq-induced LTD in the BNST and implications for anxiety treatments

In addition to using chemogenetics to identify behavioral manifestations upon engagement of endogenous signaling pathways, I observed that *ex vivo* stimulation of the hM3Dq DREADD induced a long-term depression (LTD)-like state of electrically evoked excitatory postsynaptic currents (eEPSCs). Previous electrophysiological studies conducted within the BNST show that agonists for various Gq-coupled receptors can induce an LTD of EPSCs, including the α1-adrenergic receptor and the Group 1 metabotropic glutamate receptors (mGluR) mGluR1 and mGlurR5 (Grueter et al., 2006; Grueter, McElligott, & Winder, 2007; Z. A. McElligott & Winder, 2008; Z. A. McElligott et al., 2010). These results are in agreement with findings from another study showing that stimulation of hM3Dq-expressing cells in the dorsal hippocampus induces an LTD, while hM4Di activation can alter LTP development (López et al., 2016). In addition to inducing an LTD-like state, noradrenergic signaling in the BNST can depolarize neurons via α1-adrenergic receptors and can acutely facilitate spontaneous EPSCs (sEPSCs) (Dumont & Williams, 2004; Z. A. McElligott et al., 2010). This facilitation of glutamatergic transmission requires activity of CRF1 receptors (Z. A. McElligott et al., 2010). Of note, however, α1 signaling in the BNST can facilitate GABA release and increase the frequency of inhibitory postsynaptic currents (IPSCs), possibly through depolarization of local inhibitory interneurons of the BNST (Dumont & Williams, 2004).

The complex interactions of neurotransmitters and CRF in the BNST are not limited to noradrenergic signaling. Dopamine (DA) release in the BNST facilitates glutamatergic signaling in a manner that requires CRF1 receptor activation (Kash et al., 2008). Interactions between the DA and CRF systems are required for CRF-potentiated startle responses (Meloni et al., 2006). Intriguingly, the dopaminergic afferents to the BNST arise from both the VTA and the ventrolateral periaqueductal gray (vlPAG) (Meloni et al., 2006). This connectivity positions the BNST as a relay center integrating circuits involved in pain, reward, motivation, and emotion. While I did not target projection-defined populations of neurons in the BNST, it will be interesting in future experiments to use the single-cell qPCR approach described in Chapter 2 to identify how projection-defined neurons of the BNST differ with respect to receptor expression. If we are able to identify unique receptor targets on these cells, we may be able to modulate defined behaviors while minimizing other behavioral side effects. A similar approach was used recently to identify genetic differences between basolateral amygdala (BLA) neurons that project to the nucleus accumbens (NAc) and the CeA (Namburi et al., 2015). Likewise, transgenic mouse lines that use an IEG promotor to drive expression of Cre recombinase in a tamoxifen- and activity-dependent manner, such as the Fos-Cre or Arc-Cre lines, would allow for targeting of neurons that were active during a temporally defined task. These IEG-based lines could be further crossed with a floxed-stop reporter line that produces fluorophore expression in Cre-expressing cells, thus allowing fluorophore expression in neurons that were active during a discrete time point. Such a strategy would allow for isolation of stimulus-responsive neurons, as identified by fluorescence, using FACS or similar sorting approach. Sequencing of isolated populations could then identify receptors or signaling targets that are differentially expressed in responsive neurons compared with non-responsive neurons. Perhaps manipulations of these activity-defined cell types could better prevent subsequent activity and aversive behavioral experiences. This and similar strategies have been employed to assess the contributions of neurons in the hippocampus and lateral amygdala active during fear conditioning training to driving later fear expression (X. Liu et al., 2012; Rashid et al., 2016; Yiu et al., 2014). Generally, subsequent stimulation of neuronal populations engaged during fear learning is sufficient to induce fear-related behavior, though it can be context-dependent. In keeping with this, the temporal delay between fear training in various contexts can alter the degree to which overlapping neurons are recruited to the same fear memory (Cai et

al., 2016). The mechanisms underlying the overlap may prove a critical target in preventing the development of generalized fear behavior. Ongoing studies will probe the contributions of these defined populations to emotional behavior and how perturbation of this plasticity may disrupt the progression to a disease state.

It is of interest that Gq-induced LTD in the BNST requires CB1 receptor activity given the potential for cannabinoids as a pharmacotherapy for treating anxiety disorders. The endocannabinoids anandamide (AEA) and 2-arachidonoylglycerol (2-AG) both primarily act on the CB1 receptor within the brain, while CB2 receptor expression is limited to peripheral structures. Unlike classic neurotransmitter release, endocannabinoids are released by the postsynaptic cell and act on presynaptic CB1 receptors to dampen presynaptic transmitter release. This form of retrograde transmission generates a negative feedback loop. Importantly, AEA is generated from diacylglycerol (DAG), which is created through the hydrolysis of phosphatidylinositol 4,5-bisphosphate (PIP_2). This reaction is catalyzed by PLC, which is downstream of the Gq signaling pathway. However, a separate synthesis pathway involving phospholipase D has also been observed (Freund et al., 2003). This synthesis pathway would suggest that activation of the Gq-coupled DREADD in BNST VGAT neurons leads to the generation of endocannabinoids, ultimately leading to presynaptic inhibition of transmitter release. As our *ex vivo* electrophysiological results indicate that CB1 receptor inhibition can block the reduction in evoked excitatory postsynaptic currents induced by Gq activation, it suggests this finding is mediated through the action of endocannabinoids.

In my study I did not target specific excitatory inputs to the BNST. Possible glutamatergic afferents in the BNST arise from the BLA, PFC, and ventral hippocampus. Further, given the broad and robust expression of the CB1 receptor throughout the brain, it remains unclear which particular excitatory input contributed to the LTD in the postsynaptic cell. Further, endocannabinoid signaling can result in depolarization induced suppression of inhibition (DSI), resulting in a reduction of inhibitory transmission on the postsynaptic cell. While I only assessed glutamatergic events onto BNST VGAT neurons, it is likely that GABAergic transmission was reduced as well. Similarly, I did not target Gq-DREADD expression selectively in BNST interneurons or projection neurons. Future studies assessing the contributions of Gq

signaling-induced reductions in synaptic transmission on projection-defined BNST neurons will better parse the circuits underlying the net increase in anxiety-like behavior.

The involvement of endocannabinoid release in modulating the activity of BNST neurons is interesting given the role of endocannabinoids in the stress response and anxious behavior (Hill & Tasker, 2012; Hill et al., 2010). Knockout of the CB1 receptor, or systemic administration of CB1 receptor antagonists, blunts the HPA axis response to acute stressors, though in a context dependent manner (Patel et al., 2004; Cota et al., 2007). Antagonism of CB1 receptors leads to a rise in c-fos expression in the PVN, which contains the CRF-expressing neurons that initiate the HPA stress response. Activation of PVN CRF neurons ultimately leads to the release of cortisol in humans, or corticosterone in rodents, from the adrenal glands. Endocannabinoid release can activate CB1 receptors on glutamatergic terminals that synapse onto PVN CRF-expressing neurons, thereby providing a feedback mechanism to inhibit HPA axis activity (Di et al., 2003). While I did not assess CB1 receptor involvement within the BNST in contributing to HPA axis activity, the CB1 receptor-mediated LTD induced by Gq activation in the BNST is of interest given that the BNST has direct projections to the PVN. It would be of interest to use retrograde viruses, such as an HSV-Cre injected into the PVN, followed by a cre-inducible hM3Dq DREADD into the BNST, to selectively activate Gq signaling in PVN-projecting BNST neurons. Such a study would provide mechanistic insight into how the BNST projection to the PVN contributes to the generation of anxiety states and how this functional connectivity is modulated by the release of endocannabinoids.

Together, our findings are in agreement with previous studies within the BNST demonstrating that Gq-induced signaling leads to CB1 receptor-mediated LTD (McElligott et al., 2010; Grueter et al., 2006; Glangetas et al., 2013). Prolonged changes in synaptic activity could be associated with the development of psychiatric disease. Indeed, altered CB1 receptor signaling has been implicated in anxiety-related psychiatric conditions, such as PTSD. A study in patients diagnosed with PTSD showed elevated expression of CB1 receptors throughout the brain, while levels of anandamide and cortisol were reduced (Neumeister et al., 2013). Although our results suggest that CB1 receptors may be an interesting target for modulating the activity of BNST neurons that are sufficient to drive anxiety, targeting CB1 receptors for the treatment of anxiety-related conditions poses many challenges. CB1 receptors are broadly and densely expressed throughout the brain (Herkenham et al., 1990; Glass et al., 1997), thus, large-scale

dampening of synaptic transmission mediated by CB1 receptor activity could produce a variety of undesirable side effects. Indeed, a clinical trial assessing the efficacy of rimonabant, a CB1 receptor antagonist, in reducing a number of cardiovascular diseases needed to be terminated due to multiple psychiatric side effects (Topol et al., 2010). Patients receiving rimonabant reported significantly increased gastrointestinal problems, neuropsychiatric conditions, suicidal ideation, and multiple participants completed suicide. Other pharmacological manipulations of endocannabinoid signaling, such as reuptake blockers, offer alternative approaches that may yield more beneficial results (Griebel & Holmes, 2013; Micale et al., 2013).

4.3 Considerations of brain-wide metabolic mapping during behavioral states

Interestingly, we observed with DREAMM imaging that activation of Gq-coupled signaling altered metabolic activity throughout the brain in regions associated with anxiety in human patients experiencing anxiety. Specifically, acute activation of the Gq-DREADD in BNST VGAT neurons of mice resulted in enhanced activity within the BNST, the VTA, the BLA and CEA, the PBN, LC, and other areas of the hindbrain. While the BNST has direct projections to many of these structures, we also observed elevated activity in the regions that do not receive direct BNST innervation, such as the PFC. The PFC sends afferents to the BNST, so enhanced activity in the PFC may reflect the engagement of polysynaptic feedback loops. It would be interesting to assess in future studies if neurons that project from the PFC to the BNST are directly activated following activation of the hM3Dq DREADD in the BNST. This could be accomplished by injecting both a retrograde trafficking virus encoding a fluorophore along with a virus encoding an hM3Dq DREADD into the BNST. Following CNO-induced activation of the hM3Dq, staining for the IEG c-fos or arc could be used to assess changes in activity of the defined populations of the PFC. This would be particularly useful given that while DREAMM imaging does provide insights into changes of metabolic activity of a region, it is based upon the uptake of glucose, which occurs at both pre- and postsynaptic sites. Therefore, I cannot say with certainty whether the changes in metabolic activity represent alterations in pre- or postsynaptic responses. Similarly, the genetic identity of a postsynaptic cell would be unclear, making it impossible to discern whether cells with increased activity represent local interneurons, projecting neurons, or a combination of the two.

While there are limitations and caveats for metabolic mapping, a biological map of altered metabolic activity throughout the brain provides insights into the circuits engaged during emotional and behavioral states. If we are able to generate an endophenotype of the brain-wide metabolic activity of disease states, then we may be able to use this readout to assess whether treatments have indeed restored normal brain-wide network patterns of activity. Future studies will assess how engagement of the other G protein coupled pathways alters metabolic demand throughout the brain. These findings can be expanded upon by assessing how perturbations of BNST activity following stressors or withdrawal from drugs of abuse and alcohol affect network function. Of particular interest, chronic activation of GPCR signaling can induce metabolic changes that differ from acute activity. For example, DREAMM imaging results following acute activation of Gq-coupled signaling in DR 5-HT neurons using CNO produces a pattern of activity that differs from results observed when Gq signaling was chronically activated by CNO availability in drinking water (Urban et al., 2015). Specifically, while acute Gq signaling within DR 5-HT neurons elevates metabolic activity in areas of forebrain cortex including somatosensory and motor cortices, chronic treatment with CNO results in a reduction in metabolic activity of somatosensory and motor cortex (Urban et al., 2015). The driving force behind the differences remains to be determined. It is unclear if the broad network effects are the result of prolonged stimulation of 5-HT release from DR serotonergic neurons, if Gq-mediated events within 5-HT DR neurons produce long-term changes in release, or if there is a combination of long-term plasticity induced alterations throughout the entire network resulting in broad functional differences. It will be informative in future studies if chronic CNO treatment is coupled with either systemic or local application of particular receptor antagonists to assess the contributions of both neurotransmitter modulation and postsynaptic GPCR-based activity on subsequent network responses. If using the metabolic map as an endophenotype of a disease state, then this approach will provide ways of targeting the unique signaling contributions that generate prolonged aberrations of metabolic network patterns.

4.4 Serotonin interactions with CRF in the BNST to generate anxiety and implications for therapeutics

Using a single-cell qPCR approach to identify endogenous Gq-coupled receptors expressed within BNST VGAT neurons, I generated a list of Gq coupled receptors expressed by BNST VGAT

neurons (Figure 2.6). We ultimately focused on the 5-HT2C receptor as serotonin has been widely implicated in anxiety and emotional disorders, and the colocalization of CRF containing neurons and 5-HT terminals in the BNST provided complex interactions between the 5-HT and CRF systems. Although there was robust expression of mGluR1 and mGluR5, these receptors are broadly expressed at both pre- and postsynaptic sites throughout the brain, so they are unlikely candidates for modulating discrete behaviors within a nuclei of interest. It will be interesting for future studies to probe the contributions of M1 receptor and neurotensin 2 receptor signaling in the BNST in driving anxiety-like states. We identified that agonism of the 5-HT2C receptor of the BNST *in vivo* was sufficient to induce an increase in startle amplitude, indicative of an increase in anxiety-like behavior. This is of high interest as it demonstrates that 5-HT signaling through actions at Gq-coupled receptors in the BNST can drive anxiety states. Coupled with the data described above, these data generated a locus within the BNST for investigating the role of 5-HT signaling on discrete cell types as defined by neurotransmitter and neuropeptide content.

In particular, given that selective serotonin reuptake inhibitors (SSRIs) are the most common pharmacological treatment for an array of anxiety and depression disorders, it is of interest that we identified acute signaling via the 5-HT2C receptor in the BNST is sufficient to promote anxiety-like behavior. In Chapter 3 we demonstrate that 5-HT has opposing effects on membrane polarization in BNST CRF neurons that is dependent on 5-HT2R expression with respect to connectivity. 5-HT-induced depolarization of BNST CRF neurons could be blocked by antagonism of the 5-HT2C receptor. This effect was only identified in BNST CRF neurons that do not project to the LH or VTA, thus highlighting the anatomical specificity of the effect. Intriguingly, optical stimulation of serotonergic inputs to the BNST increased 5-HT release as assessed *ex vivo* and increased anxiety and fear expression *in vivo*. These findings were critical as they provide a node for 5-HT induced increases in anxiety and fear behavior. Further, they identify opposing effects of 5-HT on membrane properties of BNST CRF-expressing cells, which are known to be located near serotonergic fibers.

These findings build on the long observed connection between serotonergic activity and emotional behavior. Following benzodiazepines, which act as an agonist at the GABA-A receptor, the 5-HT1A receptor partial agonist buspirone became the first pharmacotherapeutical option for patients with

generalized anxiety disorder (GAD) (Goldberg & Finnerty, 1979; Rickels et al., 1982; Griebel & Holmes, 2013). While the therapeutic efficacy of buspirone did not translate to all anxiety-related conditions, such as panic disorder, it pointed to the involvement of serotonin receptors as candidate targets for regulating emotional disorders. The first-line pharmacotherapeutic for multiple anxiety and depression conditions today remains SSRIs that enhancing synaptic levels of 5-HT through inhibition of the presynaptic serotonin transporter.

As previously observed, acute SSRI pretreatment can exacerbate cued fear recall, and we identified that systemic treatment with a CRF1 receptor antagonist is sufficient to block SSRI-induced potentiation of fear. These data position CRF1 receptor antagonists as a potential pharmacotherapeutic option for alleviating the acute aversive effects of SSRIs. Patients taking SSRIs have cited aversive side effects, as well as an exacerbation of preexisting symptoms, as contributors to their decisions to abstain from continued SSRI treatment. Therefore, coupling CRF1 receptor antagonism to the early stages of SSRI-based treatment regimens may aid in reducing aversive side effects and lead to better adherence to SSRI treatment schedules.

It is worth noting that the CRF1 receptor has been a previous target for alleviation of symptoms in patients with anxiety, depression, or addiction, with various results. Early preclinical studies demonstrated CRF1 receptor antagonism reduces multiple aversive conditions in rodents and non-human primates without changes in HPA axis activity. The first small clinical trial in human subjects with the CRF1 receptor antagonist R121919 showed a reduction in the Hamilton Depression Rating Scale (HAM-D) in some patients suffering from major depressive disorder (MDD) (Zobel et al., 2000). However treatment at a variety of doses remained ineffective or worsened symptoms in some patients (Zobel et al., 2000). This study was also limited by its lack of a placebo control group, randomization in group assignment, and blinding of investigators. A subsequent clinical trial using a different CRF1 receptor antagonist, CP-316,311, saw no differences in HAM-D scores in patients with MDD relative to a placebo control, while the SSRI sertraline improved symptoms (Binneman et al., 2008). Similarly, the CRF1 receptor antagonist pexacerfont failed to reduce anxiety relative to a placebo in patients suffering from GAD (Coric et al., 2010).

While clinical trial results aiming to treat anxiety and depression have had discouraging results, CRF1 receptor antagonists may still hold promise for the treatment of diseases featuring an exacerbated response to discrete stressors that result in elevated CRF levels. That is, if a stressor evokes CRF release, then antagonism of CRF receptors may still present a promising avenue for the alleviation of stress-induced aversive states. In accordance with this, rats receiving multiple infusions across days of the CRF receptor agonist urocortin (Ucn) into the BLA show elevated anxiety-like behavior that persists a month following the last Ucn injection. The persistent behavioral changes are accompanied by alterations in synaptic transmission within the BLA, including increased excitability and a reduction in inhibitory postsynaptic transmission (Rainnie et al., 2004). Co-administration of Ucn and the NMDA receptor antagonist AP-5 abolished the behavioral and subsequent inhibitory transmission changes normally induced by chronic Ucn treatment (Rainnie et al., 2004). Critically, these data suggest that blockade of CRF receptors during periods of elevated CRF release induced by stressors, particularly long-lasting stressors that generate sustained CRF release, may be able to prevent the long-term plasticity effects that remain in the absence of continued CRF secretion. The blockade of Ucn-induced plasticity through inhibition of NMDA receptors is also noteworthy in light of evidence that NMDA receptor antagonism with ketamine has shown promise as a way to generate long-lasting improvements in mood in patients suffering from major depression (Murrough, 2016; Zarate et al., 2006).

In keeping with this, a study comparing rodent and human responses to antagonism of CRF1 receptors with NBI-34041 observed reductions in stress-induced ACTH levels in rodents and reduced ACTH and cortisol following a Trier Social Stress Test (TSST) in human subjects (Ising et al., 2007). However, intravenuous administration of CRF increased ACTH and cortisol levels despite CRF1 receptor antagonism (Ising et al., 2007). Together, these results highlight the importance of CRF1 receptor antagonism in reducing stress-evoked increases in behavior that are upstream of increases in stress-induced CRF release. Basal levels of ACTH and cortisol remain unaltered with CRF receptor antagonism, again pointing to the role of these receptors in blocking CRF receptor-induced increases in downstream ACTH and cortisol release. These findings are particularly intriguing in light of our finding that CRF1 receptor antagonism can reduce SSRI-induced increases in learned fear. In Chapter 3 we presented data showing that we observed increased electrical activity during fear conditioning within the BNST as

assessed by *in vivo* electrophysiology, and immunohistochemical analysis revealed that that serotonergic DR neurons projecting to the BNST had elevated c-fos immunoreactivity relative to non-shocked mice. Further, we saw that 5-HT release in the BNST can depolarize a subpopulation of CRF-expressing cells through a postsynaptic 5-HT2C receptor-dependent mechanism. Given that the BNST has direct projections to the paraventricular nucleus of the hypothalamus (PVN), it would be interesting to assess if increases in ACTH or corticosterone levels in mice following shock exposure require activity of BNST CRF neurons, and if 5-HT input arising from the DR onto BNST CRF neurons contributes to modulation of downstream stress hormone release. Such a study would be of particular relevance given the broad disruption of HPA axis activity across mood disorders.

Although the clinical efficacy of coadministration of CRF1 receptor and SSRIs remains to be explored, we have identified that broad suppression of BNST CRF neurons reduces the acute aversive effects of SSRI pretreatment and these neurons may yield other promising targets. GPCRs enriched in BNST CRF neurons may provide useful targets for blunting the adverse effects of acute elevations of 5-HT levels. Given that data with DREADDs have demonstrated that Gs-mediated signaling pathways contribute to peptide release, functionally opposing this signaling pathway in BNST CRF neurons may provide another potential avenue for treatment (Nakajima et al., 2016). Gs-mediated signaling results in the downstream activation of adenylyl cyclase and the production of cyclic AMP (cAMP), ultimately stimulating protein kinase A (PKA) activity and further downstream phosphorylation events. Conversely, Gi-mediated signaling inhibits activity of adenylyl cyclase, thus opposing the actions of Gs-coupled GPCRs. In light of this, stimulation of Gi-coupled receptors within BNST CRF neurons, or within neurons that express the CRF1 receptor may provide a target to alleviate anxiety and fear that is mediated through BNST CRF neuron circuitry. In agreement with this, I show in Chapter 3 that activation of Gi-coupled signaling using the hM4Di DREADD in BNST CRF neurons blocks SSRI-induced increases in fear. Further, NPY is known to functionally oppose the actions of CRF and acts on a family of Gi-coupled receptors. Preclinical research has observed promising anxiolytic effects of NPY and its receptors across multiple anxiety assays, and NPY over-expressing mice show an anxiolytic phenotype, so modulation of NPY signaling may be a useful future target for alleviation of emotional disorders discussed here. Future studies assessing how NPY interacts with SSRI-induced changes in anxiety and fear will provide more

insight into discrete cells and receptors for alternative alleviations of SSRI-induced adverse treatment outcomes.

Given our findings that 5-HT2C receptor expressing neurons in the BNST contribute to anxiety-like behavior, it is interesting that a pair of recent studies assessing anxiety and depression in cancer patients observed reductions in both of these measures following treatment with the 5-HT2A receptor agonist psilocybin (Griffiths et al., 2016; Ross et al., 2016). 5-HT2A receptors, like 5-HT2C receptors, are Gq-coupled and are densely expressed in the prefrontal cortex as well as the BNST (Hammack, Guo, et al., 2009). In both studies, a single dose of psilocybin, coupled with psychotherapy, reduced scores of anxiety and depression as long as six months following treatment. While both studies assessing clinical efficacy of psilocybin were limited to patients with cancer, it remains encouraging that select modulation of 5-HT receptor activity can produce long-lasting and rapid reductions in anxiety and depression. In a separate study assessing the effects of psilocybin on the blood oxygen level-dependent (BOLD) response using functional magnetic resonance imaging (fMRI), acute treatment led to reductions in BOLD signals in the medial PFC (Carhart-Harris et al., 2012). However, this study was conducted in healthy volunteers, so it is unclear if network activity patterns following psilocybin would differ in patients suffering from anxiety or depression. As the BNST expresses 5-HT2A receptors and receives glutamatergic afferents from the PFC, it would be of interest to assess if the therapeutic benefits of 5-HT2A receptor agonism require activity within the BNST. Further, it is unknown whether 5-HT2A receptor expression is limited to BNST interneurons or projection neurons. As SSRI treatment enhances synaptic 5-HT levels, thereby increasing receptor binding at a variety of 5-HT receptor families, it will be important to discern how 5-HT2A receptor activity within the BNST contributes to anxiety-like behavior.

Altogether, the work described in this dissertation identifies novel signaling contributions within the extended amygdala to anxiety-related behavior and characterizes discrete cell types and projection pathways involved in mediating the exacerbation of fear following acute treatment with SSRIs. Untangling the precise circuits underlying both these conditions and the effects of phamaracological therapy on the physiology of these circuits is critical as SSRIs remain the predominant form of treatment for anxiety and depression disorders. Here we have shed light on some of the signaling pathways and interactions between 5-HT and CRF within the BNST in generating an anxious state. We have also identified a

brainwide map of metabolic activity that correlated with a time point of increased anxiety-like behavior following activation of Gq-coupled signaling in GABAergic neurons of the BNST. This biomarker may serve as an endophenotype to recognize regions involved in anxiety, and further studied characterizing metabolic activity of these same regions at various time points along the progression to pathology may be useful in determining what structures to target to restore baseline circuit activity. As we better discern the exact contributions of transmitters, peptides, and network function in generating aversive states, we will provide targets for more selective, and more efficacious, means of treating an array of psychiatric illnesses.

REFERENCES

Adamantidis, A.R., Zhang, F., Aravanis, A.M., Deisseroth, K., Lecea, L. De, & de Lecea, L., 2007. Neural substrates of awakening probed with optogenetic control of hypocretin neurons. *Nature*, 450(7168), pp.420–4.

Adhikari, A., 2014. Distributed circuits underlying anxiety. *Frontiers in behavioral neuroscience*, 8(April), p.112.

Agulhon, C., Boyt, K.M., Xie, A.X., Friocourt, F., Roth, B.L., & McCarthy, K.D., 2013. Modulation of the autonomic nervous system and behaviour by acute glial cell Gq protein-coupled receptor activation in vivo. *The Journal of physiology*, 591(22), pp.5599–609.

Airan, R.D., Thompson, K.R., Fenno, L.E., Bernstein, H., & Deisseroth, K., 2009. Temporally precise in vivo control of intracellular signalling. *Nature*, 458(7241), pp.1025–9.

Alexander, G.M., Rogan, S.C., Abbas, A.I., Armbruster, B.N., Pei, Y., Allen, J.A., Nonneman, R.J., Hartmann, J., Moy, S.S., Nicolelis, M.A., McNamara, J.O., & Roth, B.L., 2009. Remote control of neuronal activity in transgenic mice expressing evolved G protein-coupled receptors. *Neuron*, 63(1), pp.27–39.

Alheid, G.F. & Heimer, L., 1988. New perspectives in basal forebrain organization of special relevance for neuropsychiatric disorders: the striatopallidal, amygdaloid, and corticopetal components of substantia innominata. *Neuroscience*, 27(1), pp.1–39.

Anderson, D.J. & Adolphs, R., 2014. A framework for studying emotions across species. *Cell*, 157(1), pp.187–200.

Anderson, S.A.R., Michaelides, M., Zarnegar, P., Ren, Y., Fagergren, P., Thanos, P.K., Wang, G.J., Bannon, M., Neumaier, J.F., Keller, E., Volkow, N.D., & Hurd, Y.L., 2013. Impaired periamygdaloid-cortex prodynorphin is characteristic of opiate addiction and depression. *Journal of Clinical Investigation*, 123(12), pp.5334–5341.

Aponte, Y., Atasoy, D., & Sternson, S.M., 2011. AGRP neurons are sufficient to orchestrate feeding behavior rapidly and without training. *Nature neuroscience*, 14(3), pp.351–355.

Armbruster, B.N., Li, X., Pausch, M.H., Herlitze, S., & Roth, B.L., 2007. Evolving the lock to fit the key to create a family of G protein-coupled receptors potently activated by an inert ligand. *Proceedings of the National Academy of Sciences of the United States of America*, 104(12), pp.5163–8.

Asan, E., Steinke, M., & Lesch, K.P., 2013. Serotonergic innervation of the amygdala: Targets, receptors, and implications for stress and anxiety. *Histochemistry and Cell Biology*, 139(6), pp.785–813.

Atasoy, D., Betley, J.N., Su, H.H., & Sternson, S.M., 2012. Deconstruction of a neural circuit for hunger. *Nature*, 488(7410), pp.172–177.

Austin, M.C., Bradley, C.C., Mann, J.J., & Blakely, R.D., 1994. Expression of Serotonin Transporter Messenger RNA in the Human Brain. *Journal of Neurochemistry*, 62(6), pp.2362–2367.

Avery, S.N., Clauss, J.A., & Blackford, J.U., 2016. The Human BNST: Functional Role in Anxiety and Addiction. *Neuropsychopharmacology : official publication of the American College of Neuropsychopharmacology*, 41(1), pp.126–41.

Awwad, H.O., Gonzalez, L.P., Tompkins, P., Lerner, M., Brackett, D.J., Awasthi, V., & Standifer, K.M., 2015. Blast overpressure waves induce transient anxiety and regional changes in cerebral glucose metabolism and delayed hyperarousal in rats. *Frontiers in Neurology*, 6(MAY), p.132.

Bale, T.L. & Vale, W.W., 2004. CRF and CRF receptors: role in stress responsivity and other behaviors.

Annual review of pharmacology and toxicology, 44(1), pp.525–57.

Ballenger, J.C., 1999. Clinical guidelines for establishing remission in patients with depression and anxiety. *The Journal of clinical psychiatry*, 60 Suppl 2(suppl 22), pp.29–34.

Barnes, N.M. & Sharp, T., 1999. A review of central 5-HT receptors and their function. *Neuropharmacology*, 38(8), pp.1083–1152.

Bath, B.D., Michael, D.J., Trafton, B.J., Joseph, J.D., Runnels, P.L., & Wightman, R.M., 2000. Subsecond adsorption and desorption of dopamine at carbon-fiber microelectrodes. *Analytical chemistry*, 72(24), pp.5994–6002.

Bechara, A., Tranel, D., Damasio, H., Adolphs, R., Rockland, C., & Damasio, A.R., 1995. Double dissociation of conditioning and declarative knowledge relative to the amygdala and hippocampus in humans. *Science*, 269(25 August), pp.1115–1118.

Behan, D.P., De Souza, E.B., Lowry, P.J., Potter, E., Sawchenko, P., & Vale, W.W., 1995. Corticotropin releasing factor (CRF) binding protein: a novel regulator of CRF and related peptides. *Frontiers in neuroendocrinology*, 16(4), pp.362–82.

Belzung, C. & Griebel, G., 2001. Measuring normal and pathological anxiety-like behaviour in mice: A review. *Behavioural Brain Research*, 125(1–2), pp.141–149.

Belzung, C., Le Guisquet, a M., Barreau, S., & Calatayud, F., 2001. An investigation of the mechanisms responsible for acute fluoxetine-induced anxiogenic-like effects in mice. *Behavioural pharmacology*, 12(3), pp.151–62.

Berger, M., Gray, J.A., & Roth, B.L., 2009. The expanded biology of serotonin. *Annual Review of Medicine*, 60(August 2016), pp.355–366.

Berndt, A., Yizhar, O., Gunaydin, L.A., Hegemann, P., & Deisseroth, K., 2009. Bi-stable neural state switches. *Nature neuroscience*, 12(2), pp.229–34.

Binneman, B., Feltner, D., Kolluri, S., Shi, Y., Qiu, R., & Stiger, T., 2008. A 6-week randomized, placebo-controlled trial of CP-316,311 (a selective CRH1 antagonist) in the treatment of major depression. *American Journal of Psychiatry*, 165(5), pp.617–620.

Blackmer, T., Larsen, E.C., Bartleson, C., Kowalchyk, J.A., Yoon, E.-J., Preininger, A.M., Alford, S., Hamm, H.E., & Martin, T.F.J., 2005. G protein betagamma directly regulates SNARE protein fusion machinery for secretory granule exocytosis. *Nature neuroscience*, 8(4), pp.421–425.

Blair, K., Shaywitz, J., Smith, B.W., Rhodes, R., Geraci, M., Jones, M., McCaffrey, D., Vythilingam, M., Finger, E., Mondillo, K., Jacobs, M., Charney, D.S., Blair, R.J.R., Drevets, W.C., & Pine, D.S., 2008. Response to emotional expressions in generalized social phobia and generalized anxiety disorder: Evidence for separate disorders. *American Journal of Psychiatry*, 165(9), pp.1193–1202.

Bodnoff, S.R., Suranyi-Cadotte, B., Aitken, D.H., Quirion, R., & Meaney, M.J., 1988. The effects of chronic antidepressant treatment in an animal model of anxiety. *Psychopharmacology*, 95(3), pp.298–302.

Bota, M., Sporns, O., & Swanson, L.W., 2012. Neuroinformatics analysis of molecular expression patterns and neuron populations in gray matter regions: The rat BST as a rich exemplar. *Brain Research*, 1450, pp.174–193.

Bourane, S., Duan, B., Koch, S.C., Dalet, A., Britz, O., Garcia-Campmany, L., Kim, E., Cheng, L., Ghosh, A., Ma, Q., & Goulding, M., 2015. Gate control of mechanical itch by a subpopulation of spinal cord interneurons. *Science (New York, N.Y.)*, 350(6260), pp.550–4.

Boyden, E.S., Zhang, F., Bamberg, E., Nagel, G., & Deisseroth, K., 2005. Millisecond-timescale, genetically targeted optical control of neural activity. *Nature neuroscience*, 8(9), pp.1263–8.

Brown, J.S., Kalish, H.I., & Farber, I.E., 1951. Conditioned fear as revealed by magnitude of startle response to an auditory stimulus. *Journal of Experimental Psychology*, 41(5), pp.317–328.

Burghardt, N.S., Bush, D.E.A., McEwen, B.S., & LeDoux, J.E., 2007. Acute Selective Serotonin Reuptake Inhibitors Increase Conditioned Fear Expression: Blockade With a 5-HT2C Receptor Antagonist. *Biological Psychiatry*, 62(10), pp.1111–1118.

Burghardt, N.S., Sullivan, G.M., McEwen, B.S., Gorman, J.M., & Ledoux, J.E., 2004. The selective serotonin reuptake inhibitor citalopram increases fear after acute treatment but reduces fear with chronic treatment: A comparison with tianeptine. *Biological Psychiatry*, 55(12), pp.1171–1178.

Burke, L.K., Doslikova, B., D'Agostino, G., Greenwald-Yarnell, M., Georgescu, T., Chianese, R., Martinez de Morentin, P.B., Ogunnowo-Bada, E., Cansell, C., Valencia-Torres, L., Garfield, A.S., Apergis-Schoute, J., Lam, D.D., Speakman, J.R., Rubinstein, M., Low, M.J., Rochford, J.J., Myers, M.G., Evans, M.L., & Heisler, L.K., 2016. Sex difference in physical activity, energy expenditure and obesity driven by a subpopulation of hypothalamic POMC neurons. *Molecular Metabolism*, 5(3), pp.245–252.

Cai, D.J., Aharoni, D., Shuman, T., Shobe, J., Biane, J., Lou, J., Kim, I., Baumgaertel, K., Levenstain, A., Tuszynski, M., Mayford, M., & Silva, A.J., 2016. A shared neural ensemble links distinct contextual memories encoded close in time. *Nature*, 534(7605), pp.115–118.

Calhoon, G.G. & Tye, K.M., 2015. Resolving the neural circuits of anxiety. *Nature neuroscience*, 18(10), pp.1394–404.

Carhart-Harris, R.L., Erritzoe, D., Williams, T., Stone, J.M., Reed, L.J., Colasanti, A., Tyacke, R.J., Leech, R., Malizia, A.L., Murphy, K., Hobden, P., Evans, J., Feilding, A., Wise, R.G., & Nutt, D.J., 2012. Neural correlates of the psychedelic state as determined by fMRI studies with psilocybin. *Proceedings of the National Academy of Sciences of the United States of America*, 109(6), pp.2138–43.

Ceccatelli, S., Villar, M.J., Goldstein, M., & Hökfelt, T., 1989. Expression of c-Fos immunoreactivity in transmitter-characterized neurons after stress. *Proceedings of the National Academy of Sciences of the United States of America*, 86(23), pp.9569–73.

Chalmers, D.T., Lovenberg, T.W., & De Souza, E.B., 1995. Localization of novel corticotropin-releasing factor receptor (CRF2) mRNA expression to specific subcortical nuclei in rat brain: comparison with CRF1 receptor mRNA expression. *The Journal of neuroscience : the official journal of the Society for Neuroscience*, 15(10), pp.6340–50.

Chang, S.E., Todd, T.P., Bucci, D.J., & Smith, K.S., 2015. Chemogenetic manipulation of ventral pallidal neurons impairs acquisition of sign-tracking in rats. *European Journal of Neuroscience*, 42(12), pp.3105–3116.

Charney, D.S., Woods, S.W., Goodman, W.K., & Heninger, G.R., 1987. Serotonin function in anxiety. II. Effects of the serotonin agonist MCPP in panic disorder patients and healthy subjects. *Psychopharmacology*, 92(1), pp.14–24.

Chen, X., Choo, H., Huang, X.P., Yang, X., Stone, O., Roth, B.L., & Jin, J., 2015. The first structure-activity relationship studies for designer receptors exclusively activated by designer drugs. *ACS Chemical Neuroscience*, 6(3), pp.476–484.

Choi, D.C., Furay, A.R., Evanson, N.K., Ostrander, M.M., Ulrich-lai, Y.M., & Herman, J.P., 2007. Bed Nucleus of the Stria Terminalis Subregions Differentially Regulate Hypothalamic – Pituitary – Adrenal Axis Activity : Implications for the Integration of Limbic Inputs. *Animals*, 27(8), pp.2025–

2034.

Chow, B.Y., Han, X., Dobry, A.S., Qian, X., Chuong, A.S., Li, M., Henninger, M.A., Belfort, G.M., Lin, Y., Monahan, P.E., & Boyden, E.S., 2010. High-performance genetically targetable optical neural silencing by light-driven proton pumps. *Nature*, 463(7277), pp.98–102.

Clarke, S.D., 1993. Regulation of fatty acid synthase gene expression: an approach for reducing fat accumulation. *Journal of animal science*, 71(7), pp.1957–65.

Commons, K.G., Connolley, K.R., & Valentino, R.J., 2003. A neurochemically distinct dorsal raphe-limbic circuit with a potential role in affective disorders. *Neuropsychopharmacology : official publication of the American College of Neuropsychopharmacology*, 28(2), pp.206–15.

Coric, V., Feldman, H.H., Oren, D.A., Shekhar, A., Pultz, J., Dockens, R.C., Wu, X., Gentile, K.A., Huang, S.P., Emison, E., Delmonte, T., D'Souza, B.B., Zimbroff, D.L., Grebb, J.A., Goddard, A.W., & Stock, E.G., 2010. Multicenter, randomized, double-blind, active comparator and placebo-controlled trial of a corticotropin-releasing factor receptor-1 antagonist in generalized anxiety disorder. *Depression and Anxiety*, 27(5), pp.417–425.

Costafreda, S.G., Brammer, M.J., David, A.S., & Fu, C.H.Y., 2008. Predictors of amygdala activation during the processing of emotional stimuli: A meta-analysis of 385 PET and fMRI studies. *Brain Research Reviews*, 58(1), pp.57–70.

Coste, S.C., Murray, S.E., & Stenzel-Poore, M.P., 2001. Animal models of CRH excess and CRH receptor deficiency display altered adaptations to stress. *Peptides*, 22(5), pp.733–741.

Cota, D., Steiner, M.-A., Marsicano, G., Cervino, C., Herman, J.P., Grübler, Y., Stalla, J., Pasquali, R., Lutz, B., Stalla, G.K., & Pagotto, U., 2007. Requirement of cannabinoid receptor type 1 for the basal modulation of hypothalamic-pituitary-adrenal axis function. *Endocrinology*, 148(4), pp.1574–81.

Crestani, C.C., Alves, F.H., Gomes, F. V, Resstel, L.B., Correa, F.M., & Herman, J.P., 2013. Mechanisms in the bed nucleus of the stria terminalis involved in control of autonomic and neuroendocrine functions: a review. *Current neuropharmacology*, 11(2), pp.141–59.

Crestani, C.C., Alves, F.H.F., Resstel, L.B.M., & Correa, F.M.A., 2010. The bed nucleus of the stria terminalis modulates exercise-evoked cardiovascular responses in rats. *Experimental physiology*, 95(1), pp.69–79.

Cryan, J.F. & Holmes, A., 2005. The ascent of mouse: advances in modelling human depression and anxiety. *Nature reviews. Drug discovery*, 4(9), pp.775–90.

Cummings, S., Elde, R., Ells, J., & Lindall, A., 1983. Corticotropin-releasing factor immunoreactivity is widely distributed within the central nervous system of the rat: an immunohistochemical study. *The Journal of neuroscience : the official journal of the Society for Neuroscience*, 3(7), pp.1355–68.

Dabrowska, J., Hazra, R., Ahern, T.H., Guo, J.D., McDonald, A.J., Mascagni, F., Muller, J.F., Young, L.J., & Rainnie, D.G., 2011. Neuroanatomical evidence for reciprocal regulation of the corticotrophin-releasing factor and oxytocin systems in the hypothalamus and the bed nucleus of the stria terminalis of the rat: Implications for balancing stress and affect. *Psychoneuroendocrinology*, 36(9), pp.1312–1326.

Dabrowska, J., Hazra, R., Guo, J.D., DeWitt, S., & Rainnie, D.G., 2013. Central CRF neurons are not created equal: Phenotypic differences in CRF-containing neurons of the rat paraventricular hypothalamus and the bed nucleus of the stria terminalis. *Frontiers in Neuroscience*, 7(7 AUG), p.156.

Daniel, S.E. & Rainnie, D.G., 2015. Stress Modulation of Opposing Circuits in the Bed Nucleus of the Stria Terminalis. *Neuropsychopharmacology*, 41(1), pp.1–23.

Davis, M., Walker, D.L., & Lee, Y., 1997. Amygdala and bed nucleus of the stria terminalis: differential roles in fear and anxiety measured with the acoustic startle reflex. *Philos.Trans.R.Soc.Lond B Biol.Sci.*, 352(1362), pp.1675–1687.

Davis, M., Walker, D.L., Miles, L., & Grillon, C., 2010. Phasic vs sustained fear in rats and humans: role of the extended amygdala in fear vs anxiety. *Neuropsychopharmacology : official publication of the American College of Neuropsychopharmacology*, 35(1), pp.105–35.

Dean Mobbs, Predrag Petrovic, Jennifer L. Marchant, Demis Hassabis, Nikolaus Weiskopf, Ben Seymour, Raymond J. Dolan, & Christopher D. Frith, 2013. When Fear Is Near:\nThreat Imminence Elicits Prefrontal–\nPeriaqueductal Gray Shifts in Humans. *Science*, 317(2007), pp.1079–1083.

Deisseroth, K., 2011. Optogenetics. *Nature Methods*, 8(1), pp.26–29.

Dekeyne, A., Denorme, B., Monneyron, S., & Millan, M.J., 2000. Citalopram reduces social interaction in rats by activation of serotonin (5-HT)(2C) receptors. *Neuropharmacology*, 39(6), pp.1114–7.

Di, S., Malcher-Lopes, R., Halmos, K.C., & Tasker, J.G., 2003. Nongenomic glucocorticoid inhibition via endocannabinoid release in the hypothalamus: a fast feedback mechanism. *The Journal of neuroscience : the official journal of the Society for Neuroscience*, 23(12), pp.4850–4857.

DiLuca, M. & Olesen, J., 2014. The cost of brain diseases: A burden or a challenge? *Neuron*, 82(6), pp.1205–1208.

Dong, H.W., Petrovich, G.D., & Swanson, L.W., 2001. Topography of projections from amygdala to bed nuclei of the stria terminalis. *Brain Research Reviews*, 38(1–2), pp.192–246.

Dong, H.W., Petrovich, G.D., Watts, A.G., & Swanson, L.W., 2001. Basic organization of projections from the oval and fusiform nuclei of the bed nuclei of the stria terminalis in adult rat brain. *Journal of Comparative Neurology*, 436(4), pp.430–455.

Dong, H.W., Petrovich, G.D., Watts, a G., & Swanson, L.W., 2001. Basic organization of projections from the oval and fusiform nuclei of the bed nuclei of the stria terminalis in adult rat brain. *The Journal of comparative neurology*, 436(4), pp.430–55.

Dong, H.W. & Swanson, L.W., 2004a. Organization of Axonal Projections from the Anterolateral Area of the Bed Nuclei of the Stria Terminalis. *Journal of Comparative Neurology*, 468(2), pp.277–298.

Dong, H.W. & Swanson, L.W., 2006a. Projections from bed nuclei of the stria terminalis, anteromedial area: Cerebral hemisphere integration of neuroendocrine, autonomic, and behavioral aspects of energy balance. *Journal of Comparative Neurology*, 494(1), pp.142–178.

Dong, H.W. & Swanson, L.W., 2006b. Projections from bed nuclei of the stria terminalis, dorsomedial nucleus: Implications for cerebral hemisphere integration of neuroendocrine, autonomic, and drinking responses. *Journal of Comparative Neurology*, 494(1), pp.75–107.

Dong, H.W. & Swanson, L.W., 2004b. Projections from Bed Nuclei of the Stria Terminalis, Posterior Division: Implications for Cerebral Hemisphere Regulation of Defensive and Reproductive Behaviors. *Journal of Comparative Neurology*, 471(4), pp.396–433.

Dong, H.W. & Swanson, L.W., 2003. Projections from the rhomboid nucleus of the bed nuclei of the stria terminalis: Implications for cerebral hemisphere regulation of ingestive behaviors. *Journal of Comparative Neurology*, 463(4), pp.434–472.

Dong, J., Zuo, S., Liu, M., Gan, Y., Chen, B., & Zou, S., 2006. Influence of connexin43 on the bystander effect induced by double suicide genes system in vitro and in vivo. *Chinese-German Journal of Clinical Oncology*, 5(2), pp.108–112.

Dumont, E.C. & Williams, J.T., 2004. Noradrenaline triggers GABAA inhibition of bed nucleus of the stria terminalis neurons projecting to the ventral tegmental area. *The Journal of neuroscience : the official journal of the Society for Neuroscience*, 24(38), pp.8198–204.

Dunn, A.J. & Berridge, C.W., 1990. Physiological and behavioral responses to corticotropin-releasing factor administration: is CRF a mediator of anxiety or stress responses? *Brain Research Reviews*, 15(2), pp.71–100.

Elharrar, E., Warhaftig, G., Issler, O., Sztainberg, Y., Dikshtein, Y., Zahut, R., Redlus, L., Chen, A., & Yadid, G., 2013. Overexpression of corticotropin-releasing factor receptor type 2 in the bed nucleus of stria terminalis improves posttraumatic stress disorder-like symptoms in a model of incubation of fear. *Biological Psychiatry*, 74(11), pp.827–836.

Erb, S., Salmaso, N., Rodaros, D., & Stewart, J., 2001. A role for the CRF-containing pathway from central nucleus of the amygdala to bed nucleus of the stria terminalis in the stress-induced reinstatement of cocaine seeking in rats. *Psychopharmacology*, 158(4), pp.360–5.

Erb, S. & Stewart, J., 1999. A role for the bed nucleus of the stria terminalis, but not the amygdala, in the effects of corticotropin-releasing factor on stress-induced reinstatement of cocaine seeking. *The Journal of neuroscience : the official journal of the Society for Neuroscience*, 19(20), p.RC35.

Etkin, A., Prater, K.E., Hoeft, F., Menon, V., & Schatzberg, A.F., 2010. Failure of anterior cingulate activation and connectivity with the amygdala during implicit regulation of emotional processing in generalized anxiety disorder. *American Journal of Psychiatry*, 167(5), pp.545–554.

Fakhoury, M., 2016. Revisiting the Serotonin Hypothesis: Implications for Major Depressive Disorders. *Molecular Neurobiology*, 53(5), pp.2778–2786.

Fenno, L.E., Mattis, J., Ramakrishnan, C., Hyun, M., Lee, S.Y., He, M., Tucciarone, J., Selimbeyoglu, A., Berndt, A., Grosenick, L., Zalocusky, K.A., Bernstein, H., Swanson, H., Perry, C., Diester, I., Boyce, F.M., Bass, C.E., Neve, R., Huang, Z.J., & Deisseroth, K., 2014. Targeting cells with single vectors using multiple-feature Boolean logic. *Nature methods*, 11(7), pp.763–72.

Fergusson, D., Doucette, S., Glass, K.C., Shapiro, S., Healy, D., Hebert, P., & Hutton, B., 2005. Association between suicide attempts and selective serotonin reuptake inhibitors: systematic review of randomised controlled trials. *Bmj*, 330(7488), p.396.

Forray, M.I., Gysling, K., Andrés, M.E., Bustos, G., & Araneda, S., 2000. Medullary noradrenergic neurons projecting to the bed nucleus of the stria terminalis express mRNA for the NMDA-NR1 receptor. *Brain research bulletin*, 52(3), pp.163–9.

Fox, A.S., Shelton, S.E., Oakes, T.R., Davidson, R.J., & Kalin, N.H., 2008. Trait-like brain activity during adolescence predicts anxious temperament in primates. *PLoS ONE*, 3(7), p.e2570.

Fox, J.H., Hammack, S.E., & Falls, W.A., 2008. Exercise is associated with reduction in the anxiogenic effect of mCPP on acoustic startle. *Behavioral Neuroscience*, 122(4), pp.943–948.

Freund, T.F., Katona, I., & Piomelli, D., 2003. Role of endogenous cannabinoids in synaptic signaling. *Physiological reviews*, 83(3), pp.1017–66.

Funk, D., Li, Z., & Lê, A.D., 2006. Effects of environmental and pharmacological stressors on c-fos and corticotropin-releasing factor mRNA in rat brain: Relationship to the reinstatement of alcohol seeking. *Neuroscience*, 138(1), pp.235–43.

Fuxe, K., 1965. Evidence for the existence of monoamine neurons in the central nervous system. *Zeitschrift für Zellforschung und Mikroskopisch*, 596(65), pp.573–596.

Gafford, G.M., Guo, J.-D., Flandreau, E.I., Hazra, R., Rainnie, D.G., & Ressler, K.J., 2012. Cell-type

specific deletion of GABA(A)alpha 1 in corticotropin-releasing factor-containing neurons enhances anxiety and disrupts fear extinction. *Proc Natl Acad Sci U S A*, 109(40), pp.16330–16335.

Garcia-Garcia, A.L., Newman-Tancredi, A., & Leonardo, E.D., 2014. P5-HT1A receptors in mood and anxiety: Recent insights into autoreceptor versus heteroreceptor function. *Psychopharmacology*, 231(4), pp.623–636.

Gerachshenko, T., Blackmer, T., Yoon, E.-J., Bartleson, C., Hamm, H.E., & Alford, S., 2005. Gbetagamma acts at the C terminus of SNAP-25 to mediate presynaptic inhibition. *Nature neuroscience*, 8(5), pp.597–605.

Gewirtz, J.C., McNish, K.A., & Davis, M., 1998. Lesions of the bed nucleus of the stria terminalis block sensitization of the acoustic startle reflex produced by repeated stress, but not fear- potentiated startle. *Progress in Neuro-Psychopharmacology and Biological Psychiatry*, 22(4), pp.625–648.

Glangetas, C., Girard, D., Groc, L., Marsicano, G., Chaouloff, F., & Georges, F., 2013. Stress switches cannabinoid type-1 (CB1) receptor-dependent plasticity from LTD to LTP in the bed nucleus of the stria terminalis. *The Journal of neuroscience : the official journal of the Society for Neuroscience*, 33(50), pp.19657–63.

Glass, M., Dragunow, M., & Faull, R.L., 1997. Cannabinoid receptors in the human brain: a detailed anatomical and quantitative autoradiographic study in the fetal, neonatal and adult human brain. *Neuroscience*, 77(2), pp.299–318.

Goldberg, H.L. & Finnerty, R.J., 1979. The comparative efficacy of buspirone and diazepam in the treatment of anxiety. *The American journal of psychiatry*, 136(9), pp.1184–7.

Gorman, J.M., Liebowitz, M.R., Fyer, A.J., Goetz, D., Campeas, R.B., Fyer, M.R., Davies, S.O., & Klein, D.F., 1987. An open trial of fluoxetine in the treatment of panic attacks. *Journal of clinical psychopharmacology*, 7(5), pp.329–32.

Gorwood, P., 2004. Generalized anxiety disorder and major depressive disorder comorbidity: an example of genetic pleiotropy? *European psychiatry : the journal of the Association of European Psychiatrists*, 19(1), pp.27–33.

Graeff, F.G., 2002. On serotonin and experimental anxiety. *Psychopharmacology*, 163(3–4), pp.467–476.

Grammatopoulos, D.K., Randeva, H.S., Levine, M.A., Kanellopoulou, K.A., & Hillhouse, E.W., 2001. Rat cerebral cortex corticotropin-releasing hormone receptors: Evidence for receptor coupling to multiple G-proteins. *Journal of Neurochemistry*, 76(2), pp.509–519.

Greenberg, T., Carlson, J.M., Cha, J., Hajcak, G., & Mujica-Parodi, L.R., 2013. Ventromedial prefrontal cortex reactivity is altered in generalized anxiety disorder during fear generalization. *Depression and Anxiety*, 30(3), pp.242–250.

Griebel, G. & Holmes, A., 2013. 50 Years of Hurdles and Hope in Anxiolytic Drug Discovery. *Nature reviews. Drug discovery*, 12(9), pp.667–87.

Griffiths, R.R., Johnson, M.W., Carducci, M.A., Umbricht, A., Richards, W.A., Richards, B.D., Cosimano, M.P., & Klinedinst, M.A., 2016. Psilocybin produces substantial and sustained decreases in depression and anxiety in patients with life-threatening cancer: A randomized double-blind trial. *Journal of psychopharmacology (Oxford, England)*, 30(12), pp.1181–1197.

Grillon, C., Chavis, C., Covington, M.F., & Pine, D.S., 2009. Two-week treatment with the selective serotonin reuptake inhibitor citalopram reduces contextual anxiety but not cued fear in healthy volunteers: a fear-potentiated startle study. *Neuropsychopharmacology : official publication of the American College of Neuropsychopharmacology*, 34(4), pp.964–971.

Grillon, C., Levenson, J., & Pine, D.S., 2007. A single dose of the selective serotonin reuptake inhibitor citalopram exacerbates anxiety in humans: a fear-potentiated startle study. *Neuropsychopharmacology : official publication of the American College of Neuropsychopharmacology*, 32(1), pp.225–231.

Grillon, C., Morgan, C.A., Davis, M., & Southwick, S.M., 1998. Effect of darkness on acoustic startle in Vietnam veterans with PTSD. *American Journal of Psychiatry*, 155(6), pp.812–817.

Grillon, C., Pellowski, M., Merikangas, K.R., & Davis, M., 1997. Darkness facilitates the acoustic startle reflex in humans. *Biological Psychiatry*, 42(6), pp.453–460.

Grueter, B.A., Gosnell, H.B., Olsen, C.M., Schramm-Sapyta, N.L., Nekrasova, T., Landreth, G.E., & Winder, D.G., 2006. Extracellular-signal regulated kinase 1-dependent metabotropic glutamate receptor 5-induced long-term depression in the bed nucleus of the stria terminalis is disrupted by cocaine administration. *The Journal of neuroscience : the official journal of the Society for Neuroscience*, 26(12), pp.3210–9.

Grueter, B.A., McElligott, Z.A., & Winder, D.G., 2007. Group I mGluRs and long-term depression: Potential roles in addiction? *Molecular Neurobiology*, 36(3), pp.232–244.

Guettier, J.-M., Gautam, D., Scarselli, M., Ruiz de Azua, I., Li, J.H., Rosemond, E., Ma, X., Gonzalez, F.J., Armbruster, B.N., Lu, H., Roth, B.L., & Wess, J., 2009. A chemical-genetic approach to study G protein regulation of beta cell function in vivo. *Proceedings of the National Academy of Sciences of the United States of America*, 106(45), pp.19197–202.

Gungor, N.Z. & Paré, D., 2016. Functional Heterogeneity in the Bed Nucleus of the Stria Terminalis. *The Journal of neuroscience : the official journal of the Society for Neuroscience*, 36(31), pp.8038–49.

Hackler, E. a, Turner, G.H., Gresch, P.J., Sengupta, S., Deutch, A.Y., Avison, M.J., Gore, J.C., & Sanders-bush, E., 2007. 5-Hydroxytryptamine2C Receptor Contribution to m-Chlorophenylpiperazine and N-Methyl-ß-carboline-3- carboxamide-Induced Anxiety-Like Behavior and Limbic Brain Activation. *The Journal of Pharmacology and Experimental Therapeutics*, 320(3), pp.1023–1029.

Hammack, S.E., Cheung, J., Rhodes, K.M., Schutz, K.C., Falls, W.A., Braas, K.M., & May, V., 2009. Chronic stress increases pituitary adenylate cyclase-activating peptide (PACAP) and brain-derived neurotrophic factor (BDNF) mRNA expression in the bed nucleus of the stria terminalis (BNST): Roles for PACAP in anxiety-like behavior. *Psychoneuroendocrinology*, 34(6), pp.833–843.

Hammack, S.E., Guo, J.D., Hazra, R., Dabrowska, J., Myers, K.M., & Rainnie, D.G., 2009. The response of neurons in the bed nucleus of the stria terminalis to serotonin: Implications for anxiety. *Progress in Neuro-Psychopharmacology and Biological Psychiatry*, 33(8), pp.1309–1320.

Hammack, S.E., Mania, I., & Rainnie, D.G., 2007. Differential expression of intrinsic membrane currents in defined cell types of the anterolateral bed nucleus of the stria terminalis. *Journal of neurophysiology*, 98(2), pp.638–56.

Hammack, S.E., Richey, K.J., Schmid, M.J., LoPresti, M.L., Watkins, L.R., & Maier, S.F., 2002. The role of corticotropin-releasing hormone in the dorsal raphe nucleus in mediating the behavioral consequences of uncontrollable stress. *The Journal of neuroscience : the official journal of the Society for Neuroscience*, 22(3), pp.1020–1026.

Hammack, S.E., Schmid, M.J., LoPresti, M.L., Der-Avakian, A., Pellymounter, M.A., Foster, A.C., Watkins, L.R., & Maier, S.F., 2003. Corticotropin releasing hormone type 2 receptors in the dorsal raphe nucleus mediate the behavioral consequences of uncontrollable stress. *The Journal of neuroscience : the official journal of the Society for Neuroscience*, 23(3), pp.1019–1025.

Hannon, J. & Hoyer, D., 2008. Molecular biology of 5-HT receptors. *Behavioural Brain Research*, 195(1),

pp.198–213.

Hasue, R.H. & Shammah-Lagnado, S.J., 2002. Origin of the dopaminergic innervation of the central extended amygdala and accumbens shell: A combined retrograde tracing and immunohistochemical study in the rat. *Journal of Comparative Neurology*, 454(1), pp.15–33.

Hauger, R.L., Risbrough, V., Brauns, O., & Dautzenberg, F.M., 2006. Corticotropin releasing factor (CRF) receptor signaling in the central nervous system: new molecular targets. *CNS & neurological disorders drug targets*, 5(4), pp.453–79.

Hefner, K., Whittle, N., Juhasz, J., Norcross, M., Karlsson, R.-M., Saksida, L.M., Bussey, T.J., Singewald, N., & Holmes, A., 2008. Impaired fear extinction learning and cortico-amygdala circuit abnormalities in a common genetic mouse strain. *The Journal of neuroscience : the official journal of the Society for Neuroscience*, 28(32), pp.8074–85.

Heilig, M., 2004. The NPY system in stress, anxiety and depression. *Neuropeptides*, 38(4), pp.213–224.

Heilig, M. & Koob, G.F., 2007. A key role for corticotropin-releasing factor in alcohol dependence. *Trends in Neurosciences*, 30(8), pp.399–406.

Heinrichs, S.C. & Koob, G.F., 2004. Corticotropin-Releasing Factor in Brain: A Role in Activation, Arousal, and Affect Regulation. *Journal of Pharmacology and Experimental Therapeutics*, 311(2), pp.427–440.

Heisler, L.K., Zhou, L., Bajwa, P., Hsu, J., & Tecott, L.H., 2007. Serotonin 5-HT(2C) receptors regulate anxiety-like behavior. *Genes, brain, and behavior*, 6(5), pp.491–6.

Herkenham, M., Allison B. Lynn, Little, M.D., Johnson, M.R., Melvin, L.S., Costa, B.R. de, & Rice, K.C., 1990. Cannabinoid Receptor Localization in Brain. *Proceedings of the National Academy of Sciences of the United States of America*, 87(5), pp.1932–1936.

Herman, J.P., Figueiredo, H., Mueller, N.K., Ulrich-Lai, Y., Ostrander, M.M., Choi, D.C., & Cullinan, W.E., 2003. Central mechanisms of stress integration: Hierarchical circuitry controlling hypothalamo-pituitary-adrenocortical responsiveness. *Frontiers in Neuroendocrinology*, 24(3), pp.151–180.

Hill, M.N., Patel, S., Campolongo, P., Tasker, J.G., Wotjak, C.T., & Bains, J.S., 2010. Functional interactions between stress and the endocannabinoid system: from synaptic signaling to behavioral output. *The Journal of neuroscience : the official journal of the Society for Neuroscience*, 30(45), pp.14980–6.

Hill, M.N. & Tasker, J.G., 2012. Endocannabinoid signaling, glucocorticoid-mediated negative feedback, and regulation of the hypothalamic-pituitary-adrenal axis. *Neuroscience*, 204, pp.5–16.

Hitchcock, J.M. & Davis, M., 1991. Efferent Pathway of the Amygdala Involved in Conditioned Fear as Measured With the Fear-Potentiated Startle Paradigm. *Behavioral Neuroscience Crow & Alkon*, 105(6), pp.826–842.

Hoehn-Saric, R., Schlund, M.W., & Wong, S.H.Y., 2004. Effects of citalopram on worry and brain activation in patients with generalized anxiety disorder. *Psychiatry Research - Neuroimaging*, 131(1), pp.11–21.

Hoffman, E.J. & Mathew, S.J., 2008. Anxiety disorders: A comprehensive review of pharmacotherapies. *Mount Sinai Journal of Medicine*, 75(3), pp.248–262.

Huang, M.M., Overstreet, D.H., Knapp, D.J., Angel, R., Wills, T.A., Navarro, M., Rivier, J., Vale, W., & Breese, G.R., 2010. Corticotropin-releasing factor (CRF) sensitization of ethanol withdrawal-induced anxiety-like behavior is brain site specific and mediated by CRF-1 receptors: relation to stress-induced sensitization. *The Journal of pharmacology and experimental therapeutics*, 332(1), pp.298–

307.

Hur, E.E. & Zaborszky, L., 2005. Vglut2 afferents to the medial prefrontal and primary somatosensory cortices: A combined retrograde tracing in situ hybridization. *Journal of Comparative Neurology*, 483(3), pp.351–373.

Ide, S., Hara, T., Ohno, A., Tamano, R., Koseki, K., Naka, T., Maruyama, C., Kaneda, K., Yoshioka, M., & Minami, M., 2013. Opposing roles of corticotropin-releasing factor and neuropeptide Y within the dorsolateral bed nucleus of the stria terminalis in the negative affective component of pain in rats. *The Journal of neuroscience : the official journal of the Society for Neuroscience*, 33(14), pp.5881–94.

Insel, T.R., 2012. Next-generation treatments for mental disorders. *Science translational medicine*, 4(155), p.155ps19.

Ising, M., Zimmermann, U.S., Künzel, H.E., Uhr, M., Foster, A.C., Learned-Coughlin, S.M., Holsboer, F., & Grigoriadis, D.E., 2007. High-affinity CRF1 receptor antagonist NBI-34041: preclinical and clinical data suggest safety and efficacy in attenuating elevated stress response. *Neuropsychopharmacology : official publication of the American College of Neuropsychopharmacology*, 32(9), pp.1941–1949.

Janak, P.H. & Tye, K.M., 2015. From circuits to behaviour in the amygdala. *Nature*, 517(7534), pp.284–292.

Jann, M.W., Lam, Y.W., & Chang, W.H., 1994. Rapid formation of clozapine in guinea-pigs and man following clozapine-N-oxide administration. *Archives internationales de pharmacodynamie et de therapie*, 328(2), pp.243–50.

Jasinska, A.J., Lowry, C.A., & Burmeister, M., 2012. Serotonin transporter gene, stress and raphe-raphe interactions: a molecular mechanism of depression. *Trends in Neurosciences*, 35(7), pp.395–402.

Javelot, H., Weiner, L., Terramorsi, R., Rougeot, C., Lalonde, R., & Messaoudi, M., 2011. Efficacy of chronic antidepressant treatments in a new model of extreme anxiety in rats. *Depression Research and Treatment*, 2011, p.531435.

Jennings, J.H., Rizzi, G., Stamatakis, A.M., Ung, R.L., & Stuber, G.D., 2013. The inhibitory circuit architecture of the lateral hypothalamus orchestrates feeding. *Science (New York, N.Y.)*, 341(6153), pp.1517–21.

Jennings, J.H., Sparta, D.R., Stamatakis, A.M., Ung, R.L., Pleil, K.E., Kash, T.L., & Stuber, G.D., 2013. Distinct extended amygdala circuits for divergent motivational states. *Nature*, 496(7444), pp.224–228.

De Jongh, R., Groenink, L., Van Der Gugten, J., & Olivier, B., 2003. Light-enhanced and fear-potentiated startle: Temporal characteristics and effects of ??-helical corticotropin-releasing hormone. *Biological Psychiatry*, 54(10), pp.1041–1048.

Kalin, N.H., Shelton, S.E., Fox, A.S., Oakes, T.R., & Davidson, R.J., 2005. Brain regions associated with the expression and contextual regulation of anxiety in primates. *Biological Psychiatry*, 58(10), pp.796–804.

Kash, T.L., 2012. The role of biogenic amine signaling in the bed nucleus of the stria terminals in alcohol abuse. *Alcohol*, 46(4), pp.303–308.

Kash, T.L., Nobis, W.P., Matthews, R.T., & Winder, D.G., 2008. Dopamine enhances fast excitatory synaptic transmission in the extended amygdala by a CRF-R1-dependent process. *The Journal of neuroscience : the official journal of the Society for Neuroscience*, 28(51), pp.13856–65.

Kash, T.L., Pleil, K.E., Marcinkiewcz, C.A., Lowery-Gionta, E.G., Crowley, N., Mazzone, C., Sugam, J., Hardaway, J.A., & McElligott, Z.A., 2015. Neuropeptide regulation of signaling and behavior in the BNST. *Molecules and cells*, 38(1), pp.1–13.

Kash, T.L. & Winder, D.G., 2006. Neuropeptide Y and corticotropin-releasing factor bi-directionally modulate inhibitory synaptic transmission in the bed nucleus of the stria terminalis. *Neuropharmacology*, 51(5), pp.1013–1022.

Kawahara, H., Yoshida, M., Yokoo, H., Nishi, M., & Tanaka, M., 1993. Psychological stress increases serotonin release in the rat amygdala and prefrontal cortex assessed by in vivo microdialysis. *Neuroscience Letters*, 162(1–2), pp.81–84.

Kennett, G.A., Whitton, P., Shah, K., & Curzon, G., 1989. Anxiogenic-like effects of mCPP and TFMPP in animal models are opposed by 5-HT1C receptor antagonists. *European journal of pharmacology*, 164(3), pp.445–54.

Kessler, R.C., 2005. Prevalence, Severity, and Comorbidity of 12-Month DSM-IV Disorders in the National Comorbidity Survey Replication. *Archives of General Psychiatry*, 62(6), pp.617–627.

Kessler, R.C., Angermeyer, M., Anthony, J.C., DE Graaf, R., Demyttenaere, K., Gasquet, I., DE Girolamo, G., Gluzman, S., Gureje, O., Haro, J.M., Kawakami, N., Karam, A., Levinson, D., Medina Mora, M.E., Oakley Browne, M.A., Posada-Villa, J., Stein, D.J., Adley Tsang, C.H., Aguilar-Gaxiola, S., Alonso, J., Lee, S., Heeringa, S., Pennell, B.-E., Berglund, P., Gruber, M.J., Petukhova, M., Chatterji, S., & Ustün, T.B., 2007. Lifetime prevalence and age-of-onset distributions of mental disorders in the World Health Organization's World Mental Health Survey Initiative. *World psychiatry : official journal of the World Psychiatric Association (WPA)*, 6(3), pp.168–76.

Khoshbouei, H., Cecchi, M., & Morilak, D.A., 2002. Modulatory effects of galanin in the lateral bed nucleus of the stria terminalis on behavioral and neuroendocrine responses to acute stress. *Neuropsychopharmacology : official publication of the American College of Neuropsychopharmacology*, 27(1), pp.25–34.

Kim, S.-Y., Adhikari, A., Lee, S.Y., Marshel, J.H., Kim, C.K., Mallory, C.S., Lo, M., Pak, S., Mattis, J., Lim, B.K., Malenka, R.C., Warden, M.R., Neve, R., Tye, K.M., & Deisseroth, K., 2013. Diverging neural pathways assemble a behavioural state from separable features in anxiety. *Nature*, 496(7444), pp.219–23.

Kirby, L.G., Rice, K.C., & Valentino, R.J., 2000. Effects of corticotropin-releasing factor on neuronal activity in the serotonergic dorsal raphe nucleus. *Neuropsychopharmacology : official publication of the American College of Neuropsychopharmacology*, 22(2), pp.148–62.

Klapoetke, N.C., Murata, Y., Kim, S.S., Pulver, S.R., Birdsey-Benson, A., Cho, Y.K., Morimoto, T.K., Chuong, A.S., Carpenter, E.J., Tian, Z., Wang, J., Xie, Y., Yan, Z., Zhang, Y., Chow, B.Y., Surek, B., Melkonian, M., Jayaraman, V., Constantine-Paton, M., Wong, G.K.-S., & Boyden, E.S., 2014. Independent optical excitation of distinct neural populations. *Nature methods*, 11(3), pp.338–46.

Krashes, M.J., Koda, S., Ye, C., Rogan, S.C., Adams, A.C., Cusher, D.S., Maratos-Flier, E., Roth, B.L., & Lowell, B.B., 2011. Rapid, reversible activation of AgRP neurons drives feeding behavior in mice. *Journal of Clinical Investigation*, 121(4), pp.1424–1428.

Krashes, M.J., Shah, B.P., Madara, J.C., Olson, D.P., Strochlic, D.E., Garfield, A.S., Vong, L., Pei, H., Watabe-Uchida, M., Uchida, N., Liberles, S.D., & Lowell, B.B., 2014. An excitatory paraventricular nucleus to AgRP neuron circuit that drives hunger. *Nature*, 507(7491), pp.238–42.

Kudo, T., Uchigashima, M., Miyazaki, T., Konno, K., Yamasaki, M., Yanagawa, Y., Minami, M., & Watanabe, M., 2012. Three types of neurochemical projection from the bed nucleus of the stria terminalis to the ventral tegmental area in adult mice. *The Journal of neuroscience : the official*

journal of the Society for Neuroscience, 32(50), pp.18035–46.

Lebow, M. & Chen, A., 2016. Overshadowed by the amygdala: the bed nucleus of the stria terminalis emerges as key to psychiatric disorders. *Molecular Psychiatry*, 21(4), pp.450–63.

Lebow, M., Neufeld-cohen, A., Kuperman, Y., Tsoory, M.M., Gil, S., & Chen, A., 2012. Susceptibility to PTSD-Like Behavior Is Mediated by Corticotropin-Releasing Factor Receptor Type 2 Levels in the Bed Nucleus of the Stria Terminalis. *Journal of Neuroscience*, 32(20), pp.6906–6916.

LeDoux, J., 2012. Rethinking the Emotional Brain. *Neuron*, 73(4), pp.653–676.

LeDoux, J.E., 2000. Emotion Circuits in the Brain. *Annual Review of Neuroscience*, 23(1), pp.155–184.

LeDoux, J.E., Iwata, J., Cicchetti, P., & Reis, D.J., 1988. Different projections of the central amygdaloid nucleus mediate autonomic and behavioral correlates of conditioned fear. *The Journal of neuroscience : the official journal of the Society for Neuroscience*, 8(7), pp.2517–29.

Lee, Y. & Davis, M., 1997. Role of the hippocampus, the bed nucleus of the stria terminalis, and the amygdala in the excitatory effect of corticotropin-releasing hormone on the acoustic startle reflex. *The Journal of neuroscience : the official journal of the Society for Neuroscience*, 17(16), pp.6434–46.

Lemos, J.C., Wanat, M.J., Smith, J.S., Reyes, B.A.S., Hollon, N.G., Van Bockstaele, E.J., Chavkin, C., & Phillips, P.E.M., 2012. Severe stress switches CRF action in the nucleus accumbens from appetitive to aversive. *Nature*, 490(7420), pp.402–6.

Levita, L., Hammack, S.E., Mania, I., Li, X.-Y., Davis, M., & Rainnie, D.G., 2004. 5-hydroxytryptamine1A-like receptor activation in the bed nucleus of the stria terminalis: electrophysiological and behavioral studies. *Neuroscience*, 128(3), pp.583–96.

Lewis, K., Li, C., Perrin, M.H., Blount, A., Kunitake, K., Donaldson, C., Vaughan, J., Reyes, T.M., Gulyas, J., Fischer, W., Bilezikjian, L., Rivier, J., Sawchenko, P.E., & Vale, W.W., 2001. Identification of urocortin III, an additional member of the corticotropin-releasing factor (CRF) family with high affinity for the CRF2 receptor. *Proceedings of the National Academy of Sciences of the United States of America*, 98(13), pp.7570–5.

Liang, K.C., Melia, K.R., Campeau, S., Falls, W.A., Miserendino, M.J., & Davis, M., 1992. Lesions of the central nucleus of the amygdala, but not the paraventricular nucleus of the hypothalamus, block the excitatory effects of corticotropin-releasing factor on the acoustic startle reflex. *The Journal of neuroscience : the official journal of the Society for Neuroscience*, 12(6), pp.2313–20.

Lin, J.Y., Lin, M.Z., Steinbach, P., & Tsien, R.Y., 2009. Characterization of engineered channelrhodopsin variants with improved properties and kinetics. *Biophysical Journal*, 96(5), pp.1803–1814.

Lister, R.G., 1990. Ethologically-based animal models of anxiety disorders. *Pharmacology & therapeutics*, 46(3), pp.321–40.

Liu, J., Garza, J.C., Bronner, J., Kim, C.S., Zhang, W., & Lu, X.Y., 2010. Acute administration of leptin produces anxiolytic-like effects: A comparison with fluoxetine. *Psychopharmacology*, 207(4), pp.535–545.

Liu, M.L., Liang, F.R., Zeng, F., Tang, Y., Lan, L., & Song, W.Z., 2012. Cortical-limbic regions modulate depression and anxiety factors in functional dyspepsia: A PET-CT study. *Annals of Nuclear Medicine*, 26(1), pp.35–40.

Liu, X., Ramirez, S., Pang, P.T., Puryear, C.B., Govindarajan, A., Deisseroth, K., & Tonegawa, S., 2012. Optogenetic stimulation of a hippocampal engram activates fear memory recall. *Nature*, 484(7394), pp.381–385.

Liu, Z., Zhou, J., Li, Y., Hu, F., Lu, Y., Ma, M., Feng, Q., Zhang, J. en, Wang, D., Zeng, J., Bao, J., Kim, J.Y., Chen, Z.F., ElMestikawy, S., & Luo, M., 2014. Dorsal raphe neurons signal reward through 5-HT and glutamate. *Neuron*, 81(6), pp.1360–1374.

López, A.J., Kramár, E., Matheos, D.P., White, A.O., Kwapis, J., Vogel-Ciernia, A., Sakata, K., Espinoza, M., & Wood, M.A., 2016. Promoter-Specific Effects of DREADD Modulation on Hippocampal Synaptic Plasticity and Memory Formation. *The Journal of neuroscience : the official journal of the Society for Neuroscience*, 36(12), pp.3588–99.

Lovenberg, T.W., Liaw, C.W., Grigoriadis, D.E., Clevenger, W., Chalmers, D.T., De Souza, E.B., & Oltersdorf, T., 1995. Cloning and characterization of a functionally distinct corticotropin-releasing factor receptor subtype from rat brain. *Proceedings of the National Academy of Sciences of the United States of America*, 92(3), pp.836–40.

Lowry, C.A., Rodda, J.E., Lightman, S.L., & Ingram, C.D., 2000. Corticotropin-releasing factor increases in vitro firing rates of serotonergic neurons in the rat dorsal raphe nucleus: evidence for activation of a topographically organized mesolimbocortical serotonergic system. *The Journal of neuroscience : the official journal of the Society for Neuroscience*, 20(20), pp.7728–36.

Marcinkiewcz, C.A., Dorrier, C.E., Lopez, A.J., & Kash, T.L., 2015. Ethanol induced adaptations in 5-HT2c receptor signaling in the bed nucleus of the stria terminalis: Implications for anxiety during ethanol withdrawal. *Neuropharmacology*, 89, pp.157–167.

Marcinkiewcz, C.A., Mazzone, C.M., D'Agostino, G., Halladay, L.R., Hardaway, J.A., DiBerto, J.F., Navarro, M., Burnham, N., Cristiano, C., Dorrier, C.E., Tipton, G.J., Ramakrishnan, C., Kozicz, T., Deisseroth, K., Thiele, T.E., McElligott, Z.A., Holmes, A., Heisler, L.K., & Kash, T.L., 2016. Serotonin engages an anxiety and fear-promoting circuit in the extended amygdala. *Nature*, 537(7618), pp.97–101.

Maurer-Spurej, E., Pittendreigh, C., & Misri, S., 2007. Platelet serotonin levels support depression scores for women with postpartum depression. *Journal of Psychiatry and Neuroscience*, 32(1), pp.23–29.

McElligott, Z.A., Klug, J.R., Nobis, W.P., Patel, S., Grueter, B.A., Kash, T.L., & Winder, D.G., 2010. Distinct forms of Gq-receptor-dependent plasticity of excitatory transmission in the BNST are differentially affected by stress. *Proceedings of the National Academy of Sciences of the United States of America*, 107(5), pp.2271–6.

McElligott, Z.A. & Winder, D.G., 2008. α1-Adrenergic Receptor-Induced Heterosynaptic Long-Term Depression in the Bed Nucleus of the Stria Terminalis Is Disrupted in Mouse Models of Affective Disorders. *Neuropsychopharmacology*, 33(10), pp.2313–2323.

De Mello Cruz, A.P., Pinheiro, G., Alves, S.H., Ferreira, G., Mendes, M., Faria, L., Macedo, C.E., Motta, V., & Landeira-Fernandez, J., 2005. Behavioral effects of systemically administered MK-212 are prevented by ritanserin microinfusion into the basolateral amygdala of rats exposed to the elevated plus-maze. *Psychopharmacology*, 182(3), pp.345–354.

Melón, L.C. & Boehm, S.L., 2011. GABAA receptors in the posterior, but not anterior, ventral tegmental area mediate Ro15-4513-induced attenuation of binge-like ethanol consumption in C57BL/6J female mice. *Behavioural Brain Research*, 220(1), pp.230–237.

Meloni, E.G., Gerety, L.P., Knoll, A.T., Cohen, B.M., & Carlezon, W.A., 2006. Behavioral and anatomical interactions between dopamine and corticotropin-releasing factor in the rat. *The Journal of neuroscience : the official journal of the Society for Neuroscience*, 26(14), pp.3855–63.

Merali, Z., Levac, C., & Anisman, H., 2003. Validation of a simple, ethologically relevant paradigm for assessing anxiety in mice. *Biological Psychiatry*, 54(5), pp.552–565.

Merchenthaler, I., Vigh, S., Petrusz, P., & Schally, A. V., 1982. Immunocytochemical localization of

corticotropin-releasing factor (CRF) in the rat brain. *The American journal of anatomy*, 165(4), pp.385–96.

Meunier, M., Bachevalier, J., Murray, E.A., Málková, L., & Mishkin, M., 1999. Effects of aspiration versus neurotoxic lesions of the amygdala on emotional responses in monkeys. *The European journal of neuroscience*, 11(12), pp.4403–18.

Micale, V., Di Marzo, V., Sulcova, A., Wotjak, C.T., & Drago, F., 2013. Endocannabinoid system and mood disorders: Priming a target for new therapies. *Pharmacology and Therapeutics*, 138(1), pp.18–37.

Michaelides, M., Anderson, S.A.R., Ananth, M., Smirnov, D., Thanos, P.K., Neumaier, J.F., Wang, G.J., Volkow, N.D., & Hurd, Y.L., 2013. Whole-brain circuit dissection in free-moving animals reveals cell-specific mesocorticolimbic networks. *Journal of Clinical Investigation*, 123(12), pp.5342–5350.

Michaelides, M., Pascau, J., Gispert, J.D., Delis, F., Grandy, D.K., Wang, G.J., Desco, M., Rubinstein, M., Volkow, N.D., & Thanos, P.K., 2010. Dopamine D4 receptors modulate brain metabolic activity in the prefrontal cortex and cerebellum at rest and in response to methylphenidate. *European Journal of Neuroscience*, 32(4), pp.668–676.

Mobbs, D., Yu, R., Rowe, J.B., Eich, H., FeldmanHall, O., & Dalgleish, T., 2010. Neural activity associated with monitoring the oscillating threat value of a tarantula. *Proceedings of the National Academy of Sciences of the United States of America*, 107(47), pp.20582–6.

Mochcovitch, M.D., Da Rocha Freire, R.C., Garcia, R.F., & Nardi, A.E., 2014. A systematic review of fMRI studies in generalized anxiety disorder: Evaluating its neural and cognitive basis. *Journal of Affective Disorders*, 167, pp.336–342.

Mombereau, C., Gur, T.L., Onksen, J., & Blendy, J.A., 2010. Differential effects of acute and repeated citalopram in mouse models of anxiety and depression. *The international journal of neuropsychopharmacology*, 13(3), pp.321–34.

Morin, S.M., Ling, N., Liu, X.J., Kahl, S.D., & Gehlert, D.R., 1999. Differential distribution of urocortin- and corticotropin-releasing factor-like immunoreactivities in the rat brain. *Neuroscience*, 92(1), pp.281–91.

Murrough, J.W., 2016. Ketamine for Depression: An Update. *Biological Psychiatry*, 80(6), pp.416–418.

Nagai, M., Kishi, K., & Kato, S., 2007. Insular cortex and neuropsychiatric disorders: a review of recent literature. *European psychiatry : the journal of the Association of European Psychiatrists*, 22(6), pp.387–94.

Nagel, G., Szellas, T., Huhn, W., Kateriya, S., Adeishvili, N., Berthold, P., Ollig, D., Hegemann, P., & Bamberg, E., 2003. Channelrhodopsin-2, a directly light-gated cation-selective membrane channel. *Proceedings of the National Academy of Sciences of the United States of America*, 100(24), pp.13940–5.

Nakajima, K., Cui, Z., Li, C., Meister, J., Cui, Y., Fu, O., Smith, A.S., Jain, S., Lowell, B.B., Krashes, M.J., & Wess, J., 2016. Gs-coupled GPCR signalling in AgRP neurons triggers sustained increase in food intake. *Nature Communications*, 7, p.10268.

Namburi, P., Beyeler, A., Yorozu, S., Calhoon, G.G., Halbert, S.A., Wichmann, R., Holden, S.S., Mertens, K.L., Anahtar, M., Felix-Ortiz, A.C., Wickersham, I.R., Gray, J.M., & Tye, K.M., 2015. A circuit mechanism for differentiating positive and negative associations. *Nature*, 520(7549), pp.675–8.

Neumeister, A., Normandin, M.D., Pietrzak, R.H., Piomelli, D., Zheng, M.Q., Gujarro-Anton, A., Potenza, M.N., Bailey, C.R., Lin, S.F., Najafzadeh, S., Ropchan, J., Henry, S., Corsi-Travali, S., Carson, R.E., & Huang, Y., 2013. Elevated brain cannabinoid CB1 receptor availability in post-traumatic stress

disorder: a positron emission tomography study. *Molecular psychiatry*, 18(9), pp.1034–40.

Nitschke, J.B., Sarinopoulos, I., Oathes, D.J., Johnstone, T., Whalen, P.J., Davidson, R.J., & Kalin, N.H., 2009. Anticipatory activation in the Amygdala and Anterior Cingulate in generalized anxiety disorder and prediction of reatment response. *American Journal of Psychiatry*, 166(3), pp.302–310.

O'brien, C.P., 2005. Benzodiazepine use, abuse, and dependence. *The Journal of clinical psychiatry*, 66 Suppl 2(suppl 2), pp.28–33.

Ogawa, S., Fujii, T., Koga, N., Hori, H., Teraishi, T., Hattori, K., Noda, T., Higuchi, T., Motohashi, N., & Kunugi, H., 2014. Plasma l-tryptophan concentration in major depressive disorder: New data and meta-analysis. *Journal of Clinical Psychiatry*, 75(9), pp.e906–e915.

Oh, E., Maejima, T., Liu, C., Deneris, E., & Herlitze, S., 2010. Substitution of 5-HT1A receptor signaling by a light-activated G protein-coupled receptor. *Journal of Biological Chemistry*, 285(40), pp.30825–30836.

Olive, M.F., Koenig, H.N., Nannini, M.A., & Hodge, C.W., 2002. Elevated extracellular CRF levels in the bed nucleus of the stria terminalis during ethanol withdrawal and reduction by subsequent ethanol intake. *Pharmacology Biochemistry and Behavior*, 72(1–2), pp.213–220.

Park, J., Bucher, E.S., Fontillas, K., Owesson-White, C., Ariansen, J.L., Carelli, R.M., & Wightman, R.M., 2013. Opposing catecholamine changes in the bed nucleus of the stria terminalis during intracranial self-stimulation and its extinction. *Biological Psychiatry*, 74(1), pp.69–76.

Park, J., Kile, B.M., & Wightman, M.R., 2009. In vivo voltammetric monitoring of norepinephrine release in the rat ventral bed nucleus of the stria terminalis and anteroventral thalamic nucleus. *European Journal of Neuroscience*, 30(11), pp.2121–2133.

Parr, L.A., Winslow, J.T., & Davis, M., 2002. Rearing experience differentially affects somatic and cardiac startle responses in rhesus monkeys (Macaca mulatta). *Behavioral neuroscience*, 116(3), pp.378–86.

Patel, S., Roelke, C.T., Rademacher, D.J., Cullinan, W.E., & Hillard, C.J., 2004. Endocannabinoid signaling negatively modulates stress-induced activation of the hypothalamic-pituitary-adrenal axis. *Endocrinology*, 145(12), pp.5431–5438.

Paxinos, G. & Franklin, K.B.J., 2008. The Mouse Brain in Stereotaxic Coordinates, Compact, Third Edition: The coronal plates and diagrams. , p.256.

Peirs, C., Williams, S.P.G., Zhao, X., Walsh, C.E., Gedeon, J.Y., Cagle, N.E., Goldring, A.C., Hioki, H., Liu, Z., Marell, P.S., & Seal, R.P., 2015. Dorsal Horn Circuits for Persistent Mechanical Pain. *Neuron*, 87(4), pp.797–812.

Pellow, S., Chopin, P., File, S.E., & Briley, M., 1985. Validation of open : closed arm entries in an elevated plus-maze as a measure of anxiety in the rat. *Journal of Neuroscience Methods*, 14(3), pp.149–167.

Phelix, C.F., Liposits, Z., & Paull, W.K., 1992. Serotonin-CRF interaction in the bed nucleus of the stria terminalis: A light microscopic double-label immunocytochemical analysis. *Brain Research Bulletin*, 28(6), pp.943–948.

Phelix, C.F. & Paull, W.K., 1990. Demonstration of distinct corticotropin releasing factor--containing neuron populations in the bed nucleus of the stria terminalis. A light and electron microscopic immunocytochemical study in the rat. *Histochemistry*, 94(4), pp.345–64.

Pleil, K.E., Helms, C.M., Sobus, J.R., Daunais, J.B., Grant, K.A., & Kash, T.L., 2016. Effects of chronic alcohol consumption on neuronal function in the non-human primate BNST. *Addiction Biology*, 21(6), pp.1151–1167.

Pleil, K.E., Rinker, J.A., Lowery-Gionta, E.G., Mazzone, C.M., McCall, N.M., Kendra, A.M., Olson, D.P., Lowell, B.B., Grant, K.A., Thiele, T.E., & Kash, T.L., 2015. NPY signaling inhibits extended amygdala CRF neurons to suppress binge alcohol drinking. *Nature Neuroscience*, 18(4), pp.545–552.

Pollak Dorocic, I., Fürth, D., Xuan, Y., Johansson, Y., Pozzi, L., Silberberg, G., Carlén, M., & Meletis, K., 2014. A Whole-Brain Atlas of Inputs to Serotonergic Neurons of the Dorsal and Median Raphe Nuclei. *Neuron*, 83(3), pp.663–678.

Polter, A.M. & Li, X., 2010. 5-HT1A receptor-regulated signal transduction pathways in brain. *Cellular Signalling*, 22(10), pp.1406–1412.

Poulin, J.-F., Arbour, D., Laforest, S., & Drolet, G., 2009. Neuroanatomical characterization of endogenous opioids in the bed nucleus of the stria terminalis. *Progress in Neuro-Psychopharmacology and Biological Psychiatry*, 33(8), pp.1356–1365.

Rainnie, D.G., Bergeron, R., Sajdyk, T.J., Patil, M., Gehlert, D.R., & Shekhar, A., 2004. Corticotrophin releasing factor-induced synaptic plasticity in the amygdala translates stress into emotional disorders. *The Journal of neuroscience : the official journal of the Society for Neuroscience*, 24(14), pp.3471–9.

Ramirez, S., Liu, X., MacDonald, C.J., Moffa, A., Zhou, J., Redondo, R.L., & Tonegawa, S., 2015. Activating positive memory engrams suppresses depression-like behaviour. *Nature*, 522(7556), pp.335–339.

Rashid, A.J., Yan, C., Mercaldo, V., Hsiang, H.L., Park, S., Cole, C.J., Cristofaro, A. De, Yu, J., Ramakrishnan, C., Lee, S.Y., Deisseroth, K., Frankland, P.W., & Josselyn, S.A., 2016. Competition between engrams influences fear memory formation and recall. *Science*, 353(6297), pp.383–388.

Ravinder, S., Burghardt, N.S., Brodsky, R., Bauer, E.P., & Chattarji, S., 2013. A role for the extended amygdala in the fear-enhancing effects of acute selective serotonin reuptake inhibitor treatment. *Translational psychiatry*, 3(1), p.e209.

Ravinder, S., Pillai, A.G., & Chattarji, S., 2011. Cellular correlates of enhanced anxiety caused by acute treatment with the selective serotonin reuptake inhibitor fluoxetine in rats. *Frontiers in behavioral neuroscience*, 5(December), p.88.

Reyes, T.M., Lewis, K., Perrin, M.H., Kunitake, K.S., Vaughan, J., Arias, C.A., Hogenesch, J.B., Gulyas, J., Rivier, J., Vale, W.W., & Sawchenko, P.E., 2001. Urocortin II: a member of the corticotropin-releasing factor (CRF) neuropeptide family that is selectively bound by type 2 CRF receptors. *Proceedings of the National Academy of Sciences of the United States of America*, 98(5), pp.2843–8.

Rickels, K., Weisman, K., Norstad, N., Singer, M., Stoltz, D., Brown, A., & Danton, J., 1982. Buspirone and diazepam in anxiety: a controlled study. *The Journal of clinical psychiatry*, 43(12 Pt 2), pp.81–6.

Rinker, J.A., Marshall, S.A., Mazzone, C.M., Lowery-Gionta, E.G., Gulati, V., Pleil, K.E., Kash, T.L., Navarro, M., & Thiele, T.E., 2015. Extended Amygdala to Ventral Tegmental Area Corticotropin-Releasing Factor Circuit Controls Binge Ethanol Intake. *Biological Psychiatry*, pp.1–11.

Robinson, O.J., Overstreet, C., Allen, P.S., Pine, D.S., & Grillon, C., 2012. Acute tryptophan depletion increases translational indices of anxiety but not fear: serotonergic modulation of the bed nucleus of the stria terminalis? *Neuropsychopharmacology : official publication of the American College of Neuropsychopharmacology*, 37(8), pp.1963–71.

Rogan, S.C. & Roth, B.L., 2011. Remote control of neuronal signaling. *Pharmacological reviews*, 63(2), pp.291–315.

Ross, S., Bossis, A., Guss, J., Agin-Liebes, G., Malone, T., Cohen, B., Mennenga, S.E., Belser, A., Kalliontzi, K., Babb, J., Su, Z., Corby, P., & Schmidt, B.L., 2016. Rapid and sustained symptom reduction following psilocybin treatment for anxiety and depression in patients with life-threatening cancer: a randomized controlled trial. *Journal of psychopharmacology (Oxford, England)*, 30(12), pp.1165–1180.

Roth, B.L., 2016. DREADDs for Neuroscientists. *Neuron*, 89(4), pp.683–694.

Roth, B.L., 1994. Multiple serotonin receptors: clinical and experimental aspects. *Annals of clinical psychiatry : official journal of the American Academy of Clinical Psychiatrists*, 6(2), pp.67–78.

Sahuque, L.L., Kullberg, E.F., Mcgeehan, A.J., Kinder, J.R., Hicks, M.P., Blanton, M.G., Janak, P.H., & Olive, M.F., 2006. Anxiogenic and aversive effects of corticotropin-releasing factor (CRF) in the bed nucleus of the stria terminalis in the rat: Role of CRF receptor subtypes. *Psychopharmacology*, 186(1), pp.122–132.

Sakanaka, M., Shibasaki, T., & Lederis, K., 1986. Distribution and efferent projections of corticotropin-releasing factor-like immunoreactivity in the rat amygdaloid complex. *Brain Research*, 382(2), pp.213–238.

Seasholtz, A.F., Valverde, R.A., & Denver, R.J., 2002. Corticotropin-releasing hormone-binding protein: biochemistry and function from fishes to mammals. *The Journal of endocrinology*, 175(1), pp.89–97.

Sehlmeyer, C., Schöning, S., Zwitserlood, P., Pfleiderer, B., Kircher, T., Arolt, V., & Konrad, C., 2009. Human fear conditioning and extinction in neuroimaging: A systematic review. *PLoS ONE*, 4(6).

Sergerie, K., Chochol, C., & Armony, J.L., 2008. The role of the amygdala in emotional processing: A quantitative meta-analysis of functional neuroimaging studies. *Neuroscience and Biobehavioral Reviews*, 32(4), pp.811–830.

Shackman, A.J. & Fox, A.S., 2016. Contributions of the Central Extended Amygdala to Fear and Anxiety. *The Journal of neuroscience : the official journal of the Society for Neuroscience*, 36(31), pp.8050–63.

Shackman, A.J., Fox, A.S., Oler, J.A., Shelton, S.E., Davidson, R.J., & Kalin, N.H., 2013. Neural mechanisms underlying heterogeneity in the presentation of anxious temperament. *Proceedings of the National Academy of Sciences of the United States of America*, 110(15), pp.6145–50.

Shin, L.M. & Liberzon, I., 2010. The neurocircuitry of fear, stress, and anxiety disorders. *Neuropsychopharmacology : official publication of the American College of Neuropsychopharmacology*, 35(1), pp.169–191.

Silberman, Y., Matthews, R.T., & Winder, D.G., 2013. A corticotropin releasing factor pathway for ethanol regulation of the ventral tegmental area in the bed nucleus of of the stria terminalis. *The Journal of Neuroscience*, 33(3), pp.950–960.

Singewald, N., Salchner, P., & Sharp, T., 2003. Induction of c-Fos expression in specific areas of the fear circuitry in rat forebrain by anxiogenic drugs. *Biological Psychiatry*, 53(4), pp.275–283.

Sink, K.S., Walker, D.L., Freeman, S.M., Flandreau, E.I., Ressler, K.J., & Davis, M., 2013. Effects of continuously enhanced corticotropin releasing factor expression within the bed nucleus of the stria terminalis on conditioned and unconditioned anxiety. *Molecular psychiatry*, 18(3), pp.308–19.

Somerville, L.H., Whalen, P.J., & Kelley, W.M., 2010. Human bed nucleus of the stria terminalis indexes hypervigilant threat monitoring. *Biological Psychiatry*, 68(5), pp.416–424.

Stachniak, T.J., Ghosh, A., & Sternson, S.M., 2014. Chemogenetic Synaptic Silencing of Neural Circuits Localizes a Hypothalamus→Midbrain Pathway for Feeding Behavior. *Neuron*, 82(4), pp.797–808.

Straube, T., Mentzel, H.J., & Miltner, W.H.R., 2007. Waiting for spiders: Brain activation during anticipatory anxiety in spider phobics. *NeuroImage*, 37(4), pp.1427–1436.

Stutzmann, J.M., Eon, B., Darche, F., Lucas, M., Rataud, J., Piot, O., Blanchard, J.C., & Laduron, P.M., 1991. Are 5-HT2 antagonists endowed with anxiolytic properties in rodents? *Neuroscience letters*, 128(1), pp.4–8.

Sullivan, G.M., Apergis, J., Bush, D.E.A., Johnson, L.R., Hou, M., & Ledoux, J.E., 2004. Lesions in the bed nucleus of the stria terminalis disrupt corticosterone and freezing responses elicited by a contextual but not by a specific cue-conditioned fear stimulus. *Neuroscience*, 128(1), pp.7–14.

Sun, N. & Cassell, M.D., 1993. Intrinsic GABAergic neurons in the rat central extended amygdala. *The Journal of comparative neurology*, 330(3), pp.381–404.

Swerdlow, N.R., Geyer, M.A., Vale, W.W., & Koob, G.F., 1986. Corticotropin-releasing factor potentiates acoustic startle in rats: blockade by chlordiazepoxide. *Psychopharmacology*, 88(2), pp.147–52.

Tasan, R.O., Nguyen, N.K., Weger, S., & Sartori, S.B., 2011. Europe PMC Funders Group The Central and Basolateral Amygdala Are Critical Sites of Neuropeptide Y / Y2 Receptor-Mediated Regulation of Anxiety and Depression. *The Journal of neuroscience : the official journal of the Society for Neuroscience*, 30(18), pp.6282–6290.

Theiss, J.D., Ridgewell, C., McHugo, M., Heckers, S., & Blackford, J.U., 2016. Manual segmentation of the human bed nucleus of the stria terminalis using 3T MRI. *NeuroImage*.

Topol, E.J., Bousser, M.G., Fox, K.A., Creager, M.A., Despres, J.P., Easton, J.D., Hamm, C.W., Montalescot, G., Steg, P.G., Pearson, T.A., Cohen, E., Gaudin, C., Job, B., Murphy, J.H., & Bhatt, D.L., 2010. Rimonabant for prevention of cardiovascular events (CRESCENDO): A randomised, multicentre, placebo-controlled trial. *The Lancet*, 376(9740), pp.517–523.

Tran, L., Schulkin, J., & Greenwood-Van Meerveld, B., 2014. Importance of CRF receptor-mediated mechanisms of the bed nucleus of the stria terminalis in the processing of anxiety and pain. *Neuropsychopharmacology : official publication of the American College of Neuropsychopharmacology*, 39(11), pp.2633–45.

Trouche, S., Perestenko, P. V, van de Ven, G.M., Bratley, C.T., McNamara, C.G., Campo-Urriza, N., Black, S.L., Reijmers, L.G., & Dupret, D., 2016. Recoding a cocaine-place memory engram to a neutral engram in the hippocampus. *Nature Neuroscience*, 19(4), pp.564–567.

Tsai, H.-C., Zhang, F., Adamantidis, A., Stuber, G.D., Bonci, A., de Lecea, L., & Deisseroth, K., 2009. Phasic firing in dopaminergic neurons is sufficient for behavioral conditioning. *Science (New York, N.Y.)*, 324(5930), pp.1080–4.

Tye, K.M. & Deisseroth, K., 2012. Optogenetic investigation of neural circuits underlying brain disease in animal models. *Nature Reviews Neuroscience*, 13(4), pp.251–266.

Tye, K.M., Prakash, R., Kim, S.-Y., Fenno, L.E., Grosenick, L., Zarabi, H., Thompson, K.R., Gradinaru, V., Ramakrishnan, C., & Deisseroth, K., 2011. Amygdala circuitry mediating reversible and bidirectional control of anxiety. *Nature*, 471(7338), pp.358–362.

Urban, D.J., Zhu, H., Marcinkiewcz, C.A., Michaelides, M., Oshibuchi, H., Rhea, D., Aryal, D.K., Farrell, M.S., Lowery-Gionta, E., Olsen, R.H.J., Wetsel, W.C., Kash, T.L., Hurd, Y.L., Tecott, L.H., & Roth, B.L., 2015. Elucidation of the Behavioral Program and Neuronal Network Encoded by Dorsal Raphe Serotonergic Neurons. *Neuropsychopharmacology : official publication of the American College of Neuropsychopharmacology*, 41(5), pp.1–12.

Valdez, G.R. & Koob, G.F., 2004. Allostasis and dysregulation of corticotropin-releasing factor and neuropeptide Y systems: Implications for the development of alcoholism. *Pharmacology*

Biochemistry and Behavior, 79(4), pp.671–689.

Vale, W., Spiess, J., Rivier, C., & Rivier, J., 1981. Characterization of a 41-Residue Ovine Hypothalamic Peptide that Stimulates Secretion of Corticotropin and β-endorphin. *Science*, 213(4514), pp.1394–1397.

Vardy, E., Robinson, J.E., Li, C., Olsen, R.H.J., DiBerto, J.F., Giguere, P.M., Sassano, F.M., Huang, X.-P., Zhu, H., Urban, D.J., White, K.L., Rittiner, J.E., Crowley, N.A., Pleil, K.E., Mazzone, C.M., Mosier, P.D., Song, J., Kash, T.L., Malanga, C.J., Krashes, M.J., & Roth, B.L., 2015. A New DREADD Facilitates the Multiplexed Chemogenetic Interrogation of Behavior. *Neuron*, 86(4), pp.936–46.

Vaughan, J., Donaldson, C., Bittencourt, J., Perrin, M.H., Lewis, K., Sutton, S., Chan, R., Turnbull, A. V, Lovejoy, D., & Rivier, C., 1995. Urocortin, a mammalian neuropeptide related to fish urotensin I and to corticotropin-releasing factor. *Nature*, 378(6554), pp.287–92.

Vong, L., Ye, C., Yang, Z., Choi, B., Chua, S., & Lowell, B.B., 2011. Leptin Action on GABAergic Neurons Prevents Obesity and Reduces Inhibitory Tone to POMC Neurons. *Neuron*, 71(1), pp.142–154.

Waddell, J., Morris, R.W., & Bouton, M.E., 2006. Effects of bed nucleus of the stria terminalis lesions on conditioned anxiety: aversive conditioning with long-duration conditional stimuli and reinstatement of extinguished fear. *Behavioral neuroscience*, 120(2), pp.324–336.

Walker, D.L. & Davis, M., 1997. Anxiogenic effects of high illumination levels assessed with the acoustic startle response in rats. *Biological Psychiatry*, 42(6), pp.461–471.

Walker, D.L. & Davis, M., 1997. Double dissociation between the involvement of the bed nucleus of the stria terminalis and the central nucleus of the amygdala in startle increases produced by conditioned versus unconditioned fear. *The Journal of neuroscience : the official journal of the Society for Neuroscience*, 17(23), pp.9375–83.

Walker, D.L., Miles, L.A., & Davis, M., 2009. Selective participation of the bed nucleus of the stria terminalis and CRF in sustained anxiety-like versus phasic fear-like responses. *Progress in neuro-psychopharmacology & biological psychiatry*, 33(8), pp.1291–308.

Walker, D.L., Toufexis, D.J., & Davis, M., 2003. Role of the bed nucleus of the stria terminalis versus the amygdala in fear, stress, and anxiety. *European Journal of Pharmacology*, 463(1–3), pp.199–216.

Walker, D.L., Yang, Y., Ratti, E., Corsi, M., Trist, D., & Davis, M., 2009. Differential effects of the CRF-R1 antagonist GSK876008 on fear-potentiated, light- and CRF-enhanced startle suggest preferential involvement in sustained vs phasic threat responses. *Neuropsychopharmacology : official publication of the American College of Neuropsychopharmacology*, 34(6), pp.1533–1542.

Wang, J., Fang, Q., Liu, Z., & Lu, L., 2006. Region-specific effects of brain corticotropin-releasing factor receptor type 1 blockade on footshock-stress-or drug-priming-induced reinstatement of morphine conditioned place preference in rats. *Psychopharmacology*, 185(1), pp.19–28.

Wang, L., Goebel-Stengel, M., Stengel, A., Wu, S.V., Ohning, G., & Taché, Y., 2011. Comparison of CRF-immunoreactive neurons distribution in mouse and rat brains and selective induction of Fos in rat hypothalamic CRF neurons by abdominal surgery. *Brain Research*, 1415, pp.34–46.

Ward, R.D., Winiger, V., Kandel, E.R., Balsam, P.D., & Simpson, E.H., 2015. Orbitofrontal cortex mediates the differential impact of signaled-reward probability on discrimination accuracy. *Frontiers in neuroscience*, 9(JUN), p.230.

Weiskrantz, L., 1956. Behavioral changes associated with ablation of the amygdaloid complex in monkeys. *Journal of comparative and physiological psychology*, 49(4), pp.381–391.

Westenberg, H.G. & den Boer, J.A., 1989. Serotonin-influencing drugs in the treatment of panic disorder. *Psychopathology*, 22(Suppl 1), pp.68–77.

Whalen, P.J., Johnstone, T., Somerville, L.H., Nitschke, J.B., Polis, S., Alexander, A.L., Davidson, R.J., & Kalin, N.H., 2008. A Functional Magnetic Resonance Imaging Predictor of Treatment Response to Venlafaxine in Generalized Anxiety Disorder. *Biological Psychiatry*, 63(9), pp.858–863.

Whiteford, H.A., Degenhardt, L., Rehm, J., Baxter, A.J., Ferrari, A.J., Erskine, H.E., Charlson, F.J., Norman, R.E., Flaxman, A.D., Johns, N., Burstein, R., Murray, C.J.L., & Vos, T., 2013. Global burden of disease attributable to mental and substance use disorders: Findings from the Global Burden of Disease Study 2010. *The Lancet*, 382(9904), pp.1575–1586.

Wise, C.D., Berger, B.D., & Stein, L., 1972. Benzodiazepines: anxiety-reducing activity by reduction of serotonin turnover in the brain. *Science (New York, N.Y.)*, 177(4044), pp.180–3.

Yassa, M.A., Hazlett, R.L., Stark, C.E.L., & Hoehn-Saric, R., 2012. Functional MRI of the amygdala and bed nucleus of the stria terminalis during conditions of uncertainty in generalized anxiety disorder. *Journal of Psychiatric Research*, 46(8), pp.1045–1052.

Yau, J.O.-Y. & McNally, G.P., 2015. Pharmacogenetic excitation of dorsomedial prefrontal cortex restores fear prediction error. *The Journal of neuroscience : the official journal of the Society for Neuroscience*, 35(1), pp.74–83.

Yiu, A.P., Mercaldo, V., Yan, C., Richards, B., Rashid, A.J., Hsiang, H.L.L., Pressey, J., Mahadevan, V., Tran, M.M., Kushner, S.A., Woodin, M.A., Frankland, P.W., & Josselyn, S.A., 2014. Neurons Are Recruited to a Memory Trace Based on Relative Neuronal Excitability Immediately before Training. *Neuron*, 83(3), pp.722–735.

Zarate, C.A., Singh, J., Carlson, P.J., Brutsche, N.E., Ameli, R., Luckenbaugh, D.A., Charney, D.S., & Manji, H., 2006. 1314 A Randomized Trial of an N-methyl-D-aspartate Antagonist in Treatment-Resistant Major Depression. *Archives of General Psychiatry*, 63(8), pp.856–864.

Zemelman, B. V., Lee, G.A., Ng, M., & Miesenböck, G., 2002. Selective photostimulation of genetically chARGed neurons. *Neuron*, 33(1), pp.15–22.

Zhang, F., Vierock, J., Yizhar, O., Fenno, L.E., Tsunoda, S., Kianianmomeni, A., Prigge, M., Berndt, A., Cushman, J., Polle, J., Magnuson, J., Hegemann, P., & Deisseroth, K., 2011. The microbial opsin family of optogenetic tools. *Cell*, 147(7), pp.1446–1457.

Zhang, F., Wang, L.-P., Brauner, M., Liewald, J.F., Kay, K., Watzke, N., Wood, P.G., Bamberg, E., Nagel, G., Gottschalk, A., & Deisseroth, K., 2007. Multimodal fast optical interrogation of neural circuitry. *Nature*, 446(April), pp.633–639.

Zobel, A.W., Nickel, T., Künzel, H.E., Ackl, N., Sonntag, A., Ising, M., & Holsboer, F., 2000. Effects of the high-affinity corticotropin-releasing hormone receptor 1 antagonist R121919 in major depression: the first 20 patients treated. *Journal of Psychiatric Research*, 34(3), pp.171–181.